Multiscale Manipulation of Nanocellulose Structures for Divers Sustainable Materials

Heather Wise

A dissertation

submitted in partial fulfillment of the

requirements for the degree of

Doctor of Philosophy

University of Washington

2021

Reading Committee:

Anthony Dichiara, Chair

Renata Bura

Rick Gustafson

Program Authorize to offer Degree

School of Environmental and Forest Sciences

University of Washington

Abstract

Multiscale Manipulation of Nanocellulose Structures for Diverse Sustainable Materials

Heather Wise

Chair of the Supervisory Committee:
Anthony Dichiara
Department of Bioresource Science and Engineering

Global dependence on petroleum, a finite source, is creating economic, social, and environmental unrest. The quickly depleting limited resource needs a sustainable alternative that can offer the same multifunctional benefits as petroleum. Nanocellulose, or cellulose that is approximately 2 nm in diameter with varying lengths, is sourced from renewable forms of biomass including trees and grasses. Nanocellulose is a promising sustainable alternative, but in its current applications it lacks the adaptability to fill both basic and complex functionalities and thus fails to compete with petroleum products. However, controlling the structure of nanocellulose at multiple scales offers multiple points of control increasing its potential success in basic applications such as textiles and complex applications such as small electronics, sensors, or other biomedical applications. In this work we demonstrate the massive untapped potential of nanocellulose as a diverse sustainable alternative material to petroleum. Initially we demonstrate the multiple points of control available with nanocellulose production to tailor fiber aspect ratio and surface charge, giving independent control over two critical fiber properties. The individual control over these

properties opens nanocellulose fibers to a wide range of applications not previously afforded by typical synthesis methods. Through these tailored properties we successfully designed nanocellulose for high performance in a novel pre-alignment technique involving electric field and flow focusing. The electric field provides individual CNF fiber rotation and a higher degree of alignment while the flow focusing provides a quick fiber fixation establishing permanent anisotropy. We demonstrate the positive effects of this alignment on mechanical performance and the potential of this continuous filament as an alternative textile. Finally, we further adapt this aligned filament to fill more complex applications by introducing a conductive filler to create an aligned conductive composite filament. While most report performance loss, through engineering the CNF nanostructure and carefully controlling the alignment of the composite components, we demonstrate exceptional performance beyond the qualities possible with a pure CNF filament. The alignment not only improves the mechanical properties but the electrical properties as well. The implications of this new conductive composite filament to fill complex functionalities are demonstrated through its performance as a micro wire for small electronics and a unique water sensor. This project demonstrates the potential of nanocellulose as a multifunctional and sustainably sourced alternative to petroleum.

Table of Contents

I. Introduction 12
1.0 Petroleum Dependence 12
2.0 Cellulose and Nanocellulose 13
3.0 Multiscale Manipulation of Nanocellulose Structure 15
3.1 Manipulating Nanocellulose Fiber Structure and Properties 15
3.2 Alignment of Nanocellulose Micro and Macro Structures 17
3.3 Expanding to Nanocellulose Composite Structures 22
3.4 Carbon Nanotubes 23
4.0 Summary 24
II. Materials and Methods 26
2.1 CNF Preparation via TEMPO Oxidation 26
2.2 Conductometric Titration for CNF Charge Density 27
2.3 CNF and SWNT Dispersions 27
2.3.1 CNF and SWNT Dispersion Characterization 28
2.3.2 CNF and SWNT Aspect Ratio 28
2.3.3 CNF and SWNT Bonding 29
2.4 Filament Formation (Electric Field Flow Focusing Channel) and Characterization 29
2.4.1 Filament Surface Characterization 30
2.4.2 Filament Alignment and Chemical Characterization 31
2.4.3 Filament Mechanical Properties 32
2.5 CNF/SWNT In-Situ Swelling 33
III Results and Discussion 34
1.0 Chapter 1: Controlling Nanocellulose Structure 34
1.1 Synopsis 34
1.2 Introduction 35
1.3 Nanocellulose TEMPO Oxidation 37
1.3 Controlling Surface Charge of CNF 40
1.4 Tailoring Aspect Ratio of CNF 45
1.5 Conclusion 48
2.0 Chapter 2: Field-Assisted Alignment of Cellulose Nanofibrils in a Continuous Flow-Focusing System 50
2.1 Synopsis 50
2.2 Introduction 52
2.3 Engineered CNF Characteristics 54

2.4 Continuous Aligned Filament Formation 56
2.5 Characterization of Filament Formation and Alignment 59
2.6 Anisotropic vs Isotropic Filament Mechanical Properties 64
2.7 Conclusion 66
3.0 Aligned Conductive Composite Filaments for Complex Sensing Applications 69
3.1 Synopsis 69
3.2 Introduction 71
3.3 CNF/SWNT Dispersion Characterization 75
3.4 Compound Structure of CNF with SWNT 78
3.5 CNF/SWNT Filament Characterization 83
3.6 Mechanical and Electrical Properties of Composite Filaments 85
3.7 Application of Conductive Aligned Filaments 92
3.8 Conclusion 94
IV. Conclusion and Future Work 96
V. References 100

Table of Figures

Figure 1. Chemical structure of two glucose monomers together often called cellobiose or a small cellulose chain.[7] 14
Figure 2. Chart outlining different forms of nanocellulose and their properties and applications. TEM images are included to demonstrate the different textures as well as a representative depiction of each synthesis method. 16
Figure 3. Biomass energy crop structure depicting the aligned cell wall structures and a single cell wall comprised of cellulose microfibrils coated in lignin, and hemicellulose. A magnification of the cellulose microfibril shows the structure is composed of aligned cellulose chains. The figure to the upper right demonstrates that in three of the four total tree cell walls the microfibril bundles are aligned with each other.[16,17] 18
Figure 4. Flow diagram outlining the steps required to create TEMPO oxidized CNF. Most of the steps involve purification and concentration, with two primary active steps, oxidation, and mechanical defibrillation, occurring at steps 1 through 2 and 6 through 7, respectively. 26
Figure 5. Depiction of combining two common alignment methods, electric field and flow focusing, into a novel combination electric field flow focusing channel on the right. The continuous electric field flow focusing channel is composed of 4 electrodes and is operated by a total of 5 syringe pumps resulting in an aligned filament hydrogel that is deposited into a beaker of water..... 30
Figure 6. Depiction of the full 9 step TEMPO Oxidation process for CNF production. Steps 1-2 involve a critical oxidation step followed by three purification steps that entail neutralization (step 3), concentration (step 4) and dialysis (step 5). Then the primary mechanical defibrillation to control the fiber aspect ratio (step 6 and 7) followed by one more purification step to reach the final solution of dispersed nanocellulose fibers shown in step 9. 38
Figure 7. TEMPO oxidation chemical process depicted using chemical structures. Step 1 involves the activation of TEMPO using sodium hypochlorite followed by step 2 the reaction of the C6 hydroxyl on a glucose monomer to form an aldehyde. Step 3 involves the hydration of the aldehyde and subsequent reaction to form a carboxylic acid, that is finally capped with a sodium under basic conditions. [13]..... 39
Figure 8. (A) Diagram of oxidation steps from the 9 step TEMPO oxidation process to produce CNF. The first step involves adding the three primary oxidizing chemicals and the second involves maintaining the pH at 10 with sodium hydroxide until the pH is stable and the color changes from yellow to clear. (B) Graphical conductimetric titration measurements of different types of CNF or cellulose demonstrating that the oxidation step is key to establishing CNF surface charge. 41
Figure 9. Graph depicting independent control over the charge density of CNF fibers through controlling the oxidation time. The charge density increases with oxidation time plateauing around 1 hour. Fibers at lower oxidation times were larger and visible to the naked eye but the fiber aspect ratio was maintained with additional mechanical treatment and wider distributions were observed at lower oxidation times. 42

Figure 10. Graph demonstrating the effect of sodium hypochlorite concentration on yield and charge density. Higher charge densities were achieved than possible with simply controlling oxidation time. However, quadrupling the concentration from typical quantities can lead to over processing creating degradation products lowering the overall measurable carboxylic units and yield. 44
Figure 11. Graph displaying the effect of sodium hypochlorite concentration on Fiber length and Fiber diameter. Higher concentrations of sodium hypochlorite show a shorter resulting length when undergoing the same mechanical treatment supporting the idea of increased fiber breaking. 45
Figure 12. A) Diagram highlighting the mechanical defibrillation step from the full 9 step TEMPO oxidation process. (B) AFM image of nanocellulose fibers depicting typical lengths and diameters. (C) Histogram demonstrating normal fiber length distribution of typically oxidized and mechanically treated CNF. (D) Histogram of CNF fiber diameters that underwent typical oxidation and mechanical treatment as outlined in the materials and methods. 46
Figure 13. Nanocellulose prepared with double the amount of typical sodium hypochlorite (10mmol/g CNF) and the same mechanical treatment as typical CNF batches. (A) Histogram showing the normal distribution of the fiber diameter with an average of 2.4 nm. (B) Histogram showing a shorter fiber length and a normal distribution with an average of 150 nm although the same mechanical treatment was used. 47
Figure 14. Graph comparing average fiber lengths and diameters of CNF with additional mechanical defibrillation. Increasing the sonication time causes significant reductions in fiber length but no in fiber diameter. 48
Figure 15. (A) Histogram exhibiting normal distribution of CNF fiber diameter with2nm average. (B) Histogram exhibiting normal distribution of CNF fiber length with a 620 nm average. (C) AFM image of CNF dispersion exhibiting wide narrow range of fiber length and diameter. (D) XRD analysis of nanocellulose film with a 41 % crystallinity calculated using the segal method. 55
Figure 16. Assembly of nanostructured cellulosic filaments using novel electric field flow focusing system. (A) Schematic of the field-assisted double flow-focusing channel used for the preparation of macroscopic filaments. The CNF suspension is injected in the core flow, while DI water and acid at low pH are supplied in the first and second extensional flows, respectively. Before reaching the extensional flows, the core CNF flow is exposed to four copper electrodes that are supplied a desired voltage to cause fiber polarization from the generated electric field. After the second extensional flow the CNF core undergoes a sol gel transition, and the hydrogel filament is deposited into a beaker of DI water. (B) Optical microscope image of the double flow-focusing part of the setup represented horizontally. Note that blue dyes were added to the core flow for clarity purposes. (C) Polarized optical transmission measurements of CNF alignment at various applied voltages along the core microfluidic channel, as illustrated in the above schematic. 56
Figure 17. Morphological characterization of the prepared bio-based filaments. (A) Representative SEM image of a cellulosic filament with the diameter distribution shown in the inset. (B) SEM image of the cross section of a filament showing a layered structure with

dense CNF packing and a void less core structure. Histograms representing the orientation degree of CNF threads on the surface of macroscopic filaments prepared without (C) and with (D) external electric field. High magnification SEM images of the filament surfaces, shown in the insets, and orientation factors calculated using equation 2 CNF micro bundle alignment. 59
Figure 18. Raman spectra of cellulosic filaments prepared with (red) and without (black) external electric field. The voltage applied in this case was 600 Vpp. Each spectra was collected at an excitation wavelength of 785 nm in parallel with (solid line) and perpendicular to (dashed line) the filament axis. 62
Figure 19. 2D XRD analysis of CNF alignment within the cellulosic filaments. (A) Azimuthal integration of the (200) scattering plane of the diffractograms with respect to Φ rotations for cellulosic filaments prepared at (A) 0, (B) 200, (C) 400 and (D) 600 V_{pp}. (E) Schematic illustrating the axis of rotations with respect to the filament layout on the XRD stage for the in-plane, Φ, and out-of-plane, Ψ, directions. (F) Diffractograms of cellulosic filaments prepared at various applied voltages with respect to Ψ rotations. 64
Figure 20. Mechanical properties of cellulosic filaments. (A) Histograms showing the ultimate tensile strength, strain-to-failure and Young's modulus of filaments prepared at different applied voltage. (B) Triplicate stress-strain curves of representative filaments prepared at 0 (black) and 600 V_{pp} (red). 66
Figure 21. (A) AFM Image demonstrating visual of good dispersion quality of 50 wt % CNF/SWNT dispersion. (B) Fiber length Histogram off pure CNF dispersions after 8 min sonication prepared at the same wt % of all CNF/SWNT dispersions. (C) TEM image of 50 wt % CNF/SWNT dispersions with red arrows pointing to the same single SWNT fiber. (D) STEM image of 50 wt % CNF/SWNT dispersion with one red arrow pointing to one SWNT fiber. 76
Figure 22. (A) UV-VIS absorption of the same mass of SWNTs (63 mg) with different concentrations of the same CNF. (B) Three different CNF/SWNT dispersions (pure CNF or 0 wt % and 15, 25, and 50 wt % SWNTs) prepared using double sonication for 8 min followed by 50 min centrifugation at 5500 RPM. These dispersions were prepared for application to the electric field flow focusing channel. 77
Figure 23. (A) Viscosity versus strain rate of different SWNT wt % dispersions. (E) UV-VIS absorbance of different SWNT wt % solutions prepared for application in the applied electric field flow focusing channel. (B) FTIR of films prepared from different SWNT wt % dispersions to demonstrate carboxylic acid interaction. 78
Figure 24. Schematic of Photoinduced Force Microscopy (PiFM) technique. The IR laser is focused through a series of mirrors and aligned on to the sample through parabolic mirror shifts. As the AFM cantilever probes the samples dipole-dipole force interactions from excitation are recorded in addition to typical AFM interactions to produce information on both the topographical and chemical nature of the sample. 81
Figure 25. (A) Photoinduced Force Microscopy (PiFM) of drop casted and dried CNF/SWNT at 50 wt % with seven points indicating the location of collected FTIR Spectra. (B) FTIR of seven points taken on the PiFM (color matched to locations on image A) with peaks indicated at 1612 cm^{-1}, 1347 cm^{-1}, and 1071 cm^{-1}. (C) Transmission electron microscope

(TEM) image of a single walled nanotube with rough textured nanocellulose wrapped on the SWNT surface wall. (D) PiFM Phase image depicting different material stiffness on and next to fibers. 83
Figure 26. (A) SEM image of the full cross section of a 50 w .% filament showing a solid structure with a uniform tight packing. (B) Histogram demonstrating a normal distribution of filament diameters independent of filament SWNT loading and applied voltage. (C) Higher magnification of the 50 wt % CNF/SWNT filament with applied voltage showing brighter SWNT throughout the filament core and unidirectional nanotubes aligned with the filament longitudinal axis. (D) Surface of 50 wt % CNF/SWNT filament showing a rough surface texture and micro alignment with SWNTs woven throughout the surface. 84
Figure 27. (A) Conductive imaging of 50 wt % filament created without an applied electric field showing sub surface SWNTs and a preferential alignment in the longitudinal direction. (B) Conductive imaging of 50 wt % filament with a 100V applied electric field to show SWNTs below the surface and SWNT bundles circled in red. 85
Figure 28. 2D XRD analysis of CNF alignment within the pure CNF filaments created with no applied electric field. (A) Azimuthal integration of the (200) scattering plane of the diffractograms with respect to Φ rotations for cellulosic filaments prepared with 360 nm CNF fiber length (A) and (B) 645 nm fiber length. Filaments created with shorter CNF showed no convergence indicating random orientation of CNF fibers, while longer fibers exhibited a clear inline with the filament axis. 86
Figure 29. (A) Ultimate tensile strength (UTS) and maximum strain of filaments with and without an applied electric field as a function of SWNT content. Filaments created with a 100 V applied electric field at 50 wt % SWNT showed a significantly higher strain and the same UTS as pure CNF filaments. (B) Young's Modulus and Toughness of filaments with and without an applied electric field as a function of SWNT content. The applied electric field improved the young's modulus of 15wt % and 20 wt % filaments to match the performance of pure CNF filaments. (C) Representative tensile graph of pure CNF and 50 wt % SWNT filaments prepared at both 0 V and 100 V. (D) UTS, Strain and Toughness of a filaments made with 50 wt % SWNT content and a 100 V applied electric field tested with 0 % and 35 % humidity, demonstrating significant increases in the UTS. 88
Figure 30. (A) Representative depiction of filament mounting method and inclusion in a circuit with an LED light bulb. (B) Photo of the circuit depicted in A demonstrating the successful illumination of a blue LED bulb with as little as 5 V supplied via a keithley. (C) Current as a function of voltage for 50 wt % filaments created with and without and applied electric field. (D) Resistance measurements of 50wt % filaments mounted at 15 mm in length to be used for future testing and resistance measurements. 91
Figure 31. Schematic of in-situ swelling set up demonstrating continuous real-time measurement of swelling rate and resistance changes. All filaments used for in-situ swelling measurements were 50 wt % SWNT and 15 mm length attached to microscope slide with silver adhesive paste. 93
Figure 32. (A) Relative swelling diameter and resistance changes after a 1µl drop of water is placed on 50 wt % filament produced with and without an applied electric field. (B) Swelling rate of aligned and unaligned 50 wt % filament with respect to time. (C) Cyclic

water sensing of 1μl of water on a 50 wt % filament created with an applied electric field. (D) Microscope images 50 wt % aligned dry filament (left) and swelled filament from water exposure (right)..... 94

I. Introduction

1.0 Petroleum Dependence

Petroleum is the source for a variety of daily products that exist in the world today, and its success as a material stems from application versatility. Crude oil, when harvested from the ground, is separated to make a variety of chemicals via a distillation column. This column produces different length carbon-based chemicals that are translated into several different materials including polymer-based plastics that are dependent on the chemical structure. This versatility to create fundamental products like plastic translates to crude oil comprising several daily products ranging from the basic such as textiles to the complex involving small electronic devices. This blanket use of petroleum products causes problems both because of its limited resource and its lack of biodegradability. It is commonly known that petroleum is a limited resource, and we consistently rely upon it, creating many social, economic, and environmental problems. Environmentally methods of harvesting petroleum are extremely harmful to the Earth, and socially they are extremely dangerous. In addition, the limited availability causes constant fluctuations in price creating economic and social anxiety in addition to community unrest.[1] Its imperative that an alternative material be found to offset petroleum dependence and improve global sustainability. In addition to a depleting finite petroleum source the disposal of plastics derived from crude oil also presents a large issue as every year 8 million tons of plastic waste escapes into the oceans. These large first-generation plastics (plastics directly disposed,) can cause issues, but there is also growing concern for second generation microplastic, microplastic resulting from first generation plastic degradation. Second generation microplastics have been found in several different organisms and continue to cause concern with bioaccumulation and habitat pollution. Perhaps the greatest form and concern of microplastic exists from small plastic fibers often not seen to the naked eye but that exist in the air or in the water from textile washing.[2,3] These second generation

plastics have been found to interrupt the respiration of some lobster and found in the membranes of some filter feeders.[4,5] Addressing a sustainable alternative to both of these issues will require attention to the three pillars of sustainability social, economic, and environmental.[6] Environmental sustainability encompasses all environmental impacts throughout the entire life cycle of the product including cradle to grave. Economic sustainability considers the economic success and viability of a product with considerations including capital costs, sustainable maintenance costs, and global market success. Social sustainability considers the community impact from multiple aspects including health and safety of material processes, ethics and quality of life, and education and job possibilities. All three pillars create a nearly unattainable standard, but they should be heavily considered when developing a sustainable alternative to the limited petroleum resource. It is likely to fill the large gap left by dependence on crude oil products their will need to be multiple alternatives, and these alternatives will need to be as versatile as crude oil.

2.0 Cellulose and Nanocellulose

Cellulose is one of the most abundant natural polymers in the world and can easily be found in many types of biomass, with woody biomass being the most easily identifiable form. Trees achieve incredible structural feats growing to be 120 ft tall in the case of cedars, and wood is still a structural staple in many human designed complex structures. In addition to its incredible strength, it is a naturally biocompatible and biodegradable material that can be sustainably grown while providing numerous other environmental benefits such as habitat formation, carbon sequestration, and oxygen production. Biomass itself is an attractive material solution for creating globally sustainable products because it has components satisfying all three pillars of sustainability. Environmentally biomass as a source shows promise with plantation growth or sustainable forest harvesting. In addition to a sustainable source, the natural biocompatibility

promotes quick decomposition and no secondary pollution or bioaccumulation of products. Economically biomass as a resource provides sustainable jobs in agriculture and processing, and the global availability creates a more predictable market than that of petroleum. Socially the aesthetic value and increased quality of life provided to communities through forestation and minimal plastic pollution has countless benefits. It is clear that cellulose offers major benefits in terms of sustainability, but its viability is entirely dependent of the versatility of the material. This means that cellulose will need to fill both basic needs such as textiles or plastics and more complex needs such as small electronics or biomedical devices. It seems challenging to convert a massive tree standing in nature to a shirt or even further to a small electronic device, but chemically it's entirely possible.

Chemically cellulose is simply glucose monomers attached to create long chains. These long chains are then stacked together to get something larger called cellulose microfibrils. Then these stacked bundles are put together to create large stacks of cellulose that eventually make up the tree cell.

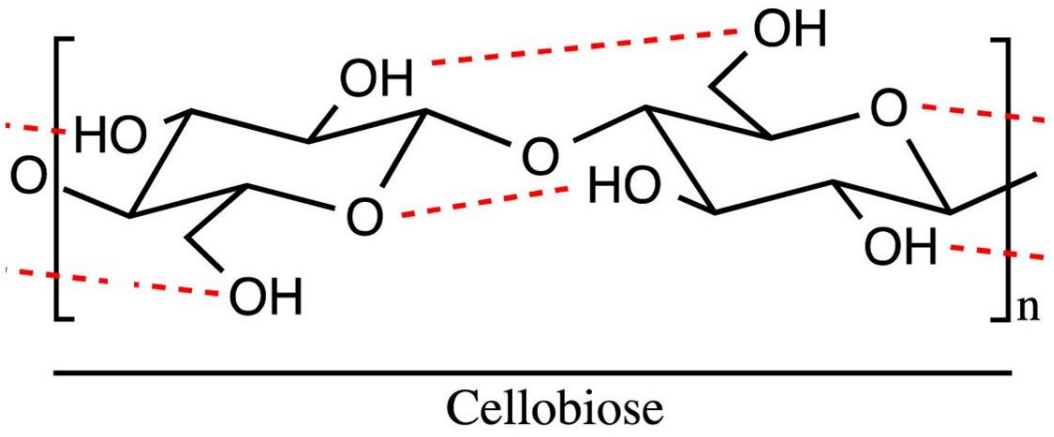

Figure 1. *Chemical structure of two glucose monomers together often called cellobiose or a small cellulose chain.*[7]

While making a tree into a textile seems challenging if we isolate the cellulose from the tree cell wall down so we have just the cellulose microfibrils, or even smaller to just single or a few long chains of cellulose bundled together, the material becomes much more moldable. These small chains or bundles of glucose chains are commonly referred to as nanocellulose or cellulose nanofibrils (CNF).

Cellulose nanofibrils (CNFs) are simply the same cellulose chains made from glucose monomers found in woody biomass but on the nano scale. The "nano" is defined as having at least one dimension in the nano scale usually associated with being less than 100 nm. This means that the nano form of the cellulose chains is still bio-based and biocompatible coming with all the same sustainable benefits as regular cellulose. However, cellulose at this small scale presents a different set of attractive material and mechanical properties due to the small scale that could serve a multitude of multifunctional applications. CNF's desirable material traits include optical transparency, high aspect ratio, and excellent mechanical properties.[8] These nanosized fibrils can vary in length from 50 nm to 1 μm, with a diameter typically from 2 to 5 nm, thus the achieving the required nano scale. Strength properties of these materials include an ultimate tensile strength from 0.1-0.8 GPa and young modulus from 5 to 55 GPa.[9] In addition to its unique nano scale properties, the fibers are incredibly versatile due to the numerous types of CNF, and the fiber structure that can be manipulated to create properties targeted toward any number of applications.

3.0 Multiscale Manipulation of Nanocellulose Structure

3.1 Manipulating Nanocellulose Fiber Structure and Properties

Generally, the fiber properties can be tailored to fit an application through the method CNF synthesis, that determines the type of CNF produced. There are two primary ways to obtain CNF; a bottom-up approach using bacteria to grow CNF, or a top-down approach using strong acids or

chemical exfoliation to break down biomass to the nano size. Each synthesis method results in specific CNF traits making the chosen synthetic method dependent upon the future application.

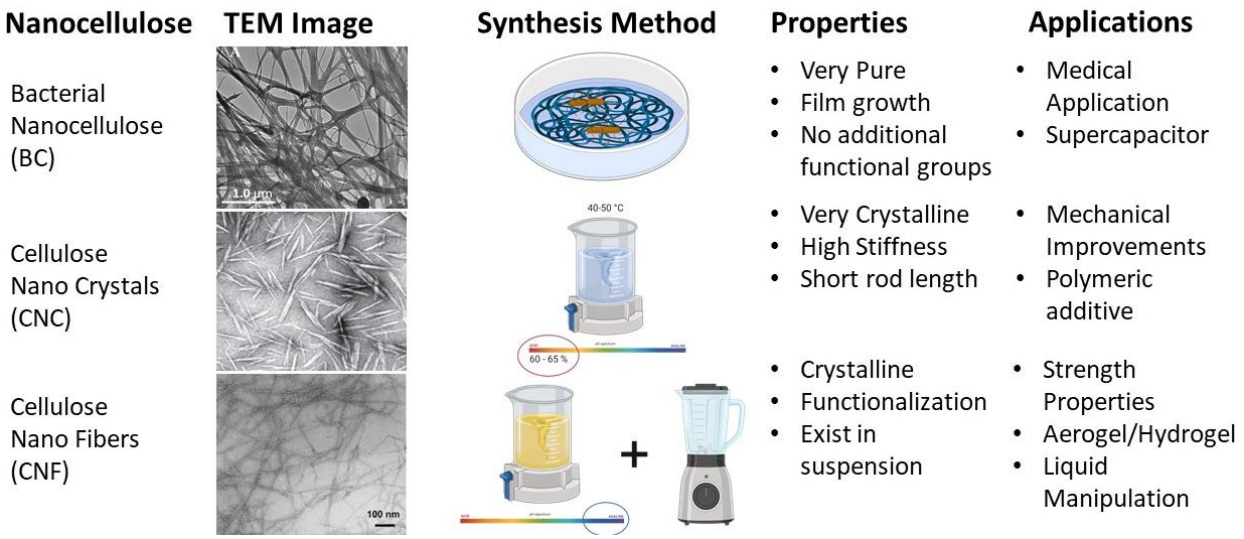

Figure 2. *Chart outlining different forms of nanocellulose and their properties and applications. TEM images are included to demonstrate the different textures as well as a representative depiction of each synthesis method.*

The bottom-up approach produces bacterial cellulose nanofibrils and they are known for their extremely high purity and lack of surface charge. Generally, the CNF is grown in sheets, so the geometry is limiting and the lack of charge on the surface makes it challenging to disperse in water without significant precipitation in solution, which greatly limits its applications. However, the excellent dielectric properties, high purity, and sheet growth are ideal for super capacitors or more commonly biomedical applications, such as biocompatible bandages for burns.[10,11] The two most common top down synthesis of CNF result in nano fiber like geometries but with different properties depending on the synthesis method. Strong acid top-down synthesis generally results in noticeably short fibers, approximately 200 nm or less, that are highly crystalline, more commonly referred to as cellulose nanocrystals (CNC). This high crystallinity creates a very high stiffness

that directly translates to its ideal use as a reinforcer in films or as an additional additive to increase material stiffness.[12] The second top down method involves chemical exfoliation methods in addition to mechanical deformation and are commonly referred to as cellulose nanofibrils or CNF. They include both the crystalline and amorphous regions of the cellulose and are known for being able to sustain high surface charges making the CNF colloidally stable in water.[13] These fiber suspensions are often desired to create a variety of pure nano cellulosic materials that typically require liquid manipulation, such as aerogels or films.[14] The liquid manipulation has the most promising outlook for multifunctionality as many industrial processes rely on liquid transportation of materials for ease of processing. The many different types and characteristics of nanocellulose further validate the material as an alternative to petroleum products because the great versatility of properties can fill numerous applications. While the types and potential applications of CNFs are boundless, nanocellulose has still not successfully been applied because of the failed transfer of properties observed at the nano level to the micro and macro levels. This failed transfer is likely because of defects in assembled structures or failed interactions between fibers, creating points of stress concentration, and ultimately mechanical failure.

3.2 Alignment of Nanocellulose Micro and Macro Structures

While current applications have not been successful in synthetically capture the amazing nano properties at the larger scales, nature has done this successfully for ages in woody biomass. As mentioned before the chemical structure of the nanocellulose is unaltered and remains to be glucose monomers, and in fact are isolated from standing strong trees. The major difference in our applied nanofibrils and those found in nature lies in the alignment of these assembled structures. In a tree cell wall nanofibrils are aligned and bundled to form microfibrils, these microfibrils are also then aligned within a tree cell wall, and even tree cells aligned within growth rings.[15]

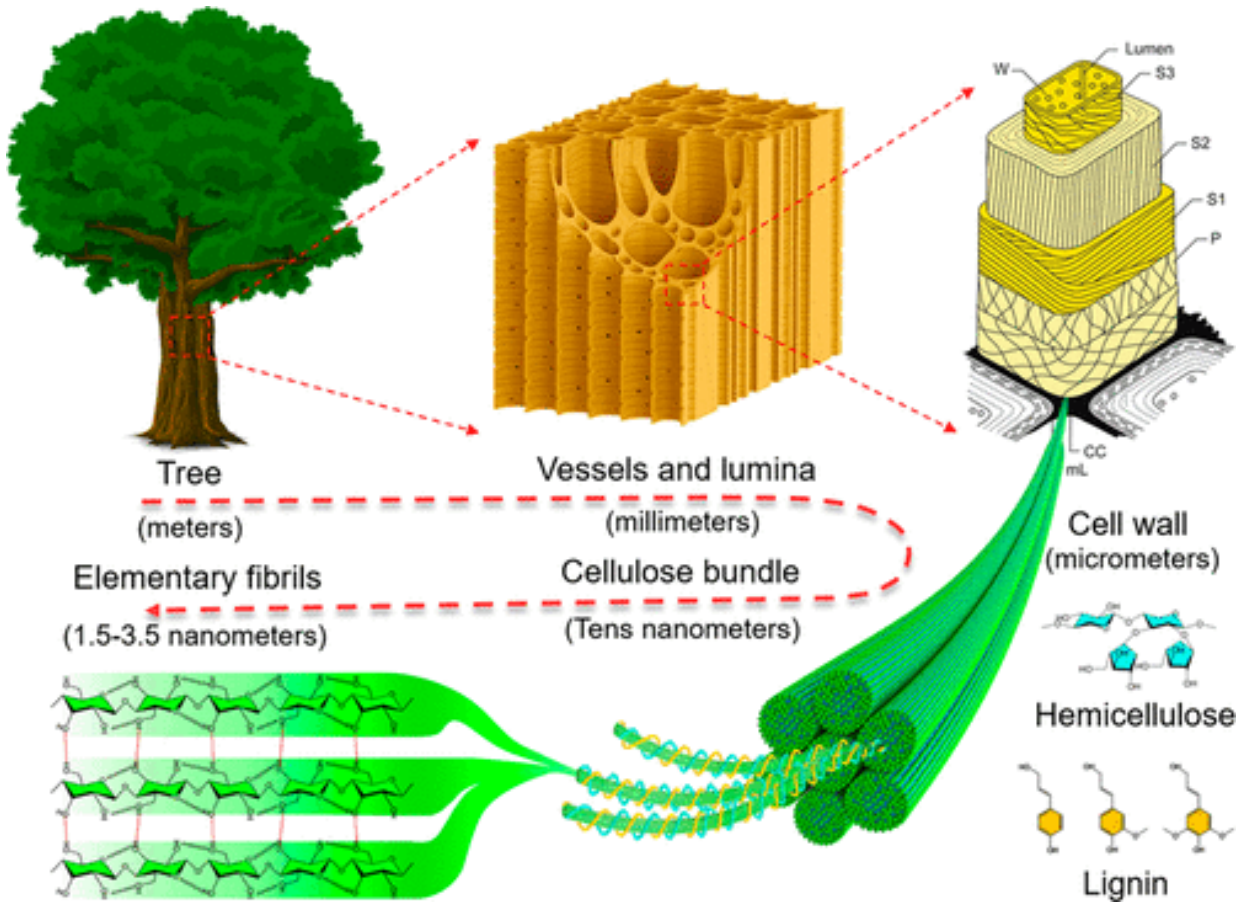

Figure 3. *Biomass energy crop structure depicting the aligned cell wall structures and a single cell wall comprised of cellulose microfibrils coated in lignin, and hemicellulose. A magnification of the cellulose microfibril shows the structure is composed of aligned cellulose chains. The figure to the upper right demonstrates that in three of the four total tree cell walls the microfibril bundles are aligned with each other.*[16,17]

This multiscale alignment beginning with the nano scale, continuing to the microscale, and even through the macroscale is responsible for the incredible anisotropic strength and adaptability of woody biomass. The alignment of microfibrils regarding each other create an exceptional amount of strength and stiffness in the aligned directions improving inter fiber bonding, while the overall microfibril alignment at multiple angles through each layer of the cell wall creates strength and

adaptability in other directions. This shows that the successful macroscale performance of CNFs is not only strongly influenced by the structure and properties established at the nano scale but also that multiscale CNF alignment is critical. Some biomimetic alignment techniques have been investigated but critical improvements are required before the versatility and sustainability required for alternative petroleum products is achieved.

Biomimetic techniques for aligning CNF can be split into two categories; those that induce alignment in an already formed solid matrix, we will call post fixation alignment, or post alignment, and those that establish alignment prior to fiber fixation, called prefixation alignment or pre-alignment.

Post alignment techniques generally involve CNF fixed in a polymer matrix creating limited fiber mobility restricting anisotropy to the bulk rather than individual fiber alignment. Typical methods involve the polymer/CNF composite enduring mechanical rubbing or drawing to drive the rotation of fiber elements.[18,19] This necessary mounting in a secondary polymer reduces the overall sustainability of the material, as it still requires a crude oil based polymer. The secondary polymer also poses a problem for fiber manipulation because a much greater force is required potential using more energy and creating difficulties working within a solid matrix. The alignment established through these processes is also flawed because a large degree of anisotropy is often lost to polymer relaxation when tension or mechanical force is removed. The strain or deformation to the solid matrix form the force can also create defects prior to its final application, ultimately detracting from mechanical performance.[20] Overall post alignment techniques lack refinement and cause damage while creating alignment netting in just a small gain in mechanical performance.

Pre-alignment entails establishing alignment prior to fiber fixation by manipulating a suspension of nanocellulose, followed by locking the alignment in place. Pre alignment techniques

require fiber suspension, before fixation generally requiring a highly viscous liquid, a surfactant, or a high fiber charge. The high fiber charge is the most desirable from a sustainability standpoint and the use of a viscous liquid or surfactant could prohibit fiber fixation resulting in poor mechanical performance. The high fiber charge makes the chemical exfoliation of CNF the most ideal form of nanocellulose for these methods because they readily exist as a stable suspension. The pre alignment method is far more attractive because the alignment is conducted independent of a solid matrix minimizing defects and improving single fiber manipulation, but it can be challenging to maintain the alignment through fiber fixation. Typical pre alignment methods include electric fields,[21–24]magnetic fields,[16–19] and liquid shear flow[29–33], followed by the chemical compound addition to induce a sol gel transition or time extensive polymer curing. These electric fields require a large voltage (~ 2000 V/cm)[22] and magnetic fields are static and require an extended amount of time (~ 180 min)[28] to establish fiber alignment and fixation. The static nature of these systems also makes it challenging to maintain alignment during extended periods of fiber fixation and limits the size of the resulting aligned CNF material.

The liquid shear flow is showing great promise for a continuous alignment and quick fiber fixation method but the alignment lacks individual fiber manipulation.[34] Aligning CNF using extensional shear flow can be challenging especially when considering CNF rather than CNC because the naturally longer fibers, fiber interactions due to charge and higher viscosity. In addition to difficulty controlling these factors flow rates are directly related to degree of fiber alignment. CNF at lower flow rates show alignment but increasing the flow rate decouple often results in no alignment because of the morphology of CNF fibers. Fibers are generally longer and have amorphous sections and high flow rates can cause fiber entanglement within a single fiber or amongst other fibers. These entanglements prohibit fiber elongation and alignment and instead

create flow obstruction and cause rotation with local vorticity. In addition, shear flows can cause a rapid rotation of individual fibers and alignment can be lost quickly. The fiber length and morphology are critical to shear flow alignments and shorter fibers can easily rotate establishing alignment quickly, but this anisotropy can be quickly lost to Brownian motion as well. Alternatively longer fibers can resist Brownian motion longer but establishing the alignment becomes challenging. CNF pre-alignment methods have shown a greater potential to create a higher degree of alignment and minimize defects offering an opportunity to maximize pure CNF material performance. Perhaps considered one of the most successful flow focusing methods is the one developed by Mittal et al. This flow method involves a primary focusing flow on CNF downward followed by an extensional flow of water that functions as a protective sheath flow and to establishes some initial alignment. Then semi- aligned core CNF flow than continues downward encountering a secondary extensional flow of a weak acid that serves to induce a sol gel transition between fibers. The first shear flow demonstrated a decrease in fiber order due to flow deceleration but then due to flow acceleration after focusing order increased, and the second shear flow showed this same behavior. These momentary drops in order still resulted in an extremely strong filament with an ultimate tensile strength at approximately 1300 MPa and young's Modulus at roughly 80 GPa. Their work also pointed out that fiber size and timing was critical to the resulting aligned material, with success occurring in instances when the time for sol gel transition was quicker than the time for Brownian motion to restore random order, and these time scales are greatly determined by the fiber length. Mittal also concluded that the surface charge of filaments was not relevant to the alignment from shear flow focusing. It is clear from this great success in created aligned CNF filaments that the pre-alignment method shows far greater potential, and that the fiber structure and properties are key to establishing and maintaining alignment.

These aligned pure CNF filaments show great potential filling basic needs such as applications as an alternative textile, or even as reinforcing structures in other polymer matrices. Although there are forms of cellulose filaments currently used as textile alternatives such as Rayon, these processes cannot be considered sustainable because of the infamously dangerous and toxic synthesis causing harm to both process engineers creating the product and the environment. Numerous fatalities from mere minutes of exposure to carbon disulfide, a necessary chemical for rayon synthesis, causes massive losses in neurological function and the fatalities from this process are so great that a book about the harms of Rayon "Fake Silk: The Lethal History of Viscose Rayon" gained much attention.[35,36] The flow focusing process used for the CNF alternative textile requires mostly pure water with the only hazard being a weakly concentrated acid, making it a far more sustainable option to current cellulose textile alternatives. Beyond a basic application these nano fibers also need to fulfill other functions currently filled by petroleum-based polymers that in are included in more complex applications. One way to achieve a high multifunctionality is through the incorporation of another structure that can add to the multifunctionality of the CNF.

3.3 Expanding to Nanocellulose Composite Structures

Controlling CNF nanostructure and alignment cannot only improve mechanical performance and bolster functionality in basic applications requiring pure CNF such as textiles or pure plastics, but they will be critical in achieving more complex functionalities, such as small electronics or biomedical sensing. These complex applications will require properties that are not native to the material, but rather they can be achieved in composite forms of CNF materials.[34,37] A composite form of CNF will be a mixture of CNF and some other secondary material or chemical that possess the desired trait. Typically adding secondary materials becomes increasingly complex because both the mechanical performance of the CNF and the secondary trait need to be successfully

transferred throughout various size scales. Generally, people report a loss in CNF mechanical performance when adding secondary material structures, or to preserve CNF performance a tertiary chemistry is used that often sacrifices the desired added functionality.

3.4 Carbon Nanotubes

As previously mentioned, electrical conductivity is a key trait necessary for complex functionality and most recently this is achieved with the addition of carbon nanotubes. Carbon nanotubes are purely carbon-based materials known for their sp^2 hybridization much like graphene, but rather in a tubular morphology. These nanotubes are known to have unique properties including good chemical stability, thermal stability, mechanical performance, and electrical conductivity. Among nanotubes there are subdivisions generated based on size and chemical functionality. Single walled carbon nanotubes considered a one-dimensional material, are a single tube of graphene rolled up into a single cylinder, while multi walled carbon nanotubes are tubes consisting of multiple stacked walls of concentric rolled graphene tubes. The properties of both materials are heavily dependent on the morphology, chirality, and chemical nature, which can be determined through the growth processes or secondary treatments. Chemical functionality of nanotubes is one method of adapting nanotubes by changing the surface chemistry that can lead to additional functionalities in sensing different molecules etc.

Choosing carbon nanotubes as a composite filler will expand the possibilities of aligned CNF structures and provide yet another point of control on the final product. This filler could have implications in small electronics, in biomedical sensing, or in tissue growth amongst many other complex functionalities. There are great challenges that come when working with nanotubes especially in solutions of water like those that would be used for CNF pre-alignment techniques. Nanotubes are hydrophobic in nature, and sometimes this can be overcome with chemical

functionalization of the tube, but generally the workable mass is greatly limited. Generally harsh solvents or surfactants are required as the medium for suspension, but this would again reduce the overall sustainability and likely cause issues in the final structures.

However, the structure of CNF and the tailorable surface charge of fibers opens the possibility for nanocellulose itself to function as both a polymer matrix and a surfactant. This would maintain the sustainability and functionality of the filaments while still providing added functionality. CNF filament performance will likely be maximized with single walled nanotubes (SWNT) because the diameter more closely matches the individual CNF fibers, and the geometry of the nanotube, similar more rigid structure to CNF, presents an opportunity to align both components. Through controlling the nanostructure of the CNF and the alignment of both materials, with the application in mind, most significant losses to mechanical and secondary performance will be minimized. This reveals the key to CNF multifunctionality especially in filling complex applications lies in the control of the CNF nanostructure and the material alignment.

4.0 Summary

The future of sustainability will require alternative materials to petroleum reducing the overall global dependence. Cellulose is a promising alternative to petroleum offering a sustainable alternative source, but its success is dependent on its ability to fill a multitude of functionalities much like petroleum-based products. Currently the greatest potential for successful application is cellulose in the nano form or nanocellulose. This nanocellulose comes in many forms and most importantly its traits can be tailored through manipulation of its structure and thus properties. Aligning nanocellulose offers a further point of engineering making nanocellulose a material with multiple facets of control throughout production. These multiple points of control increase its

potential for success in both basic applications such as textiles but also in more complex applications such as small electronics, sensing, or biomedical applications.

In this work, we demonstrate the massive untapped potential of nanocellulose as a diverse sustainable material through three key objectives. Initially we demonstrate the multiple points of control available with nanocellulose production to tailor fiber aspect ratio and surface charge, giving independent control over two critical fiber properties. The individual control over these properties opens nanocellulose fibers to a wide range of applications not previously afforded by typical synthesis methods. Through these tailored properties we successfully designed a nanocellulose for high performance in a novel pre-alignment technique involving electric field and flow focusing. The electric field provides individual CNF fiber rotation and a higher degree of alignment while the flow focusing provides a quick fiber fixation establishing permanent anisotropy. We demonstrate the benefits of this alignment in the continuous filament produced with potentials in alternative textiles. Finally, we further adapt this aligned filament to fill more complex applications by introducing a conductive filler to create an aligned conductive composite filament. While most reports lose performance, through engineering the CNF nanostructure and carefully controlling the novel pre-alignment method, we demonstrate exceptional performance beyond the qualities possible with a pure CNF filament. The implications of this new conductive composite filament are demonstrated through testing it as a unique water sensor. The alignment also improves the sensitivity of fibers demonstrating success as a sensor filling a complex need. This project demonstrates the potential of multifunctional materials made with sustainable CNF offering a sustainable alternative to petroleum.

II. Materials and Methods

2.1 CNF Preparation via TEMPO Oxidation

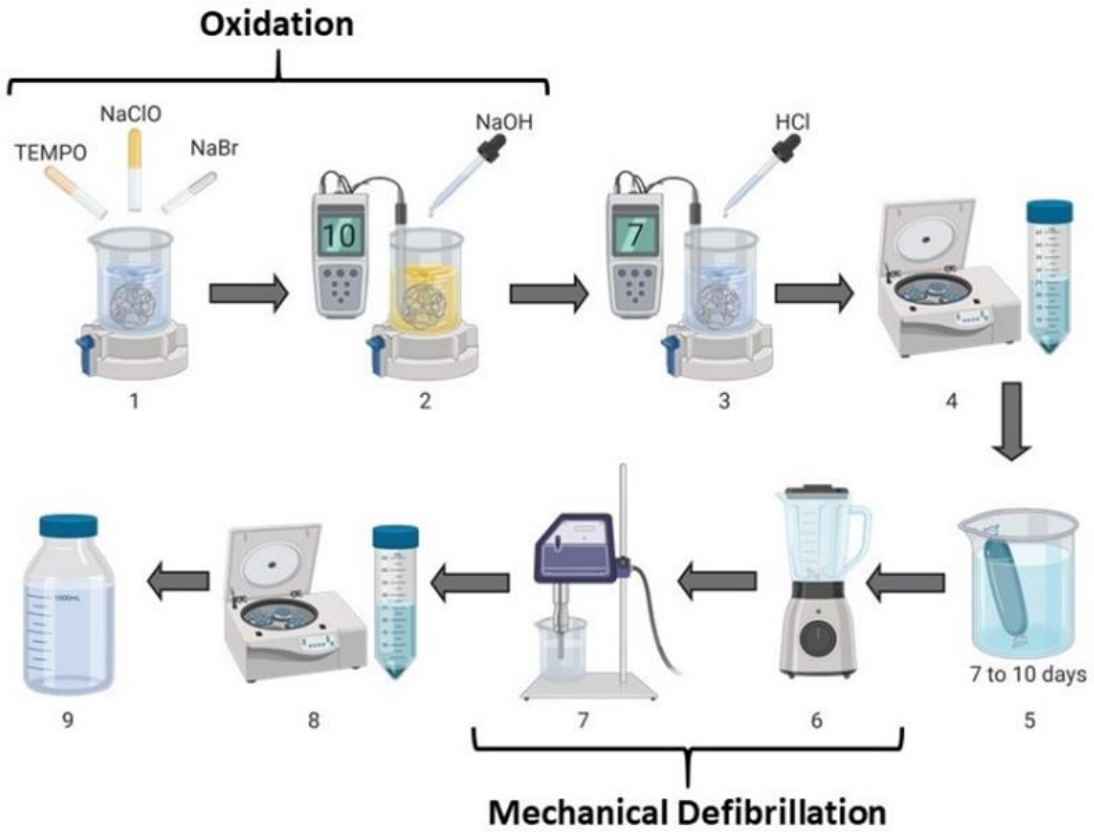

Figure 4. *Flow diagram outlining the steps required to create TEMPO oxidized CNF. Most of the steps involve purification and concentration, with two primary active steps, oxidation, and mechanical defibrillation, occurring at steps 1 through 2 and 6 through 7, respectively.*

CNFs were prepared using 2,2,6,6-Tetramethyl-1-piperidinyloxy (TEMPO) oxidation from bleached softwood pulp kindly provided by WestRock (mixture of 50/50 Doulgas fir and Hemlock).[3] Briefly, cellulose fibers were dispersed in water and mixed in a solution of TEMPO, sodium bromide, and sodium hypochlorite. After the solution was mixed, 1 M sodium hydroxide was added until the pH stabilized at 10. The pH of the solution was adjusted to 7 with 1 M HCl and then centrifuged at 5000 rpm for 15 min (Allegra 25R Centrifuge, Beckman Coulter). The

precipitate was dialyzed against deionized water for five days. The dialyzed solution was blended for 30 min (Oster, Sunbeam Products inc.) followed by horn sonication for 2 min (750 W, 100 % amplitude, Sonics Vibracell VCX). The suspension was centrifuged at 5000 rpm for 15 min and the supernatant was characterized and stored for further processing in the electric field-assisted flow focusing system.

2.2 Conductometric Titration for CNF Charge Density

Charge Density of CNF dispersions were measured using conductimetric titration to ensure that the TEMPO oxidation process changed the surface chemistry of the CNF. Briefly, 50ml of 0.1 wt % CNF dispersion and 1 ml of 0.1 M hydrochloric acid were mechanically stirred to protonate carboxylic acid groups. Then 100 ul allocates of 0.02M NaOH were added, and the conductivity measured and recorded after each addition. The volume of NaOH needed to stabilize the charge was calculated to give the concentration of carboxylic acid per gram of CNF.

2.3 CNF and SWNT Dispersions

Complex dispersions involving both CNF and SWNTs were prepared using a double sonication method. CNF solutions at 0.32 wt% were measured into 50 ml allocates and placed in a tall beaker to maximize exposure to sonic horn tip. SWNTs functionalized with carboxylic acid groups (cheaptubes.com) were massed according to the desired weight percent using equation 1. The nanotubes were slowly added to the CNF solution while vigorously stirring to ensure SWNTs were thoroughly mixed. The dispersion was then transferred into a sonic bath and the tip of a sonic horn (750 W 40 % amplitude, Sonics Vibracell VCX) was inserted as far as possible into the beaker. The 50 ml solution was double sonicated for 8 min, removed and centrifuged for 50 min at 5500 RPM. After centrifugation, the precipitate was discarded and exactly 35 ml of the supernatant was removed and stored for future use with a shelf life of one week.

$$SWNT\ wt\% = \left(\frac{Mass\ of\ SWNTs}{Mass\ of\ CNF + Mass\ of\ SWNTs}\right) \times 100 \qquad \text{(Equation 1)}$$

2.3.1 CNF and SWNT Dispersion Characterization

CNF and SWNT dispersion quality were characterized using UV-VIS spectrometry. Dispersions were prepared with constant SWNTs (63 mg) and varying CNF concentration, and vice versa using the double sonication method described above. UV-Vis measurements were performed at room temperature on dispersions diluted 30 times using a Perkin Elmer Lambda 750 spectrophotometer operating in the 250-800 range, with a 1 nm resolution.

CNF Dispersion Viscosity (Viscometer)

The viscosity of different prepared dispersion was measured using a DV2TLV viscometer from Brookfield. The viscosity for all dispersions was measured by depositing 16 ml in a beaker and inserting ULA spindle (Brookfield) with temperature maintained at 293 K.

2.3.2 CNF and SWNT Aspect Ratio

CNF fiber length and diameter were determined by measuring at least 20 individual CNFs using Atomic Force Microscopy (AFM). Samples were prepared by drop casting 10 uL of 0.00005 wt% CNF solution on freshly cleaved mica discs (TedPella Inc., 12mm) and air dried for 2 hours prior to imaging. The AFM was used in tapping mode with a bluedrive photothermal excitation and a scan rate of 1 Hz (Asylum Research, Cypher).

CNF and SWNT Compound Structure Characterization

CNF and SWNT dispersions at 0.005 wt% were bath sonicated for 5 min and drop casted on a copper TEM grid within 30 minutes of bath sonication. Images were taken on a Tecnai G2 F20 SuperTwin TEM with a 200 kV accelerating voltage. Chemical confirmation of the compound CNF and SWNT structure was verified using photo induced force microscopy (PiFM). Samples

were prepared by drop casting 10 µL of 0.0005 wt % dispersions on freshly cleaved mica slides. PiFM images were taken using a VistaScope from Molecular Vista Inc. couple to a LaserTune LT-OEM with a range from 750-1877 cm^{-1}. The microscope was operated in tapping mode with a µmasch NCH-Pt 300kHz noncontact cantilever from Nanosensors.

2.3.3 CNF and SWNT Bonding

Fourier transform infrared (FTIR) was used to elucidate chemical interactions between CNF and SWNT in a solid state. Films of varying CNF/SWNT dispersions were created by oven drying 15 ml of solution at 50℃. Spectra were collected from 1100 to 3500 cm^{-1} using a Shimadzu FTIR spectrophotometer with a resolution of 1 cm^{-1} in attenuated total reflectance (ATR) mode.

2.4 Filament Formation (Electric Field Flow Focusing Channel) and Characterization

The microfluidic channel consisted of a 1 x 1 mm^2 primary flow channel and two secondary flow channels, all controlled by 5 syringe pumps (**Figure S4**). The primary downward flow (red) of CNF, at the top of the channel, was approximately 0.3 wt % and flowed at a rate of 2.4 ml/ hr. As the CNF moved down the channel, just before the introduction of the first extensional flow, there were four electrodes made of copper. All the electrodes were 4 mm in diameter and 14mm apart from each other (measured center to center) with one side in direct contact with the CNF flow. The electrodes were supplied an AC sinusoidal voltage from a function generator and then amplified using a high voltage amplifier. The downward flow continued for approximately 5 mm past the last electrode (measured at center) and then encountered the first shear extensional flow, comprised of DI water (Blue) flowing at a rate of 6 ml/hr. Approximately 3 mm after the first extensional flow, the CNF reached the second extensional flow of 1 M hydrochloric acid flowing at a rate of 3.6 ml/hr. The compound flows continued downward until they were ejected into a beaker of DI water. The gelled filaments were then removed and dried under tension in controlled

humidity and temperature. To collect polarized optical data and deduce the degree of fibril alignment, images were taken though a pair of crossed polarized filters with a CCD camera (Mako U-029B). The light source was a He-Ne laser (130 mW) with a 5 mm radius irradiating circle.

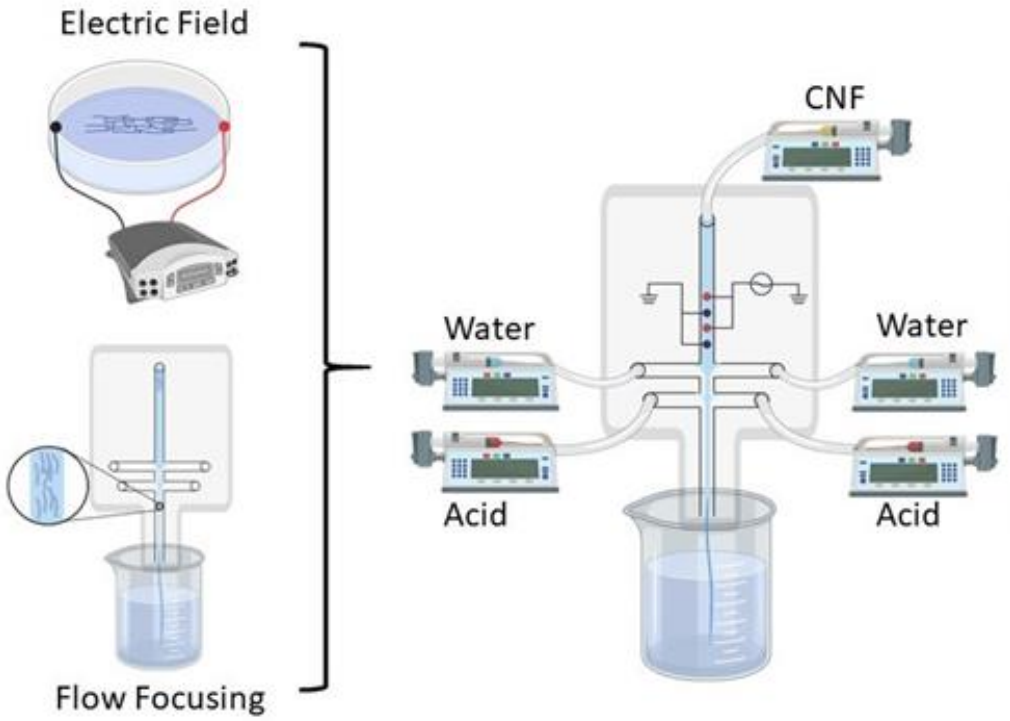

Figure 5*. Depiction of combining two common alignment methods, electric field and flow focusing, into a novel combination electric field flow focusing channel on the right. The continuous electric field flow focusing channel is composed of 4 electrodes and is operated by a total of 5 syringe pumps resulting in an aligned filament hydrogel that is deposited into a beaker of water.*

2.4.1 Filament Surface Characterization

Each pure CNF filaments surface, morphology and uniformity were characterized using Scanning Electron Microscopy (SEM, XL830, FEI Company, Hillsboro, OR, USA). The filaments were mounted using carbon tape and prepared by sputter coating with a gold/palladium target for 30 seconds at a deposition rate of 13 nm per minute. The SEM was operated using a 5 kV

accelerating voltage and 5 mm working distance. The following equation was used in tandem with SEM image analysis to assess filament degree of orientation and alignment at the micro scale. FWHM refers to the fullwidth half maximum of fitted peaks created through histograms or plotted intensities measured using 2D XRD, or SEM image analysis.

$$f_c = \frac{(180 - FWHM)}{180} \qquad \text{(Equation 2)}$$

Composite CNF and SWNT filaments were imaged on a ThermoFisher Scientific Apreo SEM equipped with a standard ETD in chamber SE Detector, a back scatter electron detector (BSE), and an in- column SE detector. Filaments were mounted on carbon tape and left uncoated so observe surface and subsurface topography. Different detectors were used to examine different filament qualities, in general surface images were taken using the in-chamber ETD detector at a 2kV accelerating voltage and subsurface images were taken using the in- column SE detector with a 20 kV accelerating voltage. Filament cross sections used a combination of detectors operating at 2kV to capture high contrast and clarity.

2.4.2 Filament Alignment and Chemical Characterization

2D X-ray Diffraction was used to characterize the crystallinity index of CNF and nano scale orientation of crystalline regions for individual CNF filaments. Samples were mounted directly on a silicon dioxide wafer and a Bruker D8 powder diffractometer was used with a high-efficiency Cu anode microfocus X-ray source and a Pilatus 100K large-area 2D-detector. The beam was generated at 50 kV and 1000 μA and adjusted to 0.10 mm spot using a beam collimator. For crystallinity index diffractograms were taken from 10 ° to 90 ° with 11 ° increments and a 30 s exposure time per increment. Crystallinity Index (CI) was calculated using the Segal method described in Equation 3, where I_t is the Intensity of the crystalline peak at 2θ = 22.7 ° and I_a is the Intensity of the amorphous peak (110) at 2θ = 18.1 ° (Segal, Nam). For alignment measurements

the x-ray source and 2D detector were kept at the 2θ = 18 °, with an 11 ° increment and had a total exposure time of 150 s.

$$Crystallinity\ Index = \frac{I_t - I_a}{I_t} \quad \text{(Equation 1)}$$

A Renishaw InVia Raman Microscope (Leica DMIRBE inverted optical microscope) with a 785 nm laser excitation source was used to asses overall alignment of a control and treatment filaments as well as chemical alterations from the electric field. The Raman laser spot size was 20 μm focused on a single filament, using a short working distance (x50) lens. The filament was manually rotated 90 degrees to capture both the direction corresponding to the parallel and perpendicular direction of the primary flow, and asses the anisotropy of the material.

2.4.3 Filament Mechanical Properties

Both pure CNF filaments and composite CNF/SWNT filaments underwent the same mounting and mechanical testing procedures. Once the filament was formed in the channel it was removed from a beaker of DI water and suspended between to aluminum posts for drying. Once the filaments dried, they were adhered to a 1 inch piece of paper with a 30 mm hole cut in the center. The suspended filaments were then dried in an oven for 30 min to achieve 0 % humidity or stored in a humidity chamber overnight to reach 35 % humidity. After establishing the humidity of filaments, the paper mounts were loaded into a tensile rack and the sides of the paper cut to leave tension on the filament alone. The filaments were tested on a Shimadzu EZ-SX tester at 0.5 mm/min equipped with a 1 N load cell. The cross section was assumed to be circular, and the diameter determined by scanning electron microscopy (SEM). At least 20 filaments were tested for each data point, to ensure statistical significance.

CNF/SWNT Electrical Properties (Keithley and Electrodes)

Filaments were cut to 15 mm and adhered to a glass microscope slide with electrical leads that were established by adhering flat nickel chromium wire to the filament ends using silver adhesive paste. Super glue was used to further secure extensions of nickel chromium wire to the microscope slide and prevent electrode from detaching. The electrical conductivities of conductive composite filaments were measured by a voltage–current meter (Keithley 2400) using a two-probe method.

2.5 CNF/SWNT In-Situ Swelling

The conductive filaments mounted on a glass slide were placed on a light microscope (Zeiss Axiolab) equipped with a Zeiss Axiocam ERc5s digital camera. The filament once in focus with a 10x microscope objective was attached to a voltage-current meter (Keithley 2400) using a two-probe method. Then while a 1μL drop of water was placed on the filament, bandicam software was used to record active changes in filament diameter, in tandem with Realtime resistance changes from the voltage-current meter. Kinovea software was used to extract frames at 0.7s intervals and Image J software was used to measure filament diameters. These changes in filament diameter were paired with the resistance changes over time to extract in-situ swelling and resistance measurements.

III Results and Discussion

1.0 Chapter 1: Controlling Nanocellulose Structure

1.1 Synopsis

Objective: Establish control over nanocellulose properties and structure to produce idyllic characteristics for specialized applications.

Characterization Techniques:

- Conductimetric Titration to determine Charge Density
- AFM for nanocellulose fiber aspect ratio

Conclusions:

- Aspect ratio and surface charge are critical characteristics to establish anisotropy of synthesized macro materials.
- Chemi-mechanical synthesis methods increase economic and social sustainability of CNF production through reduce energy costs, and improved safety.
- TEMPO oxidation allows for independent control of CNF surface charge and fiber aspect ratio through two primary steps, surface oxidation and mechanical defibrillation.
- Surface Charge can be tailored between 0.3- 1.2 mmol COOH/g CNF by controlling oxidation time, reaching up to 0.75 mmol COOH/g CNF and sodium hypochlorite concentration, reaching up to 1.2 mmol COOH/G CNF.
- Primary oxidation step determines starting microfiber size and breaks fibers for the subsequent mechanical defibrillation.
- Mechanical defibrillation time and intensity can directly control nanofiber aspect ratio, with harsher treatments resulting in smaller fibers.

1.2 Introduction

Cellulose is one of the most abundant biopolymers on earth and is considered environmentally sustainable because of its natural abundance, biocompatibility, and biodegradability. Manipulating cellulose to fill basic and complex functions commonly filled by petroleum products would greatly improve global material sustainability.[38] While translating a standing tree into a textile or small electronic seems challenging, breaking down the cellulose into a manageable nano from presents a clear path forward. The nano form of cellulose maintains the sustainability component because of the similar chemical makeup and includes unique properties that could fulfill the more complex requirements of some petroleum-based products such as microchips. The successful application of CNF will require biomimicry of the multiscale alignment exhibited in standing biomass which has been most successfully achieved in pre-alignment techniques. These pre-alignment techniques as previously outlined are largely dependent on critical fiber structural elements such as fiber length and surface charge which allow the fibers to be easily manipulated in a suspension. These traits need to be engineered to improve the resulting CNF filaments performance and allow adaptability for the future incorporation of composite fillers.

There are primarily three different types of nanocellulose, and they are generally classified by the synthesis method and resulting material properties. The three methods can be divided into a top-down approach, referring to the breakdown of a large cellulosic material into smaller nano sized chains, and a bottom-up synthesis, that involves putting glucose monomers together to form nano sized chains. The bottom-up synthesis involves bacterial propagation of monomeric glucose into polymers and is generally considered not scalable and costly because of challenges in limited production and bacteria growth.[39] The top-down synthesis methods can further be classified into three groups mechanical, chemical, and a of combination chemical and mechanical that we will

call “chemi-mechanical”.[40,41] Mechanical synthesis involves high shear rates or large amount of mechanical agitation to mechanically break fibers down to the required nano size. This method has high energy requirements lacking economic sustainability and generates a rather wide fiber size distribution ultimately sacrifice mechanical performance.[42] The mechanical fibers also lack a sustained surface charge meaning fibers are generally exist as a precipitate in solution and thus will not be compatible with most pre-alignment techniques. The chemical synthesis often involves high temperature and concentrated hazardous chemicals to reach the desired fiber size, lacking both economic and social sustainability.[43,44] The chemical methods can create surface charges on the ends of fibers, but the harsh treatment often shortens fibers down to the crystalline size around 200 nm and thus any established anisotropy would be quickly lost to Brownian motion resulting in a randomly oriented CNF structure that would likely require a secondary polymer to be held together. The chemi-mechanical option combines both chemical and mechanical treatments making it the most economic and socially sustainable way to achieve an environmentally sustainable alternative material. Minimal harsh chemical exposure establishes a more socially sustainable option and the already chemically fractured cellulose is estimated to lower energy costs of mechanical treatment from 20,000 to 30,000 kWh/ton to 1000 kWh/ton of cellulosic fibers establishing environmental and economic sustainability.[45] In addition the chemistry involved in chemi-mechanical synthesis creates fibers with a suspended charge create a suspension of nanocellulose that flows easily and generally fibers are longer that those made with a purely chemical treatment. While chemi-mechanical treatments offer the most promise, the properties of the material need to be tailorable to its future performance in pre-alignment techniques and to further increase the viability as a multifunctional sustainable alternative.

We sought to control different nanostructure traits of CNF fibers using a known chemi-mechanical form of synthesis, to demonstrate their potential as a multifunctional sustainable material filling both basic and complex functions.[46] Both aspect ratio and charge density of nanomaterials will be critical to their manipulation in pre-alignment processes. Controlling critical traits such as aspect ratio, and fiber charge at the time of synthesis can be key to dispersion performance and alignment transferring desirable nano traits to the micro and macro level. Here we demonstrate detailed knowledge of a chemi-mechanical CNF synthesis method, TEMPO oxidation, and establish independent control over both aspect ratio and fiber charge using two key steps. This synthesis offers individual control over two critical properties and creates a sustainable material that can be easily engineered to achieve ideal mechanical and chemical performance targeted to countless applications including pre-alignment processes.

1.3 Nanocellulose TEMPO Oxidation

Chemi-mechanical TEMPO oxidation involves multiple steps that can be broken down into two active steps, a chemical and mechanical phase, with intermediate washing and concentrating throughout the process (**Figure 6**). The two primary stages are the chemical or oxidation step and the mechanical or cellulose defibrillation step. These two steps can be thought of as largely independent of each other with the oxidation controlling the CNF charge, and mechanical defibrillation controlling the CNF aspect ratio. Control over the CNF charge is critical to CNF dispersion quality and future chemical functionalization that could directly benefit the application.[47,48] Aspect ratio of CNF can be critical to the mechanical performance and individual fiber manipulation during macro material synthesis. These two characteristics will be critical to our demonstrated applications of the CNF in an alternative textile and conductive composite sensor.

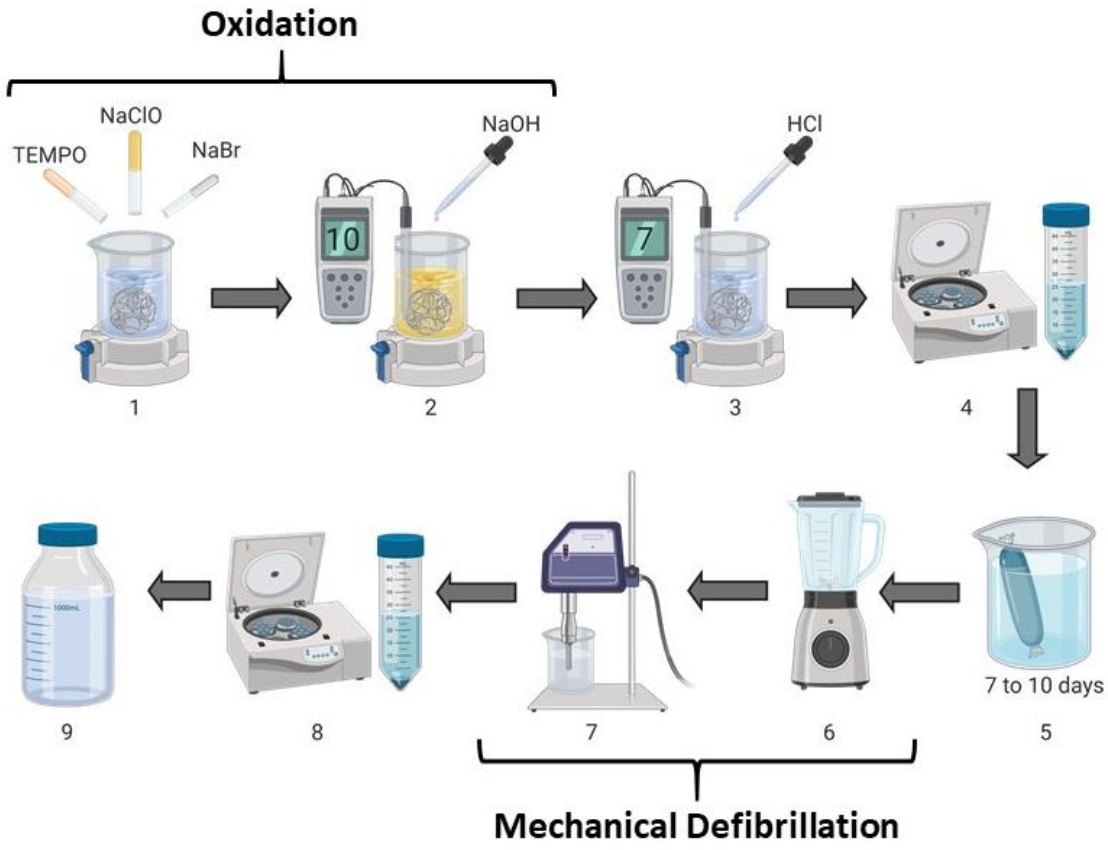

Figure 6*. Depiction of the full 9 step TEMPO Oxidation process for CNF production. Steps 1-2 involve a critical oxidation step followed by three purification steps that entail neutralization (step 3), concentration (step 4) and dialysis (step 5). Then the primary mechanical defibrillation to control the fiber aspect ratio (step 6 and 7) followed by one more purification step to reach the final solution of dispersed nanocellulose fibers shown in step 9.*

TEMPO Oxidation is a common method of oxidizing cellulose or pulp, and the nomenclature results from the reaction path that involves 2,2,6,6-Tetramethyl-1-piperidinyloxy (TEMPO). There are many different variations of TEMPO oxidized CNF, and the reactions typically include TEMPO and Sodium Hypochlorite ($NaClO^-$) as an activating agent to produce $TEMPO^+$.[49] This active version of TEMPO very selectively reacts primary alcohols to aldehydes and together with cellulose this gives a selective reaction of the C6 hydroxyl group on glucose units to an aldehyde

(**Figure 7**). These two critical chemicals are typically accompanied by a third chemical that serves to both recycle the TEMPO for continued use and further react the C6 aldehyde to a carboxylic acid group.[49] Examples of this third chemical can include additional Sodium Hypochlorite or in our case Sodium Bromide (NaBr).[13] TEMPO oxidation is primarily a surface reaction and only readily available C6 hydroxyl groups will be targeted. The hydroxyl to aldehyde and subsequent aldehyde to carboxylic acid are thought to

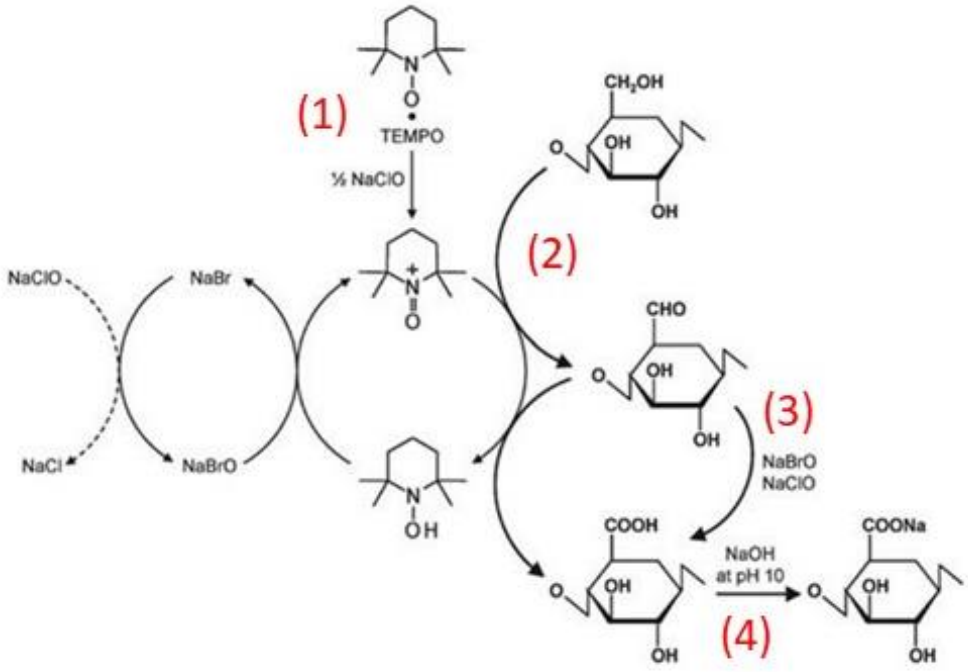

Figure 7*. TEMPO oxidation chemical process depicted using chemical structures. Step 1 involves the activation of TEMPO using sodium hypochlorite followed by step 2 the reaction of the C6 hydroxyl on a glucose monomer to form an aldehyde. Step 3 involves the hydration of the aldehyde and subsequent reaction to form a carboxylic acid, that is finally capped with a sodium under basic conditions.* [13]

1.3 Controlling Surface Charge of CNF

Figure 6 is a graphical depiction of the method of TEMPO oxidation we used involving TEMPO, Sodium Hypochlorite and Sodium Bromide. Once these chemicals are physically added to a solution of mixing bleached pulp the pH is maintained at 10 to encourage the continual oxidation of pulp fibers.

Individual control over the surface charge was confirmed by isolating different parts of TEMPO oxidized CNF process and measuring the surface charge to elucidate which step was responsible for the charge. Surface charge was determined using a conductometric titration that begins with adding an excess of acid to protonate weak carboxylic acid groups. The conductivity of the solution is then recorded while a dilute solution of sodium hydroxide is added, that serves to cap carboxylic acid groups with a sodium. The conductivity of the solution will initially drop as the sodium hydroxide will more readily neutralize excess ions from acid until a plateau is reached, during which time the sodium hydroxide is neutralizing the weak acid groups. Once the weak acid groups are consumed sodium hydroxide exists in excess and the ions will increase the conductivity of the solution linearly. The volume of sodium hydroxide consumed during the plateau can then be directly related to the number of carboxylic acid groups present. It is worth mentioning that other aldehyde groups likely exist from the TEMPO reaction but this conductimetric measures only the carboxylic acid units. Pure bleached pulp, the starting material for the TEMPO process, and pulp that only underwent the mechanical defibrillation or steps 6 and 7 showed no plateau in conductimetric titrations indicating the fibers had no method of consuming the added sodium hydroxide and thus no surface charge **Figure 8**. Fully oxidized TEMPO CNF showed an obvious plateau indicating a consumption of approximately 1.5 ml of sodium hydroxide by weak carboxylic acid groups.[49] This demonstrated that the surface charge is solely controlled by the

chemical oxidation, indicating that controlling reaction qualities of these first two oxidation steps, would allow us to control the surface charge independent of aspect ratio.

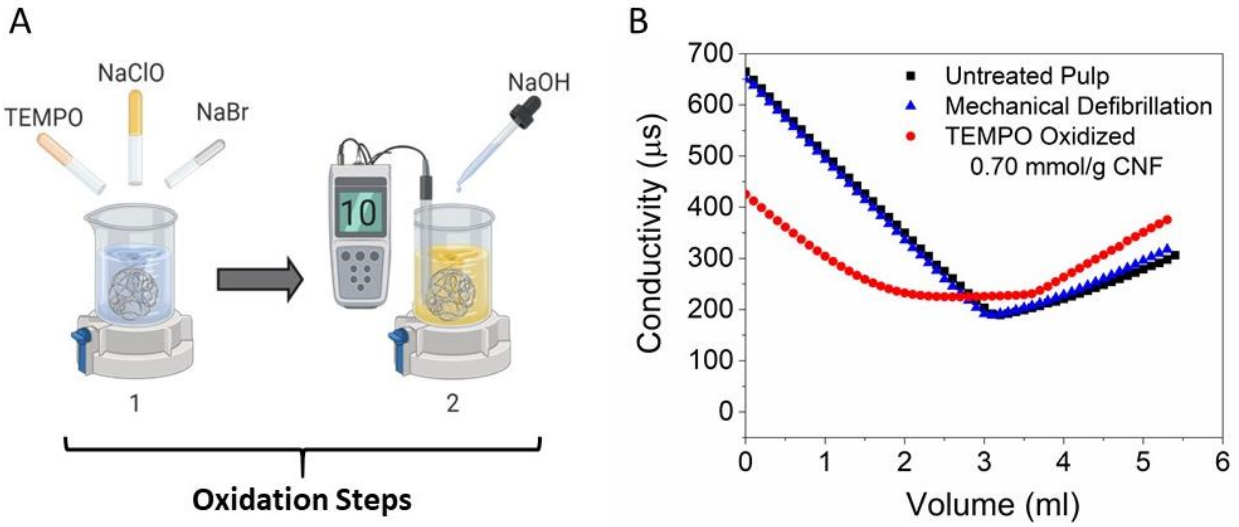

***Figure 8**. **(A)** Diagram of oxidation steps from the 9 step TEMPO oxidation process to produce CNF. The first step involves adding the three primary oxidizing chemicals and the second involves maintaining the pH at 10 with sodium hydroxide until the pH is stable and the color changes from yellow to clear. **(B)** Graphical conductimetric titration measurements of different types of CNF or cellulose demonstrating that the oxidation step is key to establishing CNF surface charge.*

The first method of controlling the surface charge is through controlling the oxidation time through manipulating the pH. During oxidation, the pH is maintained at 10 to encourage the reaction forward, and when the pH no longer drops from 10 the reaction is considered complete with the maximum surface charge achieved. When solutions were neutralized with a low concentration of acid (HCl) before completion the low pH caused oxidation to stop resulting in fewer functional groups. We manipulated the oxidation time using the pH (**Figure 9**) and found that longer oxidation times increased the surface charge up to 0.75 mmol COOH/g CNF with minimal changes occurring after 1 hour. Visual observation of CNF solutions with shorter

oxidation times such as 5 or 30 min revealed much larger fibers before mechanical defibrillation treatments. The shorter exposure time to harsh exfoliating chemicals such as sodium hypochlorite likely resulted in reduced chemical breaking or peeling.[50] The consistent aspect ratio (~ 700 nm length and ~ 2 nm fiber diameter) was achieved at each oxidation time in **Figure 9** by increasing the mechanical defibrillation intensities and time resulting in shorter fibers. This increased mechanical defibrillation also resulted in wider distributions of fiber lengths when compared to the 3-hour oxidation time. This is likely because the starting fiber size before mechanical treatment was larger with a wider distribution. A tailorable surface charge was successfully achieved through controlled oxidation time, but the charge density was still limited by the number of available groups on the pulp, because TEMPO oxidation is primarily a surface reaction. In order to further increase the surface charge to some of the highest reported in literature we examined other routes to control surface charge.

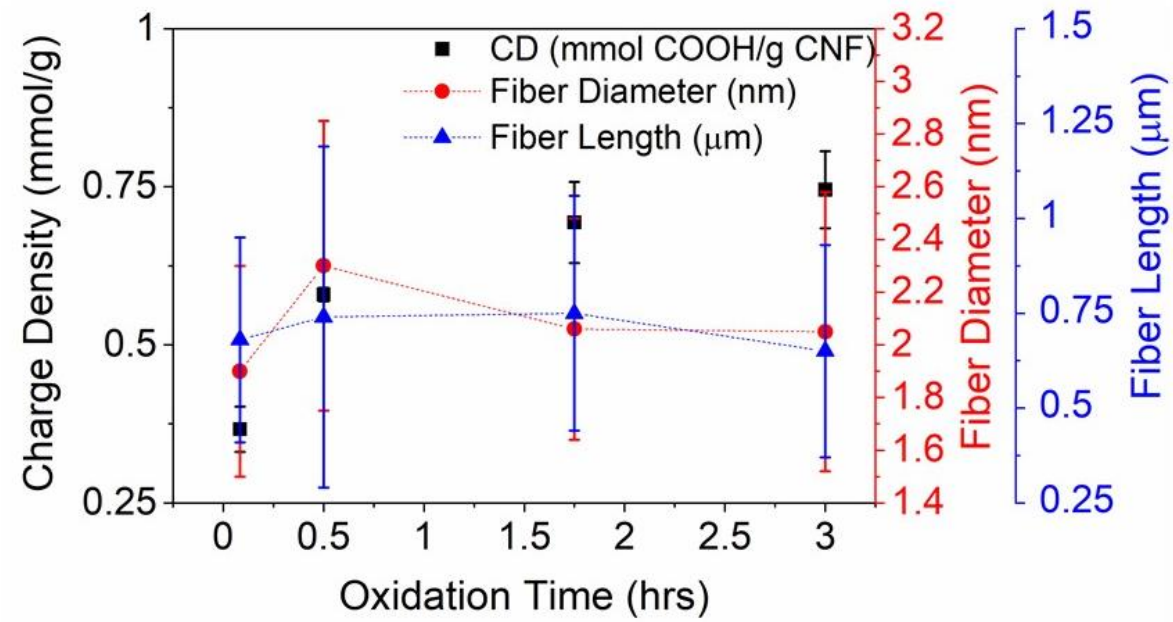

Figure 9*. Graph depicting independent control over the charge density of CNF fibers through controlling the oxidation time. The charge density increases with oxidation time plateauing around*

1 hour. Fibers at lower oxidation times were larger and visible to the naked eye but the fiber aspect ratio was maintained with additional mechanical treatment and wider distributions were observed at lower oxidation times.

The second method we discovered to control surface charge involves tailoring the exposed surface area thereby increasing the amount of primary hydroxyl groups that are available for functionalization into aldehydes.[13] We controlled the exposed surface hydroxyl groups by adjusting the ratio of sodium hypochlorite to cellulose, thus regulating the β elimination responsible for chemically breaking cellulose chains.[51] Typical concentrations reported in the literature are 5 mmol/ g of pulp but by increasing this ratio by double or even quadruple we can increase chemical exfoliation. This exfoliation allowed us to encourage or discourage the access of TEMPO to more crystalline and difficult to reach locations, allowing us to achieve a higher charge density than possible with controlled oxidation times.[52] Doubling the sodium hypochlorite from the typical 15 mmol/3 gram batch of pulp increased the overall charge density with minor decreases in CNF yield (**Figure 10**). This demonstrates charge densities between 0.70-1.2 mmol COOH/g CNF can be targeted by increasing the ratio of sodium hypochlorite to pulp, giving control over not just the lower range charge densities achieved with oxidation time but the higher ranges as well. However, increasing the sodium hypochlorite concentration further to 30 mmol/3g batch of pulp came with a greater cost to the overall fiber yield suggesting that the benefit of high charge should be carefully weighed against yield. Quadrupling the sodium hypochlorite revealed an overall lower measured carboxylic acid charge density and a significant decrease in yield indicating a maximum surface charge.[53] This decrease in charge and yield with quadruple the Sodium Hypochlorite concentration is likely a result of continual CNF degradation into small monomeric products such as tartaric acids ultimately lowering the yield and charge.[54,55]

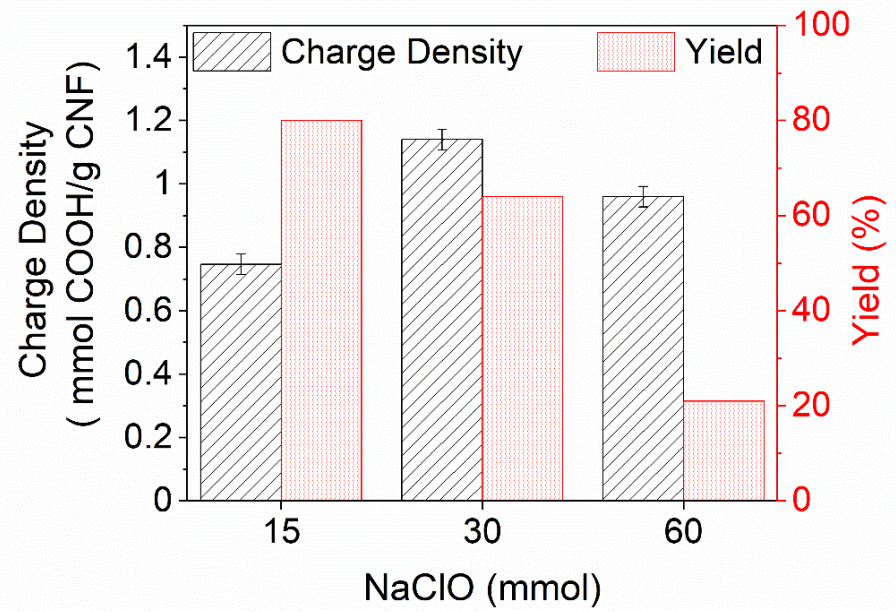

Figure 10. *Graph demonstrating the effect of sodium hypochlorite concentration on yield and charge density. Higher charge densities were achieved than possible with simply controlling oxidation time. However, quadrupling the concentration from typical quantities can lead to over processing creating degradation products lowering the overall measurable carboxylic units and yield.*

This increased fiber breaking is also supported when examining the fiber aspect ratios with increased sodium hypochlorite concentration. While excess fiber lengths from shorter oxidation times required additional mechanical defibrillation, doubling the sodium hypochlorite significantly decreased the over fiber length to 150 nm (**Figure 11**).[13] This is likely to due to the increased β elimination shortening fiber length during oxidation, causing a shorter fiber size feeding into the mechanical defibrillation. Shorter mechanical defibrillation times can be used to retain fiber length after oxidation, to compensate for the increased chemical breaking.

Both controlling oxidation time and sodium hypochlorite concentration are effective for tailoring surface charge and can primarily be done independent of fiber aspect ratio giving charge

densities between 0.3 – 1.2 mmol COOH/g CNF. Controlling oxidation time is ideal for achieving lower charge densities, while increasing the sodium hypochlorite concentration is ideal for achieving higher charge densities above 0.75 mmol/g CNF. These controlled surface charges will aid in creating free flowing suspensions for pre-alignment methods or controlling charge to maximize CNF's secondary performance as a surfactant for composite fillers. Pre-alignment techniques will also require careful control over the individual fiber length.

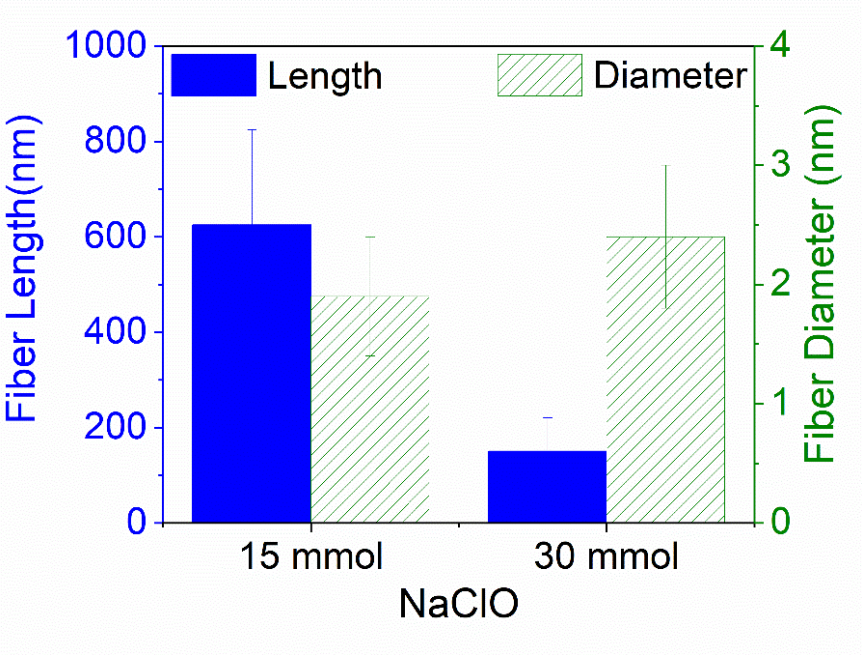

Figure 11. *Graph displaying the effect of sodium hypochlorite concentration on Fiber length and Fiber diameter. Higher concentrations of sodium hypochlorite show a shorter resulting length when undergoing the same mechanical treatment supporting the idea of increased fiber breaking.*

1.4 Tailoring Aspect Ratio of CNF

The fiber length can primarily be controlled through steps 6 and 7 otherwise known at the mechanical defibrillation stage. The mechanical defibrillation step is typically done after the chemical oxidation because the oxidation can reduce the starting fiber size and reduce the amount

of mechanical treatment necessary to reach the nano scale because of chemical treatment. Typical mechanical treatments involve blending the oxidized cellulose for approximately 30 minutes followed by a ~ 2-minute horn sonication to further cut the fibers to the nano scale while maintaining a narrow distribution (**Figure 12**).

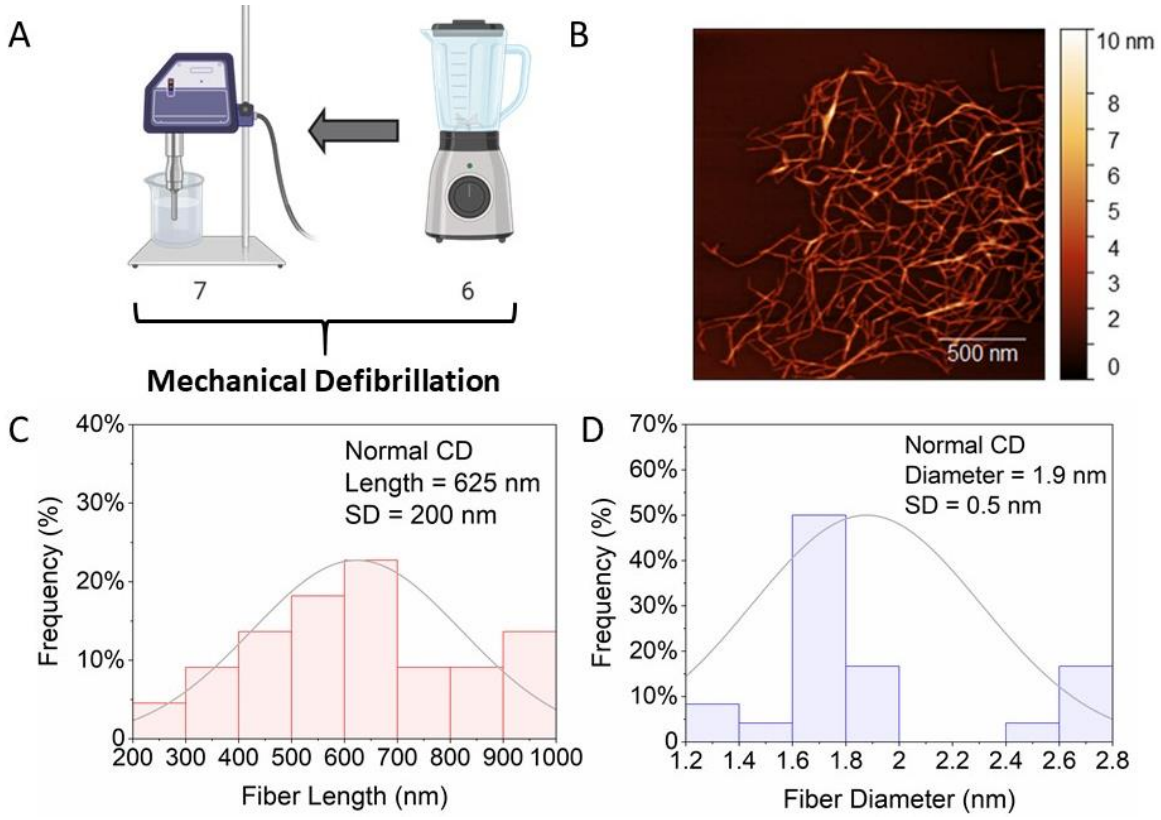

Figure 12. ***A)*** *Diagram highlighting the mechanical defibrillation step from the full 9 step TEMPO oxidation process.* ***(B)*** *AFM image of nanocellulose fibers depicting typical lengths and diameters.* (**C**) *Histogram demonstrating normal fiber length distribution of typically oxidized and mechanically treated CNF.* ***(D)*** *Histogram of CNF fiber diameters that underwent typical oxidation and mechanical treatment as outlined in the materials and methods.*

However, typically whatever the treatment type it will only reduce fiber dimensions further making the maximum attainable fiber aspect ratio the resulting size from the oxidation step.[56]

Double the charge density as mentioned before decreases the fiber size from chemical breaking so undergoing the same mechanical treatment creates a shorter aspect ratio compared to batches prepared with typical charge densities, but still maintain a narrow and normal distribution (**Figure 13**).

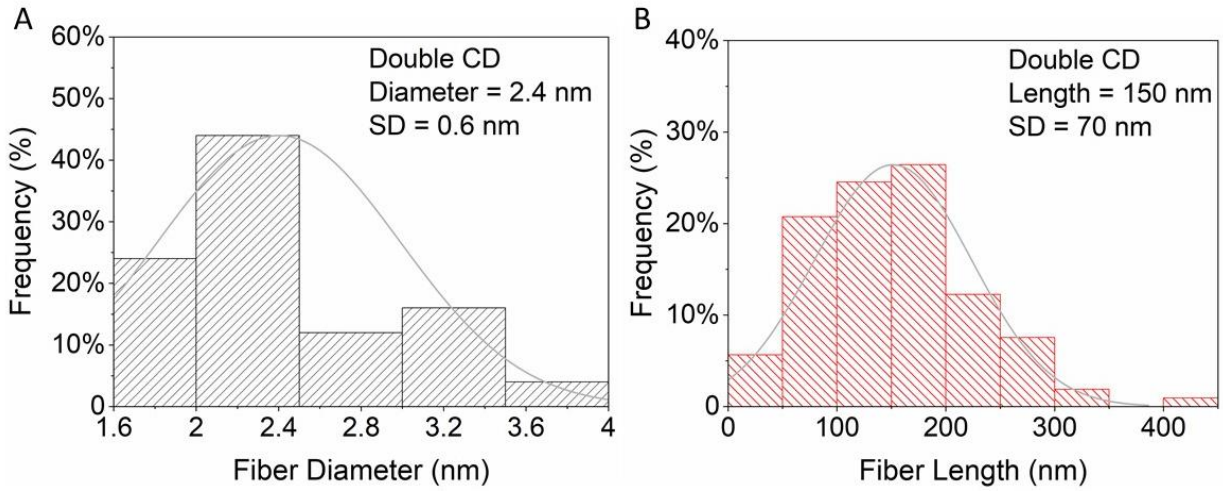

Figure 13*. Nanocellulose prepared with double the amount of typical sodium hypochlorite (10mmol/g CNF) and the same mechanical treatment as typical CNF batches.* ***(A)*** *Histogram showing the normal distribution of the fiber diameter with an average of 2.4 nm.* ***(B)*** *Histogram showing a shorter fiber length and a normal distribution with an average of 150 nm although the same mechanical treatment was used.*

While minimally dependent on the oxidation step, this phase still has independent control over aspect ratio because fibers resulting from the oxidation are generally still in the macro and micro scale, and clearly visible to the naked eye. Since fibers from the oxidation step are not yet on the nano scale mechanical defibrillation is still the major determining factor of fiber aspect ratio. Lower oxidation times give longer fibers but increasing the horn sonication time by 8 or 10 minutes, in addition to the typical two minutes, we can decrease fiber length to approximately 300

nm (**Figure 14**). Even shorter fiber lengths can be achieved with longer sonication times while still maintaining a normal distribution and consistent fiber diameter. Alternatively, higher concentrations of sodium hypochlorite result in high charge densities but a shorter fiber length, yet this length can still be maintained by decreasing the typical 2-minute sonication or 30-minute blending time. Ultimately fiber length can be controlled independent of charge density through mechanical defibrillation times and intensity, but it should be conducted after oxidation.

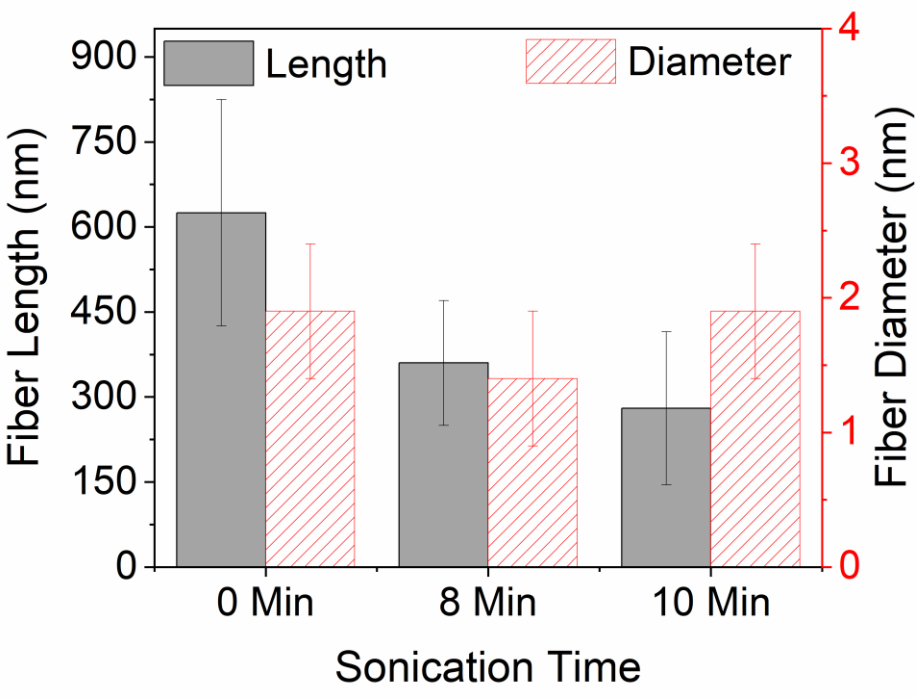

Figure 14*. Graph comparing average fiber lengths and diameters of CNF with additional mechanical defibrillation. Increasing the sonication time causes significant reductions in fiber length but no in fiber diameter.*

1.5 Conclusion

Controlling CNF charge density and aspect ratio are critical to its successful application in pre-alignment processes and as a multifunctional alternative sustainable material. These two critical qualities determine the dispersion quality and dictate the formation and response of the

fibers to externally applied forces to establish alignment. The fiber length and surface charge are also critical to transferring desirable properties from the nano to the micro and macro scale because the length can dictate the number of defects or fiber junctions while the charge can affect inter fiber bonding. Chemi-mechanical techniques of producing CNF are ideal because of the environmental and economical sustainable benefits it offers in addition to the necessary surface charge and fiber length it offers that are critical qualities needed in pre-alignment methods. The TEMPO oxidation, a form of chemi-mechanical synthesis, is ideal for CNF nanostructure control because both surface charge and aspect ratio can be controlled independently. Surface charge can be controlled from approximately 0.35-1.2 mmol COOH/g CNF by tailoring the oxidation time or sodium hypochlorite concentration. Oxidation time can be used to achieve lower surface charges while increasing sodium hypochlorite concentration can obtain higher charges with minimal loss in yield. Although oxidation can dictate the starting macro fiber size, mechanical defibrillation is the primary method of controlling the nano level aspect ratio. Nanofiber length can be decreased by increasing time and severity of mechanical defibrillation. Controlling these properties individually allows a variety of fiber size and surface charge combinations making it possible to optimize the nanostructure to pre-alignment processes and other diverse applications.

2.0 Chapter 2: Field-Assisted Alignment of Cellulose Nanofibrils in a Continuous Flow-Focusing System

2.1 Synopsis

Objective: Align nanocellulose using novel electric field flow focusing system to produce filament with improved mechanical properties.

Characterization Techniques:

- AFM
- Conductimetric Titration to determine Charge Density
- 2D XRD: Crystallinity via the Segal Method and Individual Nanofiber Alignment
- Electric Field Flow Focusing Channel for Filament Production
- SEM paired with Image J Directionality Software
- Micro-Raman
- Tensile Testing

Conclusions:

- CNF charge density and fiber length nanostructure were tailored to quickly establish and maintain anisotropy in a novel electric field flow focusing pre-alignment technique
- AC external field is significant beyond a threshold voltage (600 V) enhancing the CNF orientation factor up to 16 %
- Electric field significantly contributes to improve the CNF ordering in the bulk, through individual fiber polarization, while the CNF alignment on the filament surface is only slightly affected
- 2D X-ray diffraction shows that CNFs are densely packed anisotropically in the plane parallel to the filament axis without any preferential out of plane orientation

- The improved nano scale ordering combined with the tight CNF packing yield impressive enhancements in mechanical properties, with stiffness up to 25 GPa and more than 63 %, 46 % and 120 % increase in tensile strength, strain-to-failure and toughness, respectively.
- This study demonstrates for the first time the control over the structural ordering of anisotropic nanoparticles in a dynamic system using an electric field

2.2 Introduction

Cellulose nanofibrils (CNFs) are a class of earth-abundant bio-based and biocompatible materials with attractive properties such as lightweight, thermal stability, and good strength.[8] When assembled into macroscale materials, the mechanical and dielectric performance of the resulting components is strongly influenced by the CNF orientation in these systems.[57] The development of highly-ordered structures comprising cellulose-based nanomaterials with high aspect ratio has recently spurred great interest.[15] In this context, multiple techniques for controlling the collective alignment of colloidal nanocellulose have been explored and can be divided into two categories depending on what type of external forces are used to impose alignment. Typical external forces involve mechanical rubbing,[58,18,59,60] electric fields,[21,22,23] magnetic fields,[25,26,61] and liquid shear flow,[62,30,63,64,65] while the tendency of certain particles to self-assemble into ordered structures can be exploited in some cases without the need for external forces.[66] Although electromagnetic applications have been widely used to align various elongated nanoparticles,[67,68,69] including cellulose nanocrystals,[22,70,71,72] studies focusing on nanofibrillated cellulose remain relatively scarce.[73,74] Among these methods, only the use of AC electric field appears to be versatile enough for practical implementation. This is because the low magnetic susceptibility of cellulose requires unrealistically strong magnetic fields,[75] while the negative charges of CNF tend to generate aggregates at the anode when DC electric fields are applied.[76] When exposed to AC electric field, individual CNFs rotate and align along the field direction if their movement is not restricted by the surrounding environment.[73] This is attributed to the anisotropic nature of the material, which ensures that the dipole moment in the direction parallel to the CNF main axis is stronger than the one in the perpendicular direction. After rotation, inter-fibril interactions take place to form cellulosic chains parallel to the electric field lines, which become thicker and longer

as the electric field is applied for longer period of time. Some reports examined how the parameters of the applied electric field (*i.e.* amplitude, duration…) influence the orientation of CNFs in various solutions,[73,74] while other researchers used a combination of shear forces and electric field to improve nanocellulose alignment.[77] However, all these studies are limited to the preparation of thin films in batch experiments. To the best of our knowledge, there is no report in the literature where AC electric field has been applied in a continuous flow system to control the nano scale orientation of elongated particles.

One of the main challenges of using AC external field in a dynamic process consists of locking the field-aligned CNFs into a metastable structure as the materials travel through the electric field to prevent the time dependent relaxation toward isotropy due to Brownian diffusion. Inspired by the flow focusing approach,[63] the present study employs a set of extensional flows downstream to initiate a sol-gel transition before Brownian motion becomes dominant, hence forming highly ordered cellulose filaments. While the hydrodynamic alignment may induce non-uniform orientation profiles across the fiber width due to the inherent velocity gradient toward the channel walls,[31] the utilization of AC electric field may help to mitigate this issue for the production of anisotropic and uniform fibers with larger diameters.

In this research, TEMPO-oxidized CNFs were extracted from renewable softwood pulp to produce anisotropic fibers using an innovative field-assisted flow focusing process. The continuous production of renewable fibers with good mechanical attributes is particularly relevant considering that fibers account for more than 20 % of the overall plastic production, which was valued at $55 trillion in 2017.[78] The evolution of CNF alignment during processing with regard to the applied voltage was studied *in-situ* using polarized optical microscopy. Both surface and bulk order characterizations of the resulting filaments were conducted respectively by scanning electron

microscopy coupled with image analysis and by orientation dependent variation of the polarized Raman scattering signal. 2D-XRD was performed to examine the CNF orientation in the planes perpendicular and parallel to the filament axis. Finally, several meters of filaments were produced under different conditions to investigate how the amplitude of the AC electric field influences the mechanical properties of the resulting nanocomposites.

2.3 Engineered CNF Characteristics

CNFs were synthesized based on a previously reported TEMPO-mediated oxidation procedure with 3 mmol NaClO per g of bleached softwood pulp followed by homogenization using mechanical blending and double acoustic irradiation.[79,80,81,53] As-prepared CNFs exhibited a mean length and diameter of 620 nm and 2 nm, respectively, yielding a high aspect ratio of 310 (**Figure 15**). The tailored CNF fiber length was critical to maintain established alignment from the applied electric field. Shorter length fibers align quicker than lengthier fibers however, they typically do not retain the alignment as well as longer fibers due to Brownian motion. The carboxylate content of CNFs was 0.7 mmol/g, as measured by conductometric titration and the crystallinity index was 41%, as determined by XRD according to the Segal method (**Equation 3**).[82] The CNFs were completely dispersed at the individual nanofibril level in water by electrostatic repulsion and osmotic effects due to anionically charged carboxylate groups densely present onto the CNF surface.[83,84] The tailored polar group density established via controlled oxidation was also a key component in creating anisotropy because they are responsible for nano fiber rotation from electric field exposure.

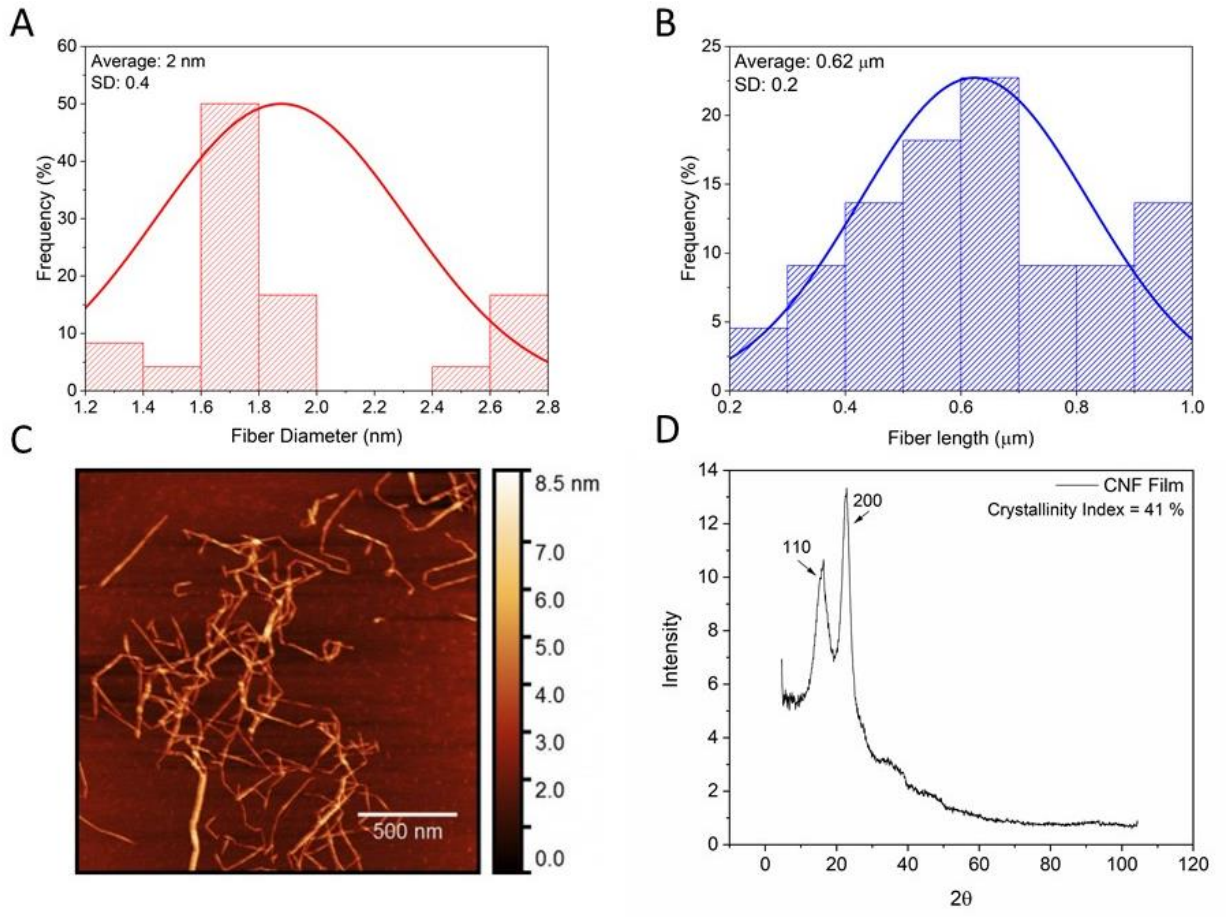

Figure 15*. **(A)** Histogram exhibiting normal distribution of CNF fiber diameter with2nm average.* ***(B)*** *Histogram exhibiting normal distribution of CNF fiber length with a 620 nm average.* ***(C)*** *AFM image of CNF dispersion exhibiting wide narrow range of fiber length and diameter.* ***(D)*** *XRD analysis of nanocellulose film with a 41 % crystallinity calculated using the segal method.*

2.4 Continuous Aligned Filament Formation

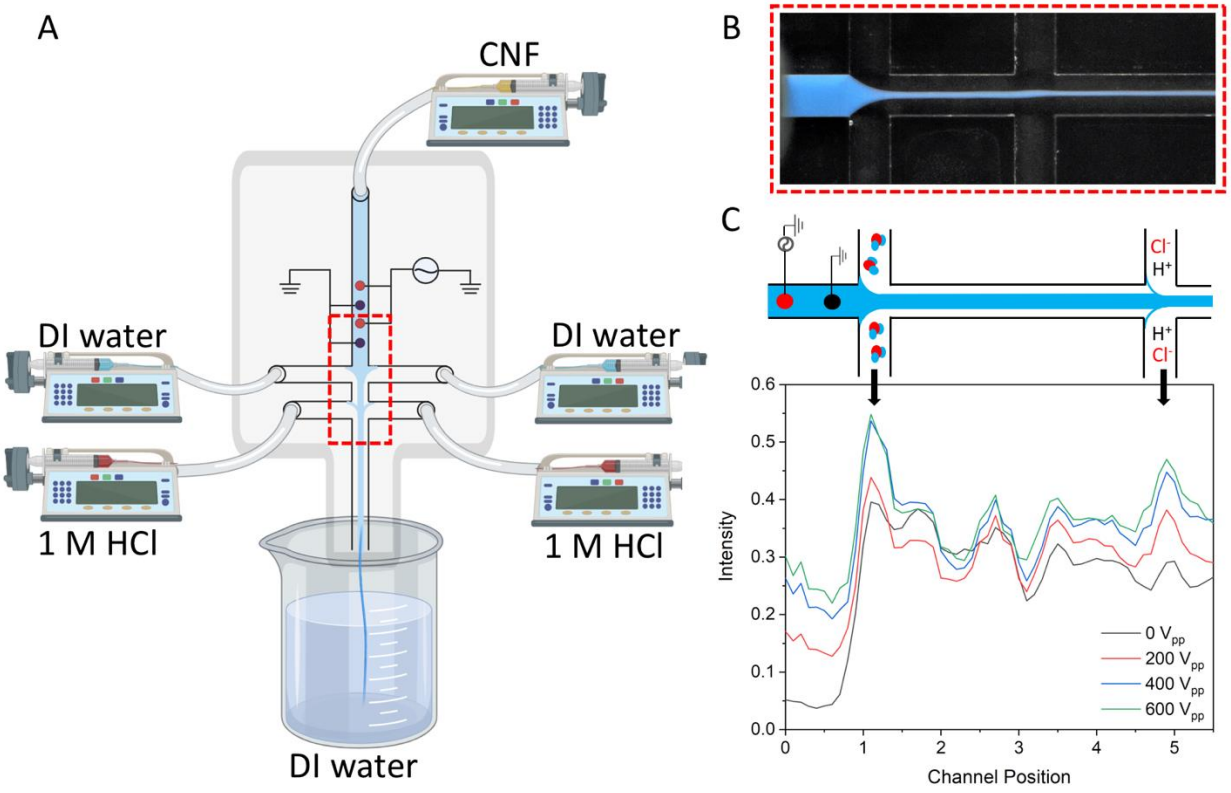

Figure 16*. Assembly of nanostructured cellulosic filaments using novel electric field flow focusing system.* ***(A)*** *Schematic of the field-assisted double flow-focusing channel used for the preparation of macroscopic filaments. The CNF suspension is injected in the core flow, while DI water and acid at low pH are supplied in the first and second extensional flows, respectively. Before reaching the extensional flows, the core CNF flow is exposed to four copper electrodes that are supplied a desired voltage to cause fiber polarization from the generated electric field. After the second extensional flow the CNF core undergoes a sol gel transition, and the hydrogel filament is deposited into a beaker of DI water.* ***(B)*** *Optical microscope image of the double flow-focusing part of the setup represented horizontally. Note that blue dyes were added to the core flow for clarity purposes.* ***(C)*** *Polarized optical transmission measurements of CNF alignment at various applied voltages along the core microfluidic channel, as illustrated in the above schematic.*

Aqueous solutions containing 0.3 wt% CNFs, exhibiting a non-Newtonian behavior with a viscosity of 13 mPa, were fed into a 1-mm microfluidic channel for the continuous fabrication of macroscopic cellulose filaments. To align the CNFs in parallel with the filament axis, the core flow was equipped with 4-mm electrodes vertically spaced every 14 mm to generate an alternating AC electric field. Two extensional flows were installed downstream with the first one composed of water and the second one comprising 1 M HCl, as illustrated in **Figure 16A**. A combination of five syringe pumps were used to control the flow rates of the core and all extensional flows, which were kept constant for all experiments. Optical transmission measurements of the core flow were collected between crossed polarizers to examine the birefringent properties of CNFs at different positions along the microfluidic channel. Experiments were conducted at different applied voltages varying from 0 to 600 V_{pp} in 200 V_{pp} increments. Voltages higher than 600 V_{pp} were not considered to prevent water electrolysis. The variations in signal intensity observed at position 0 indicate that the sole electromagnetic polarization of the core flow gave rise to the nematic ordering of CNFs in solution, which gradually improved with increasing applied AC external field. This means that the electrostatic torque exerted on the CNFs by the applied voltage was sufficient to overcome the effects of Brownian diffusion. It is also worth noting that the CNF response to the electric field was not linear and started to level off at elevated voltages, which is consistent with recent results from numerical simulations.[62] The magnitude of the field-assisted alignment at 600 V_{pp} (*i.e.* signal intensity of 0.30) was only 25% lower than the nematic CNF ordering obtained by the extensional flows at position 1 when no voltage was applied (*i.e.* signal intensity of 0.37). This demonstrates that polar moieties grafted on the CNF surface during the TEMPO-mediated oxidation enable strong CNF polarization and spontaneous alignment of dipoles under applied AC external field. In addition, the benefits of the field-assisted alignment are well maintained throughout the entire flow

focusing process despite Brownian diffusion. Besides assisting nanoparticle alignment by accelerating the core flow, the first set of extensional flows (*i.e.* position 1) generated a protecting sheath flow of DI water preventing CNF friction with the microfluidic channel wall. When 600 V_{pp} was applied compared to the baseline experiment without AC external field, the signal intensity increased by 44% and 56% at the first and second extensional flow positions (*i.e.* channel positions 1 and 5), respectively. Beyond the second set of extensional flows (*i.e.* position 5), the presence of low pH acid limited electrostatic repulsions between individual CNFs due to the protonation of carboxyl (COO^-) groups and promoted the sol-gel transition of the biopolymer, forming well-ordered macroscopic filaments.[63,85,86] These results reveal that the upstream field-assisted alignment of the core flow offers a unique opportunity to improve the downstream ordering of nanoparticles induced by extensional flows.

2.5 Characterization of Filament Formation and Alignment

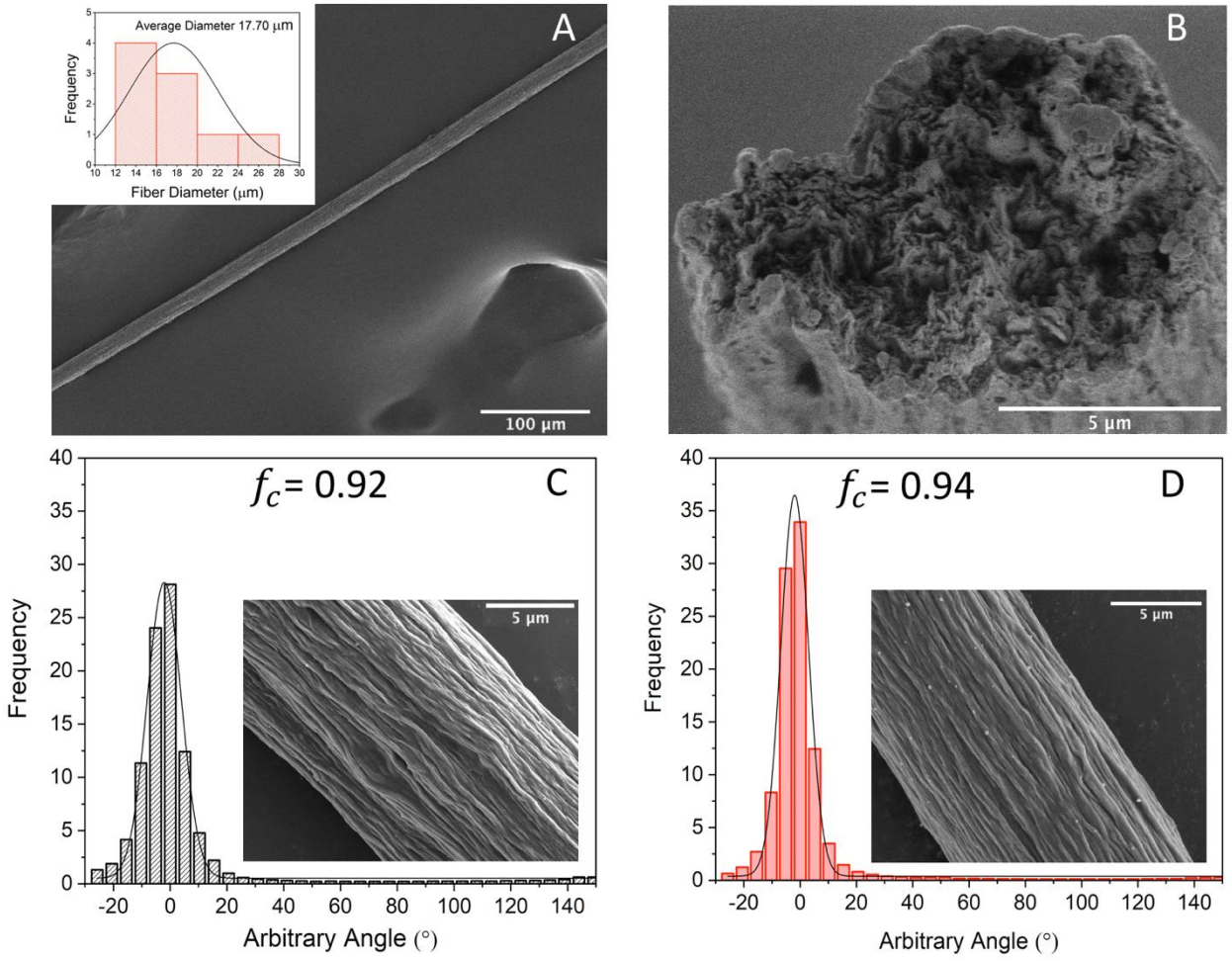

Figure 17*. Morphological characterization of the prepared bio-based filaments.* ***(A)*** *Representative SEM image of a cellulosic filament with the diameter distribution shown in the inset.* ***(B)*** *SEM image of the cross section of a filament showing a layered structure with dense CNF packing and a void less core structure. Histograms representing the orientation degree of CNF threads on the surface of macroscopic filaments prepared without* ***(C)*** *and with* ***(D)*** *external electric field. High magnification SEM images of the filament surfaces, shown in the insets, and orientation factors calculated using equation 2 CNF micro bundle alignment.*

The continuous filaments made by the field-assisted flow-focusing process were cut into small sections and air-dried under tension for further characterization. Electron microscopy analysis revealed that all filaments exhibited similar ribbed textures with a mean diameter of 17.7 +/- 4.3 □m regardless of the applied voltage **(Figure 17 A)**. The representative cross-section image of a filament in **Figure 17 B** shows that CNFs were tightly packed into a well-defined layered structure. This was consistent with the XRD pattern of macroscopic filaments, which was similar to that of CNFs with much lower intensity of cellulose peaks, suggesting a compact layout of CNFs. Observations at higher magnifications indicated that each filament was comprised of multiple CNF bundles of 1-3 □m in diameter forming aligned threads throughout the filament.[23] To assess the degree of alignment of these striations, the orientation index, f_c, was computed based on equation S2 using ImageJ software.[87] This micro-scale orientation factor was determined for filaments prepared under the same flow conditions but at different applied voltages. The high ordering of CNF bundles was confirmed by orientation factors higher than 0.9 in each case. When an external electric field was applied (**Figure 17 D**), the orientation index slightly increased from 0.92 to 0.94 compare to the baseline filament without applied voltage (**Figure 17 C**). However, there were no statistically significant differences between the orientation factors measured at various applied voltages.

While the above results provided an estimate of the microscale directionality of CNFs on the external surface of the filament, polarized Raman spectroscopy was conducted at ambient conditions to better examine the bulk orientation and the quality of the alignment of individual CNFs within the filaments.[88,89] Samples were mounted on silicon dioxide wafers and all spectra were collected at an excitation wavelength of 785 nm and normalized using the silicon dioxide signature peak at 521 cm^{-1}. The characteristic peak at 1095 cm^{-1}, commonly associated with the

C-O vibration of the cellulose backbone parallel to the molecular chain axis,[90,91]was studied due to its strong dependence on the polarization angle.[92] Since the Raman intensity of randomly oriented fibrils remains constant regardless of the polarization angle, systematic deviation from this can serve to characterize the degree of fibril alignment. **Figure 18 A** shows that when the long axis of the filament was parallel to the incident laser polarization (//), a large enhancement of the Raman intensity was observed for all specimens. Rotating the filaments from 0° to 90° reduced the intensity of the 1095 cm^{-1} band more dramatically for the filament prepared with the assistance of an external electric field. The filaments produced under applied voltage retained only 15.6 % of their maximum intensity, while the filaments synthesized without AC external field retained more than 30 % of their maximum intensity. This significant change in intensity indicates that greater optical anisotropy was achieved when the applied voltage reached 600 Vpp. Furthermore, signature peak at 380 cm^{-1} corresponds to the region describing skeletal bending of CCC, COC, OCC and OCO internal bonds, and signature peaks 1096-, 1121-, and 1152 cm^{-1} all correspond to the region dominated by CC and CO stretching motion in the backbone of cellulose chains or parallel to the cellulose chain axis.[91,93] There is no shift in any of these signature peaks with applied voltage indicating there is no change in cellulose chemical structure from exposure to the electromagnetic field. (**Figure 18 B**). The combination of electron microscopy and image analysis with polarized Raman spectroscopy revealed that an externally applied electric field improved the alignment of CNFs both on the filament surface and in the bulk. In the absence of AC electric field, however, bulk ordering was significantly reduced, while surface ordering was only slightly affected. This may be attributed to the radial velocity profile of CNFs from the core flow toward the channel walls.[31] Besides enhancing to some extent the magnitude of CNF ordering, the

utilization of AC electric field ensures a more uniform CNF orientation across the macroscale filament.

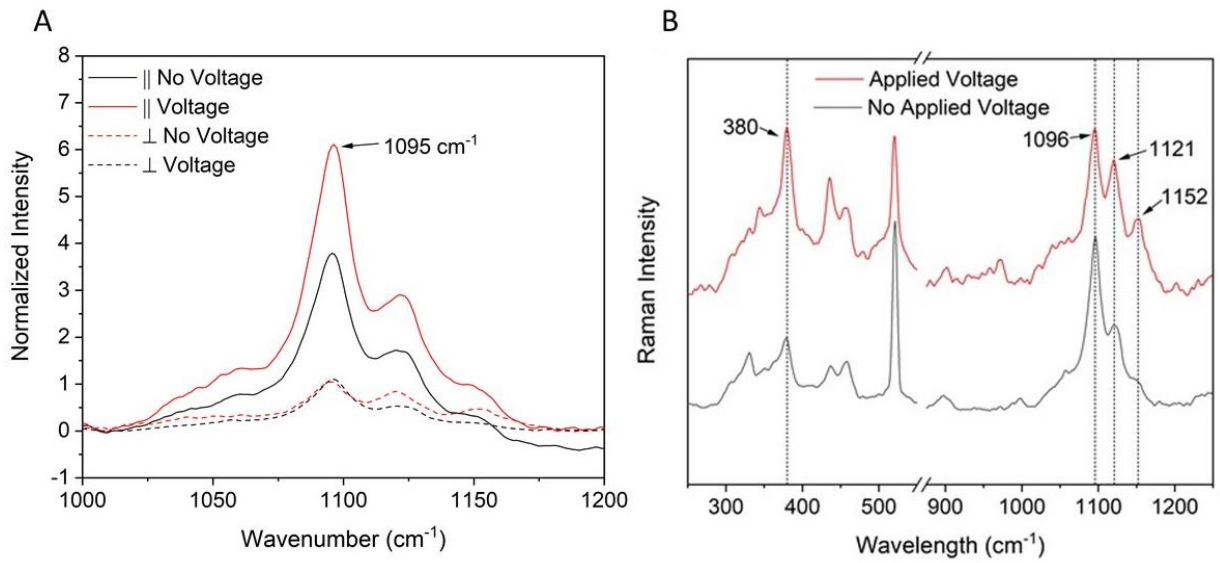

Figure 18*. Raman spectra of cellulosic filaments prepared with (red) and without (black) external electric field. The voltage applied in this case was 600 Vpp. Each spectra was collected at an excitation wavelength of 785 nm in parallel with (solid line) and perpendicular to (dashed line) the filament axis.*

To evaluate the influence of the amplitude of the electric field on the CNF ordering, filaments prepared at different applied voltages were characterized by 2D-XRD (**Figure 19**). The characteristic peak of the (200) crystallographic plane of cellulose at 2θ = 22.4°, commonly attributed to the d spacing between crystal regions of individual cellulose chains, was used to assess the CNF orientation in the filaments.[94,95] CNF orientation was analyzed both in the planes perpendicular (Ψ) and parallel (Φ) to the filament axis, as illustrated in **Figure 19E**. **Figure 19A-D** report the evolution of the (200) band intensity as a function of the in-plane rotation angle for filaments produced under different conditions. Each specimen exhibited two distinct peaks at 0°

and 180°, revealing the uniaxial orientation of CNFs along the filament axis. These peaks are obviously sharper in the case of the filaments prepared at 600 V_{pp}, while only minimal variations of the peaks' full width half maximum (FWHM) are observed for the other samples. This was consistent with the short appearance rate of the (200) band in the diffractogram of the 600 V_{pp} filament compared to the other samples. The orientation index, f_c, was computed based on equation S2 to quantify the quality of CNF alignment in the different filaments.[63,20] Note that the slight differences between the f_c values determined at 0° and 180° might be attributed to the difficulty of mounting perfectly stretched filaments onto the XRD stage. The averages between the f_c values calculated at 0° and 180° were considered for comparison purposes. The f_c values followed an upward trend and slightly increased from 0.815 to 0.865 when the applied voltage increased from 0 up to 400 Vpp. Beyond this point, the f_c culminated to 0.945 at 600 V_{pp}, representing a 16 % increase from the baseline filament synthesized without AC external field. These results reveal that, while the addition of external electric field can improve CNF ordering, its effects become significant once a threshold voltage is applied to the core channel of the flow focusing setup. This is consistent with previous batch experiments where no obvious alignment was observed in nanocellulose samples exposed to electric field lower than a certain value.[70] In the out-of-plane direction (**Figure 19F**), however, the (200) band remained clearly visible in each diffractogram when the filaments were tilted from 0° to 90° without any obvious differences between filaments prepared at various applied voltages. This indicates the absence of preferential out-of-plane CNF orientation, suggesting that the CNFs were packed isotropically in-the-plane, Ψ, but parallel to the plane, Φ.

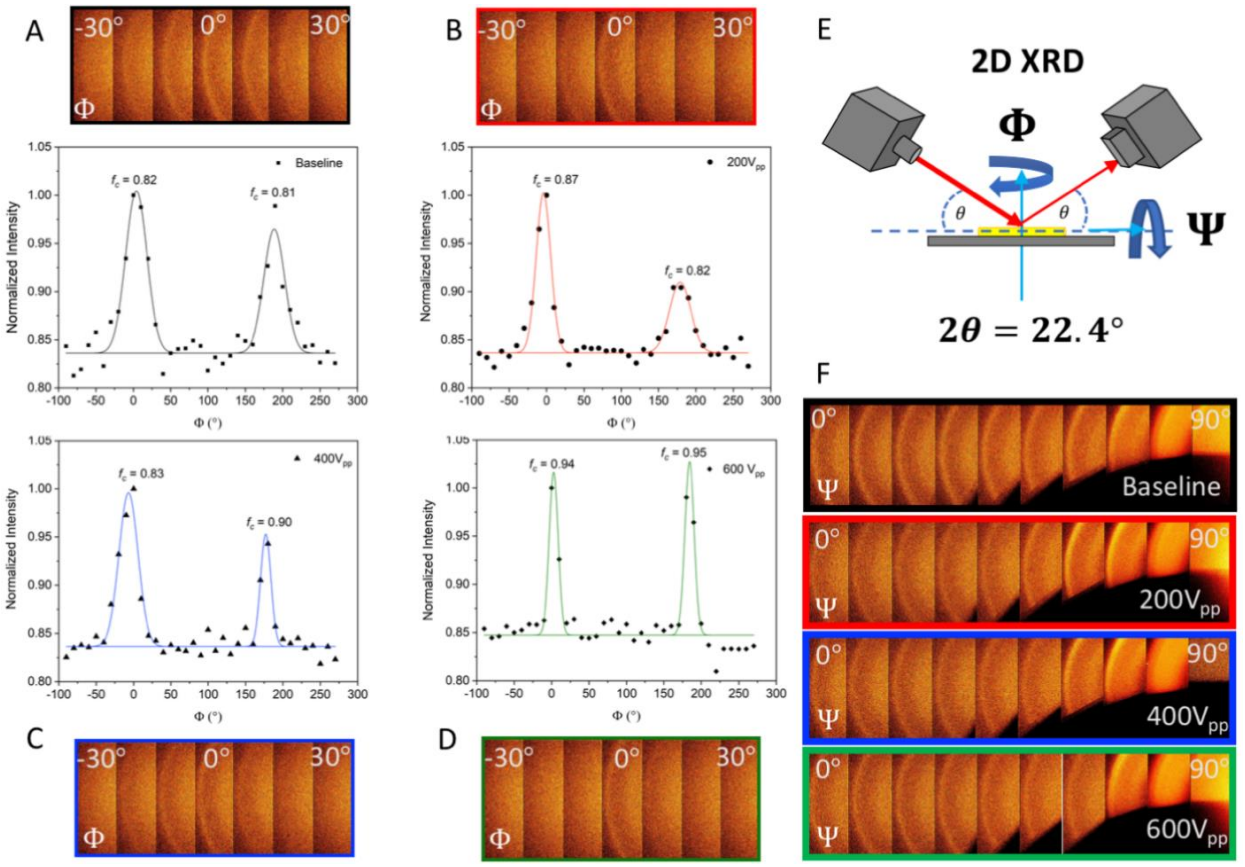

Figure 19. *2D XRD analysis of CNF alignment within the cellulosic filaments.* ***(A)*** *Azimuthal integration of the (200) scattering plane of the diffractograms with respect to Φ rotations for cellulosic filaments prepared at* ***(A)*** *0,* ***(B)*** *200,* ***(C)*** *400 and* ***(D)*** *600 V_{pp}.* ***(E)*** *Schematic illustrating the axis of rotations with respect to the filament layout on the XRD stage for the in-plane, Φ, and out-of-plane, Ψ, directions.* ***(F)*** *Diffractograms of cellulosic filaments prepared at various applied voltages with respect to Ψ rotations.*

2.6 Anisotropic vs Isotropic Filament Mechanical Properties

The influence of CNF orientation with respect to applied voltages on the mechanical response of the filaments was evaluated using stress-strain measurements. One-meter-long filaments were prepared at various applied voltages and cut into 3-cm long sections. For statistical

soundness, over 30 tensile tests were conducted for each condition and the results were subjected to one-way analysis of variance (ANOVA) and Tukey tests based on 5 % alpha level (*i.e.* 95 % confidence). Statistical significance in tensile strength, strain-to-failure and toughness were determined with p-values < 0.05. As shown in **Figure 20A**, the tensile strength and strain-to-failure for the filaments prepared at 600 V_{pp} were significantly larger than for the others samples. This was consistent with the XRD data since the largest orientation enhancements were expected to yield the greatest effects on the mechanical properties. Compared to the baseline filaments made without electric field, the filaments at 600 V_{pp} exhibited more than 63 % and 46 % augmentations in tensile strength and strain-to-failure, respectively. Such simultaneous increases in both tensile strength and strain-to-failure at 600 V_{pp} yielded an impressive improvement of the material's toughness, with nearly 120 % augmentation compared to the baseline filament prepared without AC external field. It is noteworthy, that this increase in toughness did not sacrifice the material's stiffness, as changes in the filaments' modulus of elasticity were not statistically significant. The Young's modulus hovered around 20 GPa, which is among the highest values reported for bio-based materials.[31,96,97,98] In addition, the yield point, delineating the region when the material begins to deform plastically, was raised drastically when the applied voltage increased from 0 to 600 V_{pp}, as depicted in **Figure 20B**. This reveals that important improvements in mechanical resilience can be achieved for structural materials with highly ordered nanofibrils. The good mechanical properties obtained at elevated voltages can be attributed to the anisotropic nature of the filaments combined with the tight CNF packing and limited electric field-induced structural defects.

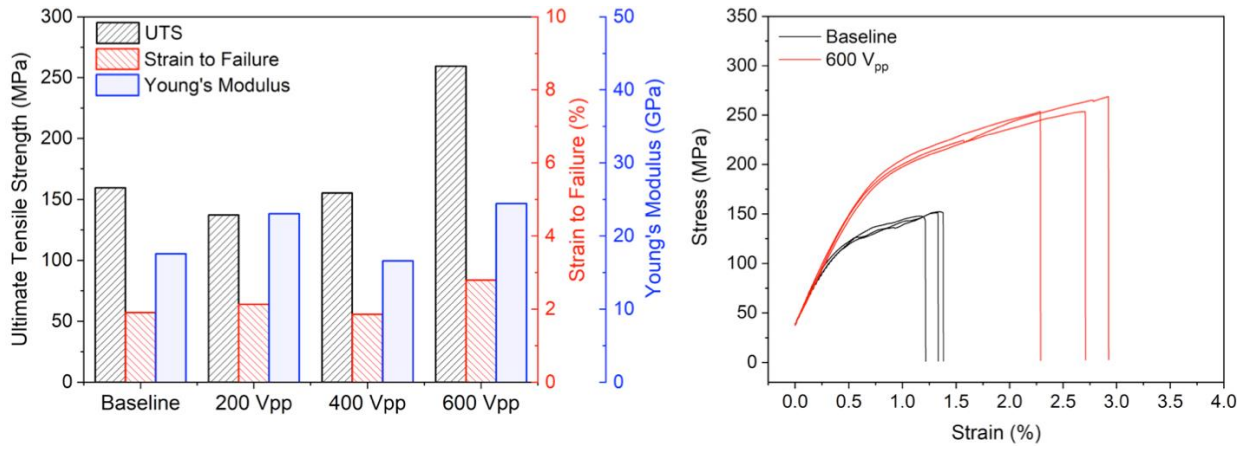

Figure 20. *Mechanical properties of cellulosic filaments.* ***(A)*** *Histograms showing the ultimate tensile strength, strain-to-failure and Young's modulus of filaments prepared at different applied voltage.* ***(B)*** *Triplicate stress-strain curves of representative filaments prepared at 0 (black) and 600* V_{pp} *(red).*

2.7 Conclusion

In summary, macroscopic filaments comprising highly-ordered TEMPO-oxidized CNFs were produced from renewable wood pulp using an innovative field-assisted flow focusing process. Tailored polar moieties established on the CNF surface via controlled oxidation enabled strong polarization and spontaneous alignment of dipoles under applied external electric field, which significantly improved the downstream nematic ordering of CNFs despite diffusion caused by Brownian motion. Fiber lengths were tailored to the appropriate length to maintain alignment from electric field and mechanical properties of individual CNF fibers. While the upstream field-assisted alignment enhanced the CNF ordering both on the filament surface and in the bulk demonstrating individual fiber manipulation, its effect became dominant once a threshold voltage was applied. Filaments produced at 600 V_{pp} had greater optical anisotropy and exhibited a 16 % augmentation in orientation index compared to filaments prepared without an AC external field.

Despite the relatively high voltages incurred, there were no signs of either electric field-induced structural defects or water electrolysis. 2D XRD analysis also revealed that the CNFs were randomly aligned in the plane along the filament length but oriented parallel to the filament axis. The high orientation degree of CNFs combined with their dense packing yielded impressive improvements in the mechanical properties of the resulting filaments, with up to 120 % increase in toughness without compromising the material's stiffness. These results demonstrate for the first time that an external electric field can be applied in a continuous flow process to control the structural ordering of anisotropic materials. Future optimization of the bio-based filaments can be made possible through the functionalization of CNFs with charged molecules and/or magnetic nanoparticles to tune the material response to an electromagnetic field and adjust inter-particle interactions for multifunctional applications.

These sustainably sourced filaments have potential applications as an alternative cellulosic based textile that could cure a growing concern for microplastic bioaccumulation. Synthetic textiles typically sourced from petroleum-based products to include polyester are detrimental when introduced to the environment either in a primary or secondary fashion. These textiles have been known to leach into groundwater, cause phytotoxicity and soil quality degradation.[99] One of the largest contributors to synthetic fibers in water systems wastewater from washing machines that gets dumped into sewage.[100] It has been discovered that 18 shores across 6 continents have microplastic accumulation in sewage with the main products being polyester, acryclic and polypropylene, and in some cases the ratio between polyesters and other additives matched common clothing compositions. [101] Creating textiles from cellulose based material could mean that as secondary fibers are generated from the inevitable washing or discarding of clothes would more easily breakdown in marine environments causing less bioaccumulation. Studies The

biocompatible nature of the fibers could also cause less harm if ingested by marine or other species. This just demonstrates how filling one basic need with cellulose, that is currently being filled by petroleum-based products, could have a large implication in multiple growing global issue. Expanding the sustainable benefits of cellulose to more complex implications could have equally as large of an impact or potentially even greater.

3.0 Aligned Conductive Composite Filaments for Complex Sensing Applications

3.1 Synopsis

Objective: Incorporate SWNTs into a composite CNF based filament and demonstrate improvements in both mechanical and electrical performance from pre-alignment techniques for a multifunctional sustainable alternative to fill complex functions.

Characterization Techniques:

- UV-VIS
- AFM
- Viscometer
- FTIR
- PiFM
- SEM and Conductive Imaging SEM
- Tensile Testing
- 2D-XRD
- Keithley Resistance Measurements
- In-Situ Swelling Rate: Light Microscope with Zeiss Camera and Keithley
    - Bandicam software used for screen capture of fiber swelling

Conclusions:

- CNF charge density, concentration, and length are critical to SWNT dispersion quality, maximum carrying capacity and alignment
- CNF disperse SWNTs through both mechanical wrapping and counterion interactions that creating a strong interface between dispersion components and individualized SWNTs

- Interfacial chemistry and individualized SWNTs is key to transferring nano properties to the macro scale
- SWNTs are the primary component maintaining alignment because of their comparatively longer fiber length, and CNF undergo secondary alignment from SWNT wrapping increasing CNF fiber matrix bonding
- The alignment and increased bonding directly increased the mechanical performance of filaments beyond the capabilities of pure CNF filaments
- Previous methods of incorporating SWNT with CNF report exceptionally low loadings of nanotubes with significant losses in mechanical performance, especially with increased SWNT loadings, compared to pure CNF filaments
- Pre-alignment techniques also increased electrical conductivity by creating intentional fiber junctions
- These intentional junctions translated to a higher sensitivity when applied as a water sensor

3.2 Introduction

Petroleum fills base applications such as textiles but can also be adapted to fill many other complex needs that involve sensing, electronics, or biomedical applications.[102] Sustainable alternatives generally succeed in filling only one specific role, making little progress in reducing global dependence on unsustainable sources. A truly impactful sustainable solution is a material that can adapt to fill not only the basic but also more complex applications, or items with compound functionality much like petroleum. Nanocellulose is a sustainable material that has been proven to fill extremely basic low functionality needs such as alternative plastic films.[103,104] Furthermore, we have increased the mechanical properties of pure nanocellulose products by tailoring CNF in tandem with pre-alignment techniques to include a variety of other base applications that require even greater mechanical performance such as textiles.[105] Adapting nanocellulose products to a composite form will create opportunities for nanocellulose products with added functionalities such as conductivity or chemical selectivity expanding the possibilities to diverse complex functionalities such as electronics, sensing or biomedical applications.[9]

Many of these complex diverse functionalities rely on conductivity as the primary mechanism, and this is particularly true for electronics and sensing devices.[106] Nanocellulose is naturally a dielectric[107] and by itself cannot strongly conduct electricity, therefore it requires a conductive filler to provide a conductive property. Single walled nanotubes (SWNTs) are an attractive material as a composite filler because of their high conductivity, and ideal mechanical performance and material properties such as a high aspect ratio, tensile strength, and stiffness.[108]

However, transferring these beneficial properties from the nano to the macro scale is a great challenge because they are hydrophobic by nature and this causes them aggregate to form large parallel bundles in the presence of water.[109] Poor SWNT dispersion quality and aggregates can

create large defects and poor bonding within polymeric matrices forming areas of stress concentration diminishing the mechanical performance.[110,111] Aggregates also decrease efficiency of the finale product giving low conductivity and to compensate for poor formation a larger mass of SWNTS must be used in order to attain a conductive network, lowering its overall economic and social sustainability. The pre-alignment techniques developed in this work and in other works that require CNF alignment for effective mechanical performance require that fibers be suspended in water for easy fiber rotation making the water compatibility an unavoidable necessity. SWNTs offer a great opportunity to create a high performing material with additional exploitable characteristics but the effective dispersion in water is critical to develop a CNF/SWNT sustainable composite.

The hydrophobic nature that largely stands in the way of achieving these two critical goals, is currently overcome by adding tertiary chemical surfactants.[112] Chemical surfactants generally consist of hydrophobic backbones and hydrophilic polarized sections to produce an overall amphiphilic nature that surrounds and coats individual or small bundles of nanotubes.[113] While the largely hydrophobic aromatic backbone can form van der waals interactions with the SWNTs pure carbon tubular structure the hydrophilic portions serve to hold the structures in solution and prevent particle precipitation. Although they can disperse nanotubes, the surfactant acts as a barrier disrupting nanotube junctions and polymer matrix bonding weakening the conductivity and mechanical properties. The tertiary surfactant would also decrease the sustainability of the overall product because common surfactants tend to be petroleum based. They would also add to the overall size of individual fibers in solution causing a lack of control over size and viscosity that could cause large problems in pre-alignment techniques, especially those requiring an electric field like the hybrid system we have developed. Overall while adding a surfactant is effective in

dispersing nanotubes the sum cost to alignment control, mechanical, and electrical performance outweighs the benefits. However, the careful control over CNF surfaced charged provides a solution that no longer requires the typical surfactant used by most.

Nanocellulose as a natural amphiphilic polymer dispersion offers a unique opportunity to both disperse nanotubes and serves as the primary polymeric matrix abandoning the tertiary surfactant requirement.[114] TEMPO oxidized nanocellulose, that allows us to independently control fiber aspect ratio and surface charge, provides an especially unique opportunity to create an ideal CNF that can maximize the ability to disperse SWNTs.[13] We can maximize the surface charge of the CNF by controlling the oxidation phase, increasing the hydrophilic nature and thus the carrying capacity of CNF dispersions. The fiber length of both components will still need to be critically controlled to ensure fiber alignment is maintained as well as the mechanical integrity of the resulting product.[115]

Typical inclusions of nanotubes in petroleum polymer-based matrices have two methods of mechanical improvement. The first is through inclusion of large amounts of SWNTs to improve contributions from the filler on the mechanical performance of the composite. The second is through the natural formation of an interphase polymer between the matrix and nanotubes that strengthens stress transfer. The polymerization in the presence of nanotubes is suspected to improve seeding and orientation of the polymer interphase. The successful individualization of large loading of nanotubes would allow for polymer interphases to be formed on a majority of SWNTs greatly increasing the mechanical properties. However, these synergistic properties between polymer matrices and nanotubes are still greatly limited by challenges of poor dispersion quality, and in most cases nanotube aggregation is detrimental to the ultimate fiber properties with loadings higher loadings greater than 10 %.[110] Although polymer seeding is unlikely with CNF

these studies make it clear that understanding the interfacial interactions between SWNTs is critical to the overall successful filament mechanical performance.

This unique dispersion of engineered CNF and SWNT (CNF/SWNT) will create opportunities to fill complex needs and their multifunctionality can be further expanded when controlling the anisotropy through pre-alignment established with the novel electric field flow focusing system. There are reports that the one-dimensional geometry of SWNTs and interaction between polymer matrices promote alignment independent of an external force, and this alignment could be amplified by the dual flow focusing system.[115] Aligning both components could greatly improve the overall mechanical properties of the filament by introducing a strong interfacial region and increasing bonding between CNF fibers. Aligning SWNT dispersions will also have positive effects on the secondary traits by creating intentional unidirectional junctions of SWNTs translating to improved electrical conductivity and lowering the overall threshold for changes in conductivity.[37]

Here we create aligned conductive composite CNF/SWNT filaments to be used for complex applications such as sensing. First, we engineered the CNF nanostructure to create an ideal dispersion of nanocellulose and single walled nanotubes that will maintain CNF fiber mechanical integrity and exploit surface charges to achieve high loadings of SWNTs. The highest achieved loading of SWNT was then investigated using electron imaging and photo induced force microscopy techniques to understand the interfacial chemistry and geometry of the CNF/SWNT compounded structure. We then applied these CNF/SWNT dispersion to the applied electric field flow focusing channel to create a CNF/SWNT composite filament. The function of the applied electric field independent of the flow focusing was investigated and it was found that the applied electric field issued a strong polarization from SWNTs translating to strong filaments with

increased conductivity. The dispersion and alignment of CNF/SWNT components was so effective that composite filaments exhibited mechanical properties exceeding that of pure nanocellulose filaments. We then go on to demonstrate the benefit of the conductive traits within CNF filaments through water sensing validating the filaments' ability to fill complex needs currently being filled by petroleum products.

3.3 CNF/SWNT Dispersion Characterization

Dispersion quality is critical to filament formation and the transfer of ideal properties from the nano to the micro and macro scale. TEMPO oxidized CNF was engineered targeting a dispersion with long fibers and a high charge density to preserve mechanical functionality and disperse a large weight percent of SWNTs, respectively.[116] The selected CNF had a charge density of 0.85 mmol COOH/g CNF established through a controlled oxidation time (3.5 hours) and a high aspect ratio with a 650 nm fiber length and a 2 nm diameter. Although higher charge densities would more effectively disperse nanotubes, we chose not to increase the sodium hypochlorite ratio to achieve higher charge densities because the additional sodium hypochlorite would greatly weaken fibers and the secondary sonication needed for SWNT dispersion would have greatly affected the overall fiber length. Single walled nanotubes (5-30 μm length and 2 nm diameter) with carboxylic acid functional groups were used achieve high quality dispersions, with the charge suspended on the SWNTs compensating for the mid-range charged CNF. It's also been demonstrated that carboxylic acid groups on SWNTs result in a stronger and faster polarization from applied electric fields compared to pure SWNTs, thus providing the SWNTs the greatest chance for polarization to establish anisotropy.[117] A variety of CNF/SWNT dispersions were prepared through double sonication with an 8-minute sonication time to achieve good dispersion quality and moderately conserved fiber length (360 nm) (**Figure 21 A and B**).[118] SWNTs were

found to be an order of magnitude longer because of the longer starting fiber length of up to 30 µm (**Figure 21 C and D**). While longer times result in higher loadings and better dispersion quality, we chose to the limit the overall time to maintain the mechanical integrity of both components in the composite.

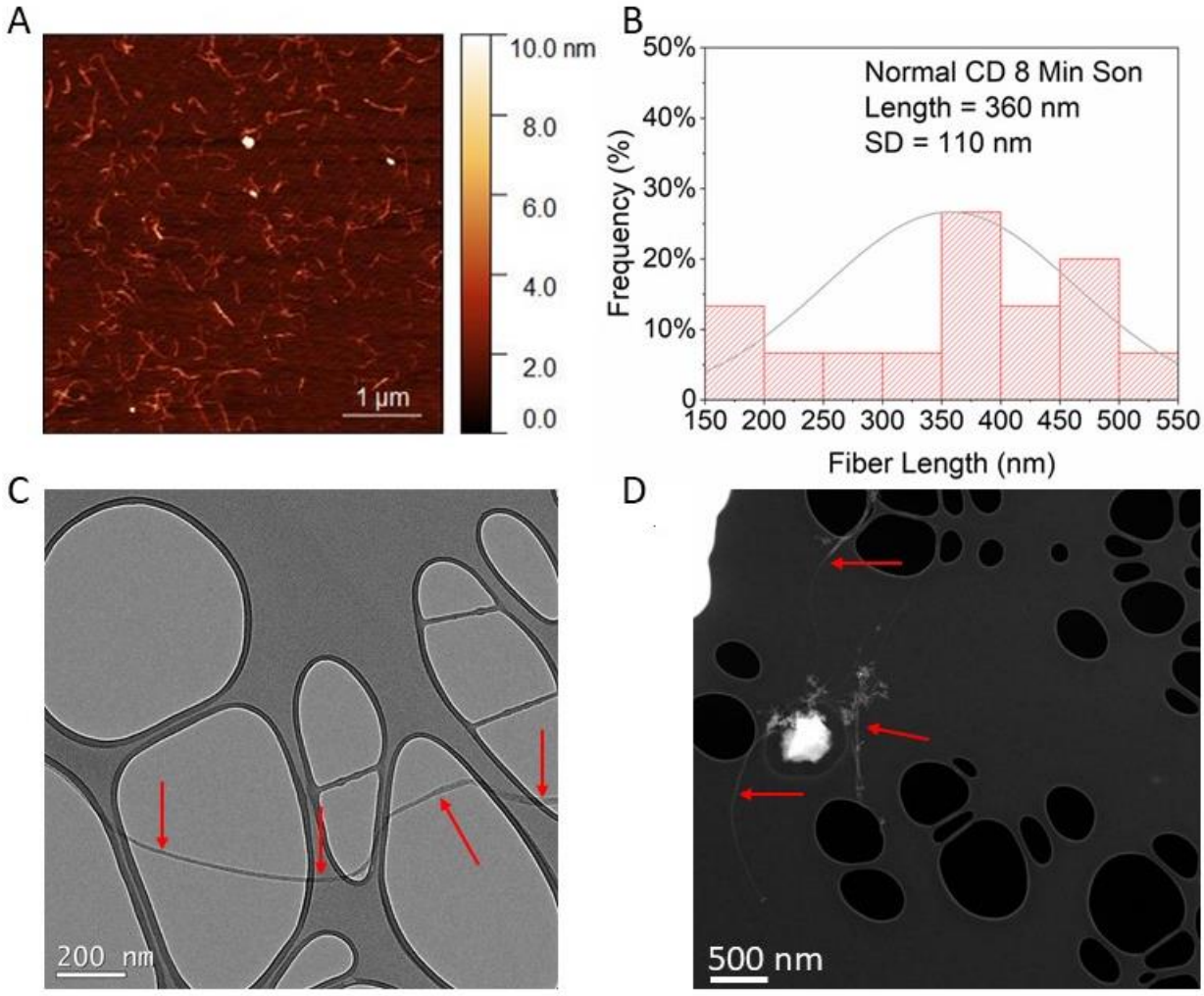

Figure 21. ***(A)*** *AFM Image demonstrating visual of good dispersion quality of 50 wt % CNF/SWNT dispersion.* ***(B)*** *Fiber length Histogram off pure CNF dispersions after 8 min sonication prepared at the same wt % of all CNF/SWNT dispersions.* ***(C)*** *TEM image of 50 wt %*

CNF/SWNT dispersions with red arrows pointing to the same single SWNT fiber. ***(D)*** *STEM image of 50 wt % CNF/SWNT dispersion with one red arrow pointing to one SWNT fiber.*

UV-VIS absorption demonstrated that the tailored CNF concentration had a significant effect on the SWNT carry capacity and individualization through increased absorption peaks at 250 nm.[119] Preparing the same CNF with different concentrations of SWNTs revealed that the CNF is primarily responsible for the SWNT dispersion with subtle contributions from carboxylic acid functionalization on the nanotubes. Three different dispersions were prepared for application to the electric field flow focusing channel including pure CNF as a comparison. CNF dispersions prepared at 0.32 wt % successfully dispersed up to 0.16 g (50 wt %) of SWNTs, and (**Figure 22 B**).[116]

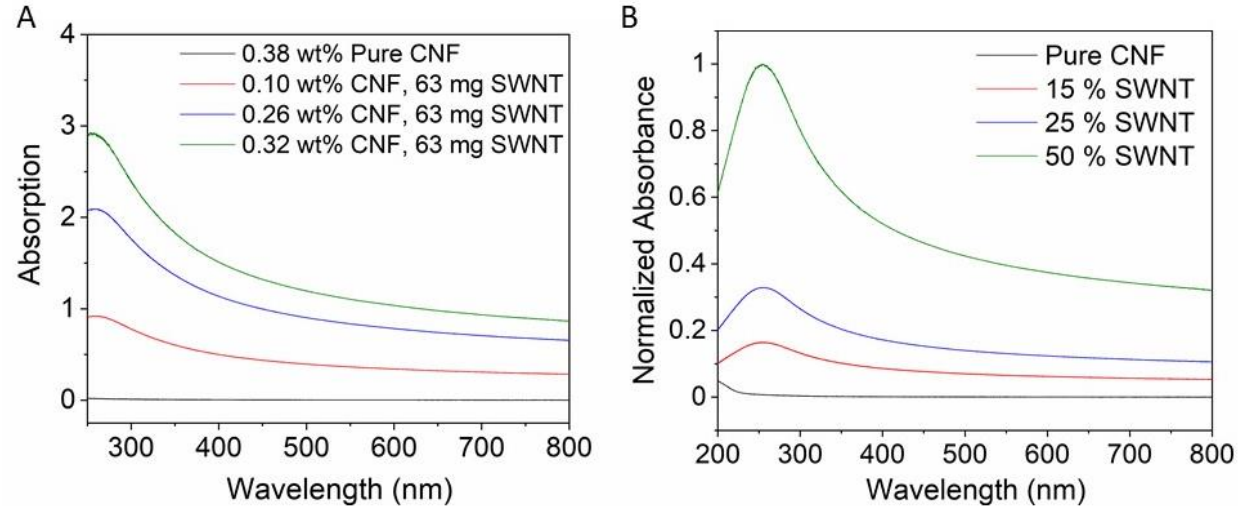

Figure 22*.* ***(A)*** *UV-VIS absorption of the same mass of SWNTs (63 mg) with different concentrations of the same CNF.* ***(B)*** *Three different CNF/SWNT dispersions (pure CNF or 0 wt % and 15, 25, and 50 wt % SWNTs) prepared using double sonication for 8 min followed by 50 min centrifugation at 5500 RPM. These dispersions were prepared for application to the electric field flow focusing channel.*

Dried CNF/SWNT films (**Figure 23 F**) demonstrated through shifts in -COOH FTIR signatures at 3329 cm^{-1}, and 1600 cm^{-1}that this dispersion involved carboxylic acid functional groups and aromatic interactions, respectively.[120] The carboxylic acid groups help with initial association and stabilization through repulsive interactions and steric hinderance. All CNF/SWNT concentrations demonstrated shear thinning with the pure CNF showing the lowest viscosity and the 50 wt % dispersion demonstrating the highest viscosity (**Figure 23 A**). This increase in viscosity is likely because of reduced repulsive forces between fibers that are occupied with SWNTs and the increasing mass of all fibers in water.[121]

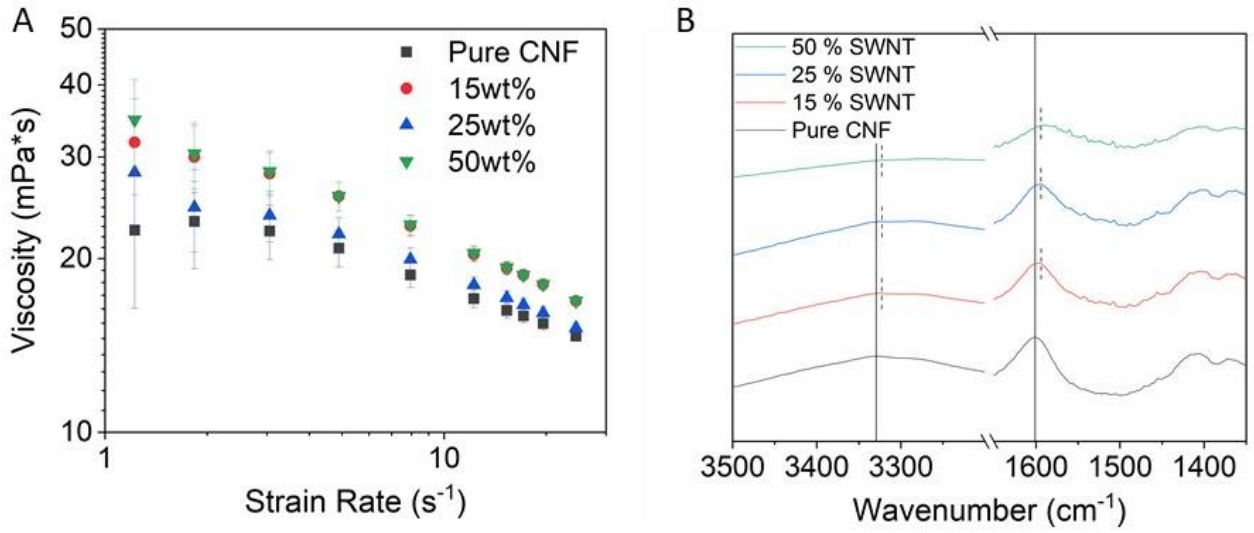

Figure 23. (A) *Viscosity versus strain rate of different SWNT wt % dispersions. (E) UV-VIS absorbance of different SWNT wt % solutions prepared for application in the applied electric field flow focusing channel.* ***(B)*** *FTIR of films prepared from different SWNT wt % dispersions to demonstrate carboxylic acid interaction.*

3.4 Compound Structure of CNF with SWNT

Understanding this CNF/SWNT compound structure created during double sonication is the key to understanding the dispersions performance in the electric field flow focusing channel,

and beneficial nano property transfer from the nano to the micro and macro scale. While the mechanism might not be the exact same as SWNT in petroleum matrices the same principles of a strong interfacial interaction and aligned structure are critical. The two common theorized methods of CNF/SWNT dispersions are either wrapping[122,123] or counterion interaction.[34] Physical wrapping has been speculated with an AFM by comparing the diameter of different components identified by speculated differences in length.[34,116,124] However, this method is challenging because the diameter of both CNF and SWNT range from 1- 4 nm and there is no guarantee that all longer elements are indeed nanotubes. Counterion interactions were discovered by force changes in a spherical AFM probe coated in CNF brought into close proximity of a graphene sheet.[34] While the structure of SWNTs and graphene both exhibit sp^2 hybridization this measurement does not account for SWNT curvature or functionalization. There has not been a definitive direct measurement of nanotubes associated with CNF both chemically and physically. Using photoinduced force microscopy (PiFM) combined with transmission electron microscopy (TEM) we demonstrated that both components interact with a combination of wrapping and chemical interaction.

Photoinduced force microscopy (PiFM) is a new technique that is critical to measuring the direct interaction between individual CNF and SWNT components. AFM alone only shows differences in surface topography and gives no information on chemical components. While the FTIR only measures the absorption or transmittance of radiation in a large given area and lacks topographical information and a small spatial resolution. PiFM can be thought of as a combination of atomic force microscopy (AFM) and an infrared laser, thus providing both topographical information and chemical component information.[125] The system works using a typical AFM that requires a cantilever that comes to an exceedingly small point that interacts with the surface of a

mounted material. As the tip scans across the surface attractive and repulsive interactions between the material and the tip cause deflections in the cantilever that are measured using a laser, and thus creating a topographical map of the material. PiFM works using the same AFM system but with the addition of an IR laser, that causes radiation absorption at specific wavelengths much like FTIR. However rather than measuring the absorption of light via transmittance the absorption is measured through force detection hence "photo induced" and "force" in the instrument name.[126] The IR laser when absorbed by the sample will cause sample excitation at signature wavelengths, and this causes a dipole-dipole interaction between the excited sample and the metal AFM tip. Then this small force interaction is detected by a laser measuring small cantilever deflection and a position sensor.[127] This force from excitation scanned at different wavelengths detected by the high spatial resolution AFM tip gives each pixel a location, and an excitation force paired with each scanned wavelength to give a topographical map that also depicts chemical signature (**Figure 24**).[128]

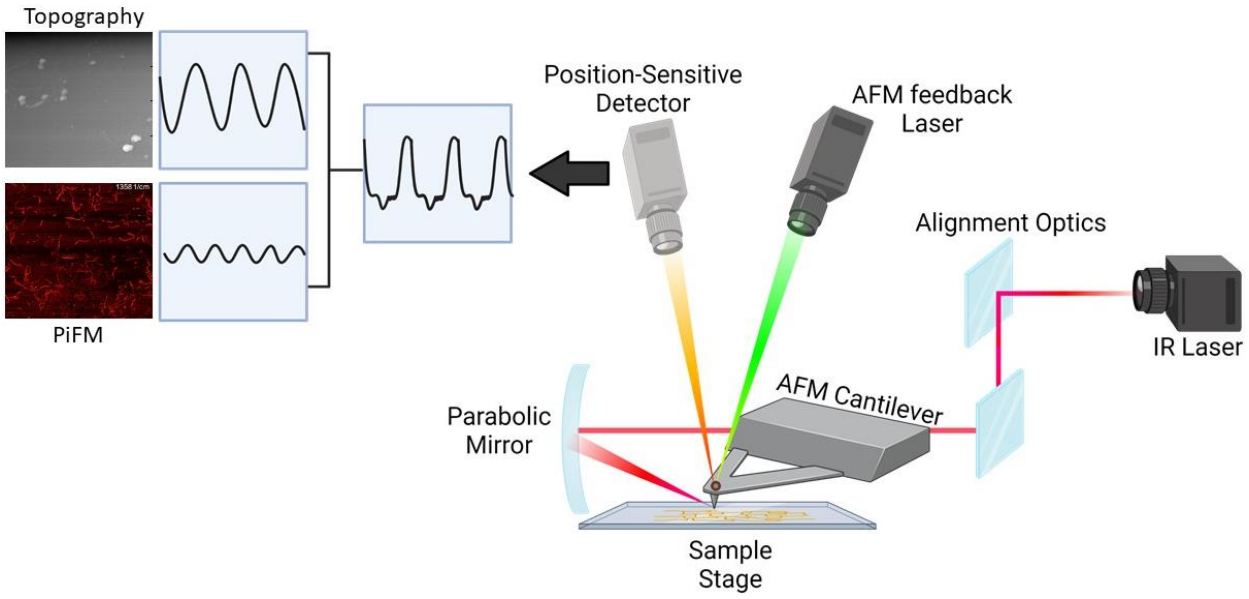

Figure 24*. Schematic of Photoinduced Force Microscopy (PiFM) technique. The IR laser is focused through a series of mirrors and aligned on to the sample through parabolic mirror shifts. As the AFM cantilever probes the samples dipole-dipole force interactions from excitation are recorded in addition to typical AFM interactions to produce information on both the topographical and chemical nature of the sample.*

Drop casted solutions on a copper TEM grid revealed long nanotubes (> 1μm) and an amorphous structure on the surface of SWNTs (**Figure 25 C**). Although a transmission image, it is likely that the CNF are wrapped on the outside wall as the diameter of CNF is close to the measured diameter of SWNTs. The AFM phase of the drop casted dispersion also showed a change in material surrounding certain portions of the SWNTs (**Figure 25 C and D**). PiFM spectra were taken at seven points along a single fiber and peak broadening was observed around the 1612 cm^{-1} wavelength in addition to a peak shift at 1347 cm^{-1} and a peak height increase at 1071 cm^{-1} (**Figure 25 A and B**). The shift and increase in the peak height are assigned to nanocellulose signature peaks[126] indicating bonding and the presence of more CNF fibers, while the 1612 cm^{-1} peak

broadening indicates aromatic interactions. These changes in FTIR signature along a single fiber indicate a compound structure between CNF and SWNT that involves both mechanical wrapping and electrostatic interactions. Electrostatic interactions can include the initial attraction caused by a fluctuation of counterions that induces a sp^2 polarization on the SWNTs structure, and hydrogen bonding from both SWNT and CNF carboxylic acid functionalization.[116] It is also speculated that the interaction of the aromatic CNF primary backbone and SWNT wall can reduce entropy also promoting strong hydrophobic interactions.[34,116] These electrostatic interactions are responsible for the chemical association observed in the FTIR but the agitation and additional energy from sonication can also cause physical interactions that can lead to wrapping.[129] This observation of strong chemical and physical interactions in the CNF/SWNT dispersion should create a strong interface between CNF and SWNT components leading to consistent filament formation and a successful transfer of mechanical properties across scales. [110]

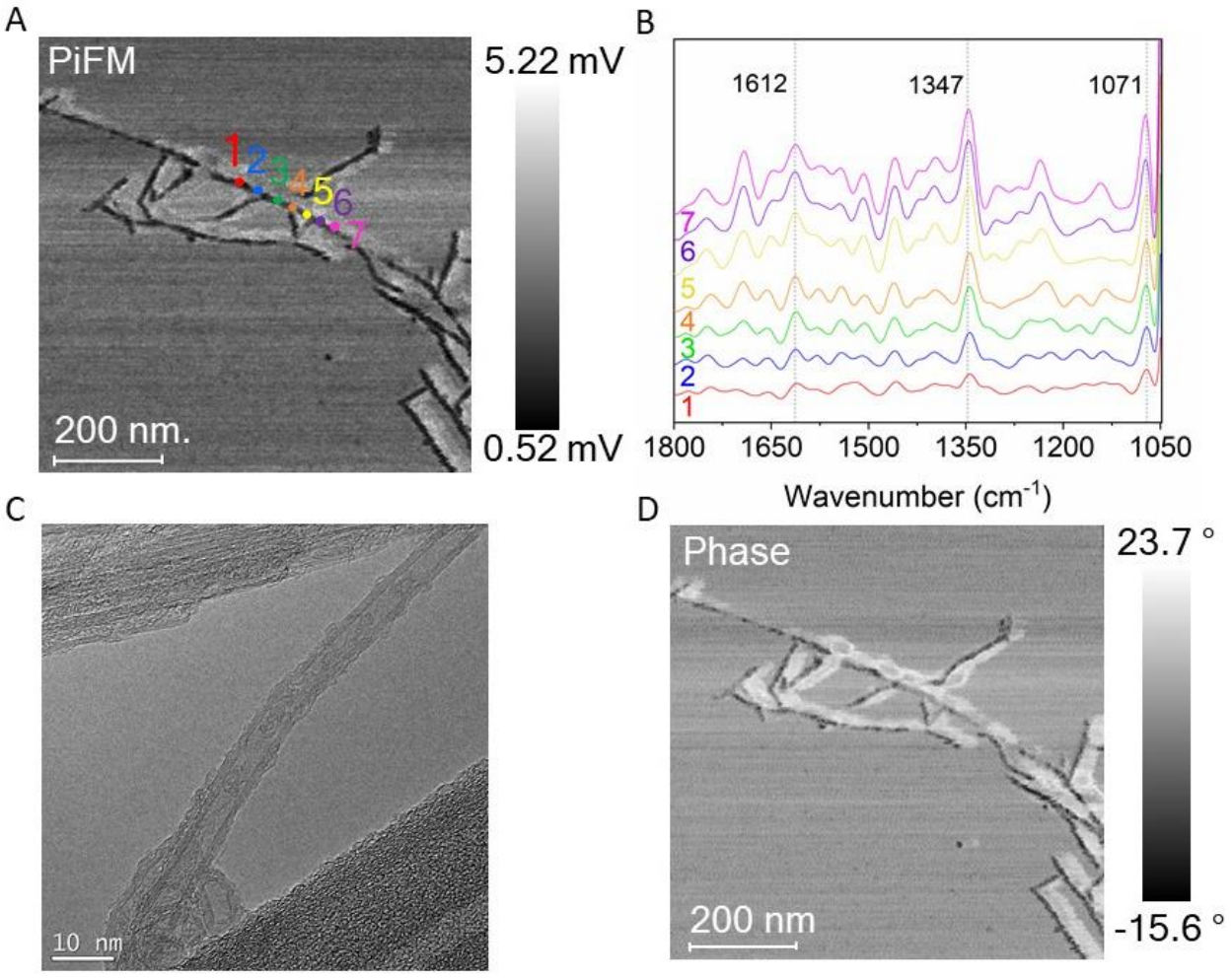

Figure 25*. **(A)** Photoinduced Force Microscopy (PiFM) of drop casted and dried CNF/SWNT at 50 wt % with seven points indicating the location of collected FTIR Spectra. **(B)** FTIR of seven points taken on the PiFM (color matched to locations on image A) with peaks indicated at 1612 cm^{-1}, 1347 cm^{-1}, and 1071 cm^{-1}. **(C)** Transmission electron microscope (TEM) image of a single walled nanotube with rough textured nanocellulose wrapped on the SWNT surface wall. **(D)** PiFM Phase image depicting different material stiffness on and next to fibers.*

3.5 CNF/SWNT Filament Characterization

Different dispersions prepared at 0 wt % (Pure CNF), 15 wt %, 25 wt %, and 50 wt % were prepared and applied to the electric field flow focusing channel with both 0 V and 100 V, to see

the effect of the electric field on filament formation and anisotropy. All filaments independent of SWNT loading and applied voltage demonstrated a uniform tightly packed core structure with no obvious voids, and an 11.5 mm diameter (**Figure 26 D**). Higher magnification of the filament ends revealed exceedingly small bundles of nanotubes evenly distributed throughout the entire filament core. The filament surface exhibited a rough and bumpy texture comparable to pure CNF filaments but with SWNTs visibly woven throughout the surface.

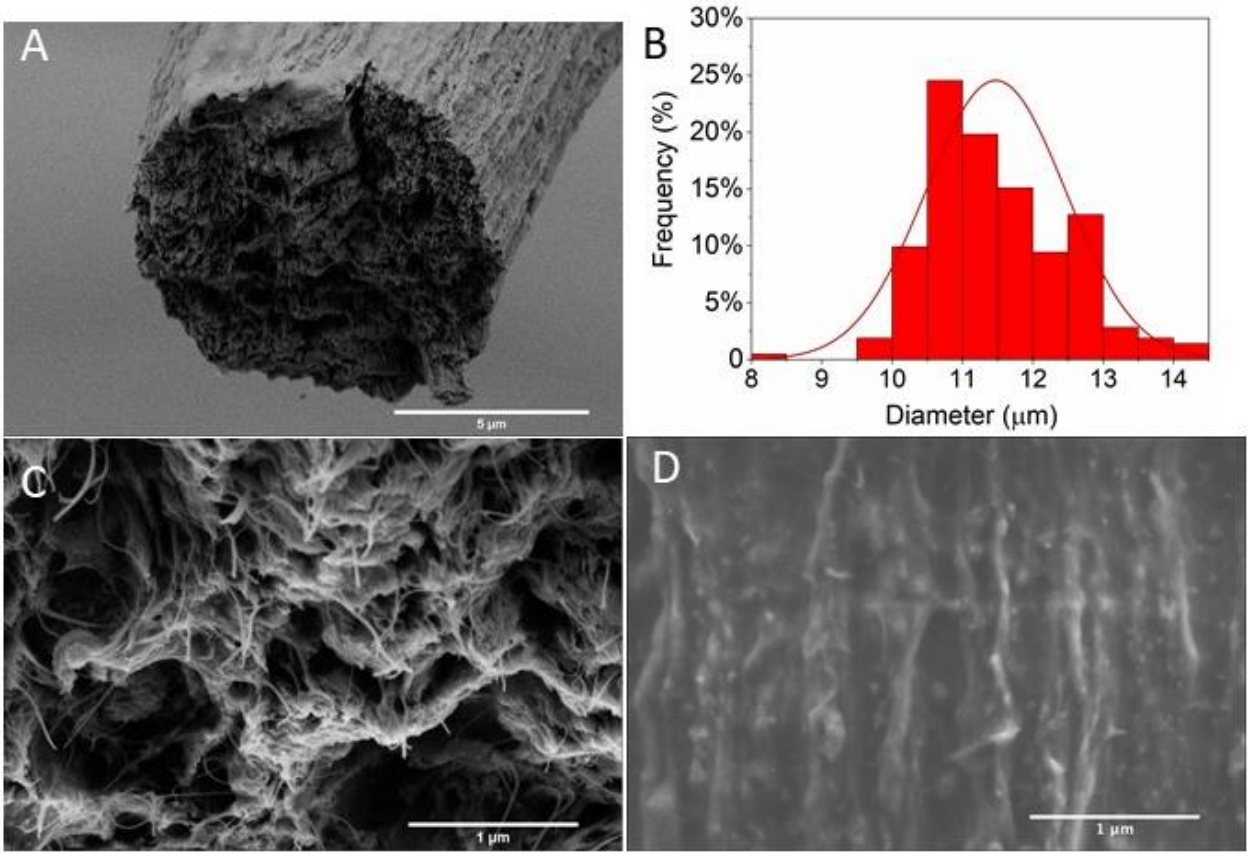

***Figure 26**. **(A)** SEM image of the full cross section of a 50 wt % filament showing a solid structure with a uniform tight packing. **(B)** Histogram demonstrating a normal distribution of filament diameters independent of filament SWNT loading and applied voltage. **(C)** Higher magnification of the 50 wt % CNF/SWNT filament with applied voltage showing brighter SWNT throughout the filament core and unidirectional nanotubes aligned with the filament longitudinal axis. **(D)** Surface*

of 50 wt % CNF/SWNT filament showing a rough surface texture and micro alignment with SWNTs woven throughout the surface.

Conductive imaging techniques showed SWNTs below the surface were aligned in both the 0 V and 100 V filaments. While both showed obvious signs of alignment the 100 V demonstrated more SWNT chaining, a characteristic common to alignment through dielectrophoresis.[70,73,117] It is clear through SEM imaging that the flow focusing alone established marginal alignment in filaments, however the chaining indicates a strong response to the electric field that and this alignment is directly translated to improved mechanical and electrical performance.

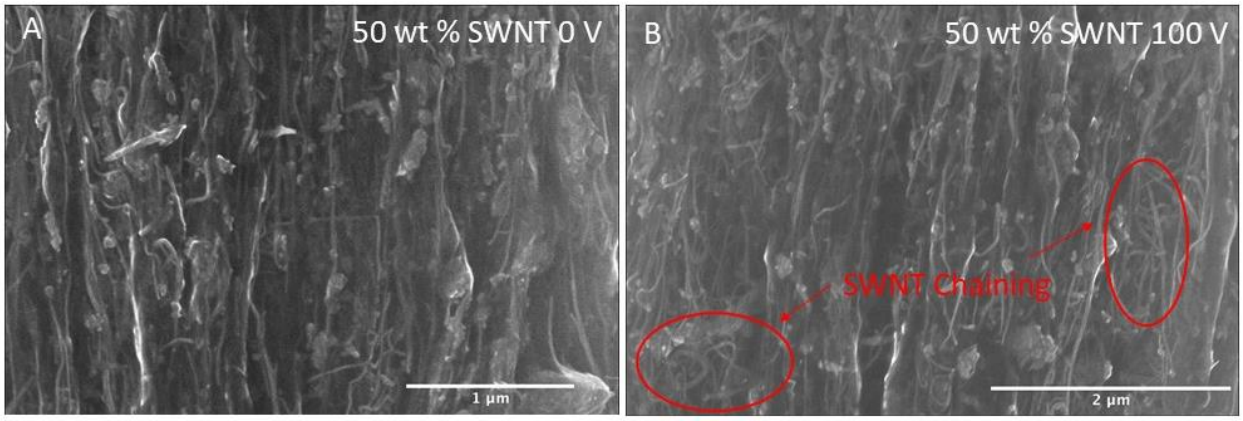

Figure 27. ***(A)*** *Conductive imaging of 50 wt % filament created without an applied electric field showing sub surface SWNTs and a preferential alignment in the longitudinal direction.* ***(B)*** *Conductive imaging of 50 wt % filament with a 100 V applied electric field to show SWNTs below the surface and SWNT bundles circled in red.*

3.6 Mechanical and Electrical Properties of Composite Filaments

All prepared dispersions (0 wt % Pure CNF, 15 wt %, 25 wt %, and 50 wt %) were applied to the electric field flow focusing system with creating filament with both 0 V and 100 V applied electric field to elucidate the response of SWNT content from the applied electric field. The applied

electric field had no significant effect on the mechanical properties of the pure CNF filament, while filaments containing 25 wt % and 50 wt % showed significant improvements. 2D XRD of pure CNF filaments with no applied electric field, indicated that crystalline regions from longer fibers maintain alignment with an f_c = 0.82 while shorter filaments showed no convergence indicating anisotropy is lost (**Figure 28**). This indicates that any improved performance from the applied electric field is likely from the polarization of longer SWNTs coated in CNF because the longer nanotubes more readily resist Brownian motion. While individualized CNF fibers do not maintain alignment the alignment of longer SWNT structures will promote secondary alignment of the wrapped CNF promoting more hydrogen bonding between wrapped elements.

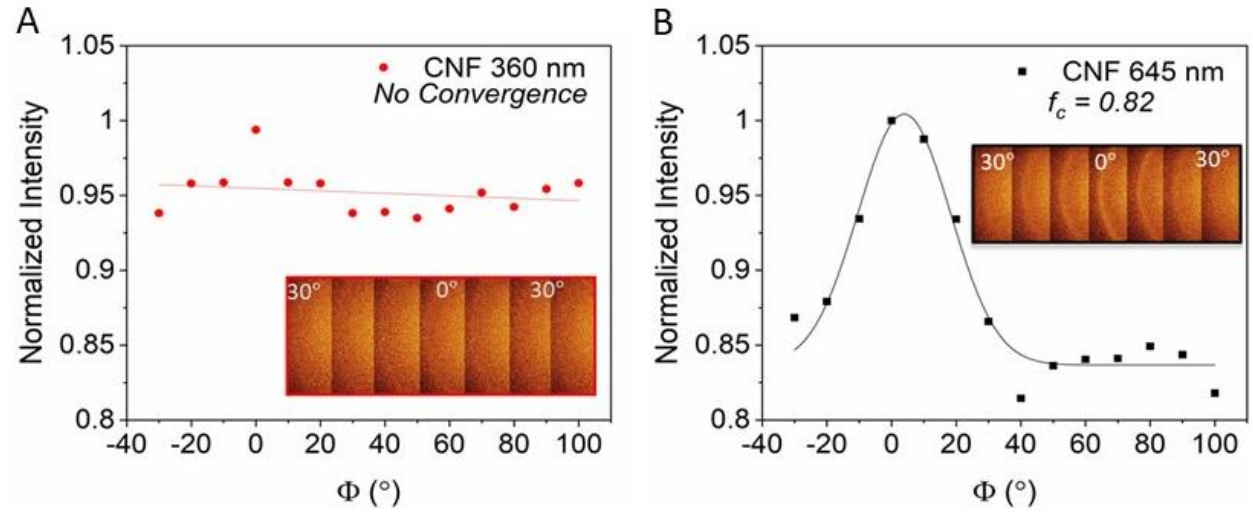

Figure 28*. 2D XRD analysis of CNF alignment within the pure CNF filaments created with no applied electric field. (A) Azimuthal integration of the (200) scattering plane of the diffractograms with respect to Φ rotations for cellulosic filaments prepared with 360 nm CNF fiber length* ***(A)*** *and* ***(B)*** *645 nm fiber length. Filaments created with shorter CNF showed no convergence indicating random orientation of CNF fibers, while longer fibers exhibited a clear inline with the filament axis.*

Although there is no established anisotropy amongst short, individualized CNF, the pure CNF filaments still show the best performance with and without an applied voltage. This indicates the SWNTs behave as a defect that improves with more SWNT mass because the mechanical properties of the SWNTs begin to overtake the composite. However, even the highest loading of SWNTs were still not able to perform as well as the pure CNF filament. The significant decrease in Y oung's modulus of 0 V filaments with SWNTs indicates that they disrupt bonding between CNF fibers overall decreasing mechanical performance compared to the pure CNF filament. This indicates that alignment is critical to increasing filament mechanical performance in addition to good interfacial bonding.

Although without the electric field the SWNTs fail to enhance performance, the minimal 100 V applied electric field becomes a great asset at 25 wt % and 50 wt % increasing the mechanical performance beyond the pure CNF filament capabilities. The applied electric field increased the ultimate tensile strength of the 25 wt % and 50 wt % filaments by 31 % and 16 %, respectively, restoring the ultimate tensile strength to equal the pure CNF filaments at 258 MPa. The 50 wt % created with no applied voltage were successful at recovering the pure CNF filament strain, but with the added 100 V the additional alignment from the electric field surpassed the pure CNF filament strain by 47 % (**Figure 29 A**). This superior strain translated to a 51 % increase in filament toughness beyond the pure CNF filament granting superior mechanical performance to the aligned 50 wt % CNF/SWNT filament. The young's modulus, an indicator of internal bonding, offers a good explanation for the improved mechanical performance with the applied electric field. The applied electric field restored the young's modulus of the 15 wt % and 25 wt % filaments back to the pure CNF filament indicating that alignment improves inter fiber bonding both between all participating components, owing to the improved mechanical performance (**Figure 29 B**). The 50

wt % aligned filament mechanical performance was further improved by increasing the humidity of the testing environment to 35 % improving the UTS by 23 % to 333 MPa.[29,130] This increase in UTS and toughness has been accredited to increase hydrogen bonding density caused by water bridges, however, this phenomenon has an upper limit relative humidity above 60 %.[130]

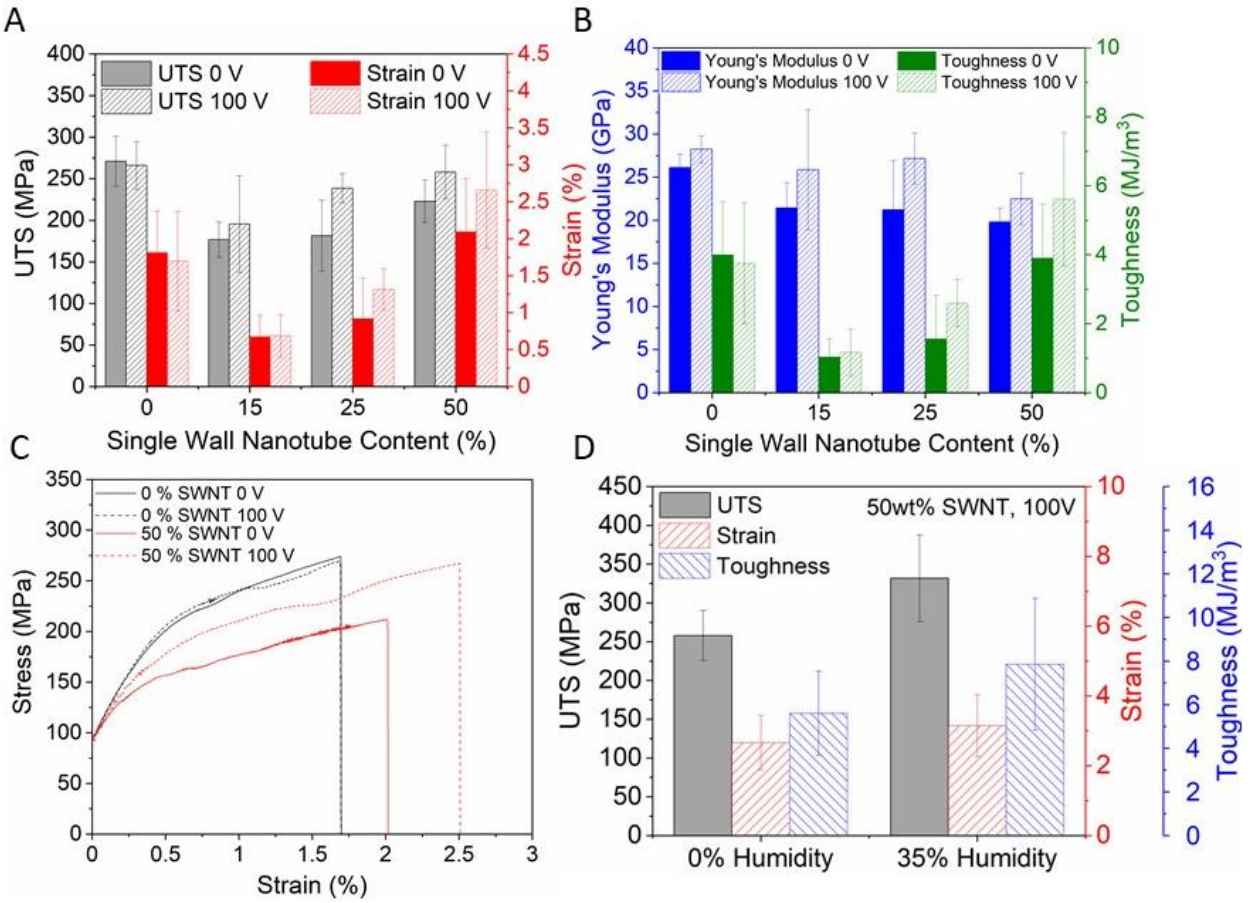

Figure 29**. **(A)** Ultimate tensile strength (UTS) and maximum strain of filaments with and without an applied electric field as a function of SWNT content. Filaments created with a 100 V applied electric field at 50 wt % SWNT showed a significantly higher strain and the same UTS as pure CNF filaments. **(B)** Young's Modulus and Toughness of filaments with and without an applied electric field as a function of SWNT content. The applied electric field improved the young's modulus of 15wt % and 20 wt % filaments to match the performance of pure CNF filaments. **(C)

Representative tensile graph of pure CNF and 50 wt % SWNT filaments prepared at both 0 V and 100 V. ***(D)*** *UTS, Strain and Toughness of a filaments made with 50 wt % SWNT content and a 100 V applied electric field tested with 0 % and 35 % humidity, demonstrating significant increases in the UTS.*

This increased mechanical performance result with 50 wt % SWNT filaments is uniquely different from previous reports of CNF and carbon nanotube composite fibers because no one has been able to recover or improve mechanical performance beyond pure CNF filaments. Typically increasing the carbon nanotube content decreased the mechanical performance and the highest performing loadings were achieved with the lowest nanotube wt % (**Table 1**).[34,124,131,132] This demonstrates the importance of controlled dispersion quality and the significant effects it has on interface between SWNT and CNF, as well as creating a preferred alignment of both composite components. Once again, the applied electric field flow focusing systems ability to individually polarize elements leads to a successful transfer of nano properties to the macro scale through dielectrophoretic continuous nano alignment.

Table 1. *Mechanical properties of different CNF and nanotube aligned filaments created with different carbon nanotube types, loadings, and alignment methods. Differences in humidity are denotes with a "% H" and the method of alignment is denoted in the "Notes" column.*

Author	Carbon Nanotubes (Wt%)	UTS (MPa)	Strain (%)	Youngs (GPa)	Notes:
Hamedi M.	43 SWNT	220	2.1	14	Flow Focusing Channel
Yuan Yuan L.	50 CNT	247	4.5	-	3D printing Method
Haisong Q.	8 MWCNT	78.3	5.2	6.3	Wet Spinning
Zhangmin Wan	50 SWNT	263.2 (12 % H) 223.2 (50 % H)	2.31(12 % H) 4.05(50 % H)	~ 18 or 19 ~15 or 16	Core Shell Structure
This Work	50 SWNT-COOH	258 (0 % H) 331 (30 % H)	2.6 (0 % H) 3.1 (30 % H)	22.4 (0 % H) 14.6 (30 %H)	Electric Field Flow Focusing

This unique nano alignment not only improved the mechanical performance but also the electrical conductivity of filaments.[117,133,134] Filaments with 50 wt % SWNT were mounted on a glass slide using silver adhesive paste and flat nickel chromium wire was attached using the same silver adhesive to extend the electrode for easy hookup. Ohmic contacts were revealed from the linear trend that emerged from current- voltage curves (I-V Curve) created using a wide range of voltages (**Figure 30 C**).[131] Filaments with the applied electric field revealed a 26 % decrease in

resistance from the creation of more intentional end to end junctions between SWNTs. We successfully transformed a dielectric pure CNF filament into a semiconductive filament by incorporating nanotubes, and we were able to increase the conductivity by influencing the SWNT alignment using the applied electric field. A blue LED was lit up using our conductive composite filaments as proof of concept for their applications in small complex electronics. The viability of this conductive composite filament for other complex multifunctional applications was further investigated with an in-situ water sensing system.

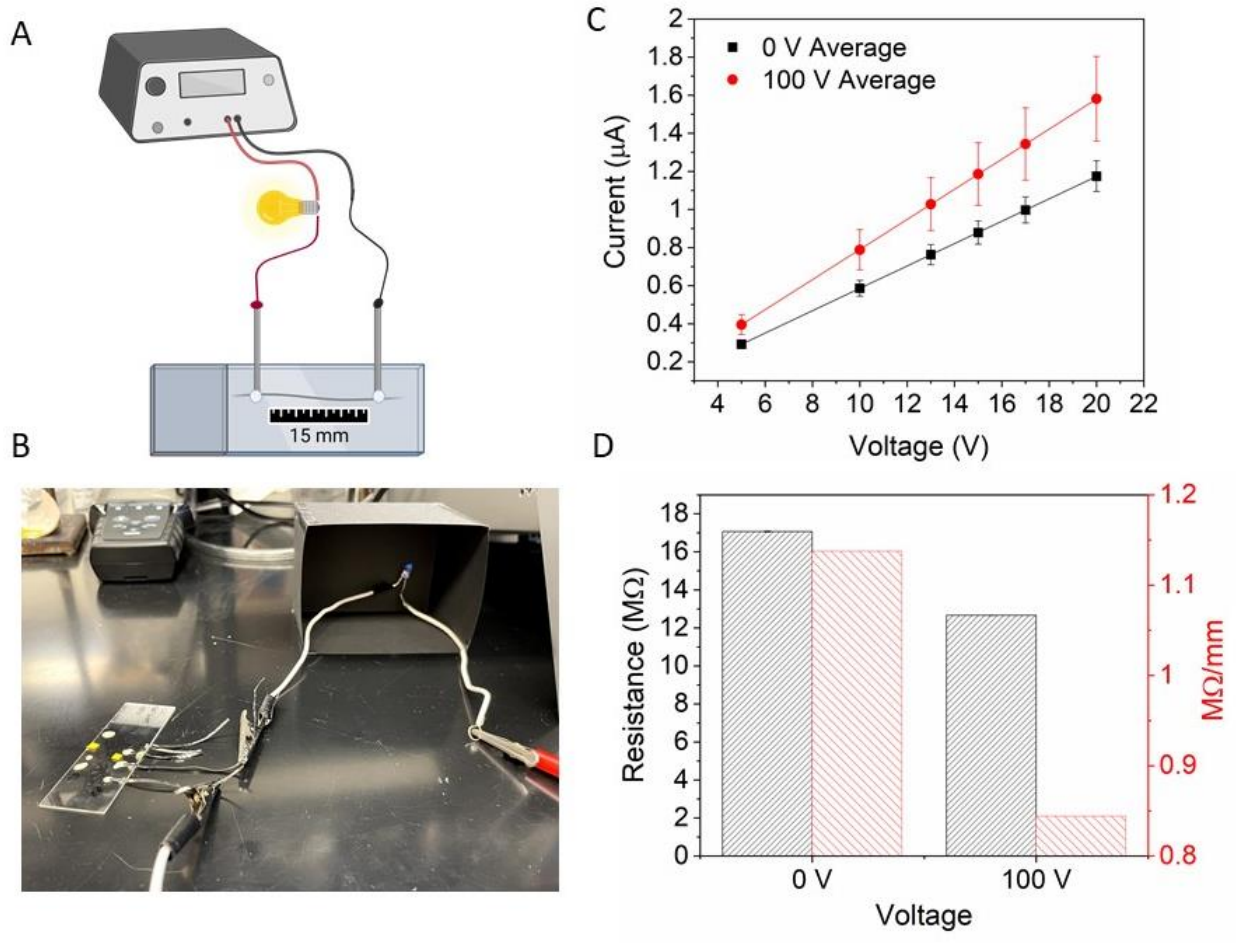

Figure 30*. **(A)** Representative depiction of filament mounting method and inclusion in a circuit with an LED light bulb. **(B)** Photo of the circuit depicted in A demonstrating the successful*

illumination of a blue LED bulb with as little as 5 V supplied via a keithley. ***(C)*** *Current as a function of voltage for 50 wt % filaments created with and without and applied electric field.* ***(D)*** *Resistance measurements of 50wt % filaments mounted at 15 mm in length to be used for future testing and resistance measurements.*

3.7 Application of Conductive Aligned Filaments

The hygroscopic nature of cellulose and intentional small filament microstructure is ideal for piezoresistive water sensing because interruptions in conductivity will be more direct and readily identified unlike most large surface area films.[37,135] Filaments with 50 wt % SWNTs were mounted on a microscope stage with a camera and attached to a Keithley for real-time resistance measurements (**Figure 31**). After identifying the initial filament diameter and resistance a 1 μl drop of water was pipetted onto the filament surface and resistance changes were recorded in tandem with video feed from the attached microscope camera. The filament diameters were then measured by extracting frames every seven tenths of a second and measuring each frames filament diameter.

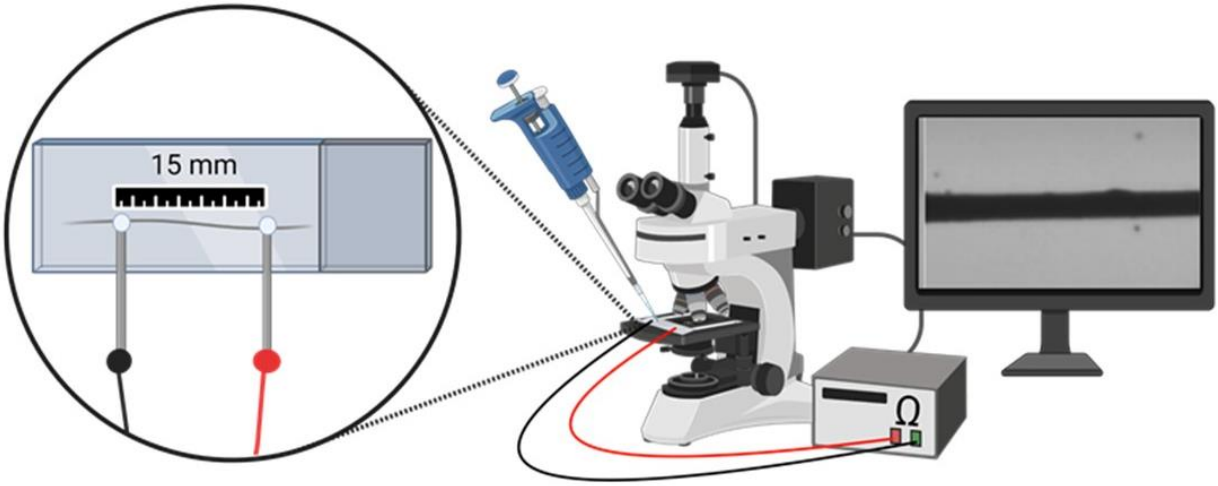

Figure 31*. Schematic of in-situ swelling set up demonstrating continuous real-time measurement of swelling rate and resistance changes. All filaments used for in-situ swelling measurements were 50 wt % SWNT and 15 mm length attached to microscope slide with silver adhesive paste.*

Both filaments exhibited the same initial sharp increase, but those created with the applied electric field revealed a secondary slower upwards trend while the more isotropic fiber exhibited a plateau. The resistance follows the same trend as the relative diameters and although both filaments swell to approximately 80 % relative diameter the aligned filament demonstrated a 1.5 times greater change in relative resistance over the unaligned (**Figure 32 A**). The filament swelling rate for each filament was 11.5 μm/s regardless of applied voltage used during synthesis (**Figure 32 B**). This significant increase in response from aligned filaments is likely due to the intentional junctions created through aligning the SWNTs. Cyclic testing of the filaments revealed that water evaporation does significantly drop the resistance, but it does not return to the starting resistance indicating some structural changes occurred in the filament (**Figure 3 C**). It is possible with a few repeated cycles that the hysteresis would disappear once a new oriented equilibrium nanostructure is achieved.[131] The pre-alignment method was not only key to improving the mechanical

properties, but it also has significant implications on lowering sensing thresholds and increasing sensitivity opening the possibility for numerous other multifunctional applications.

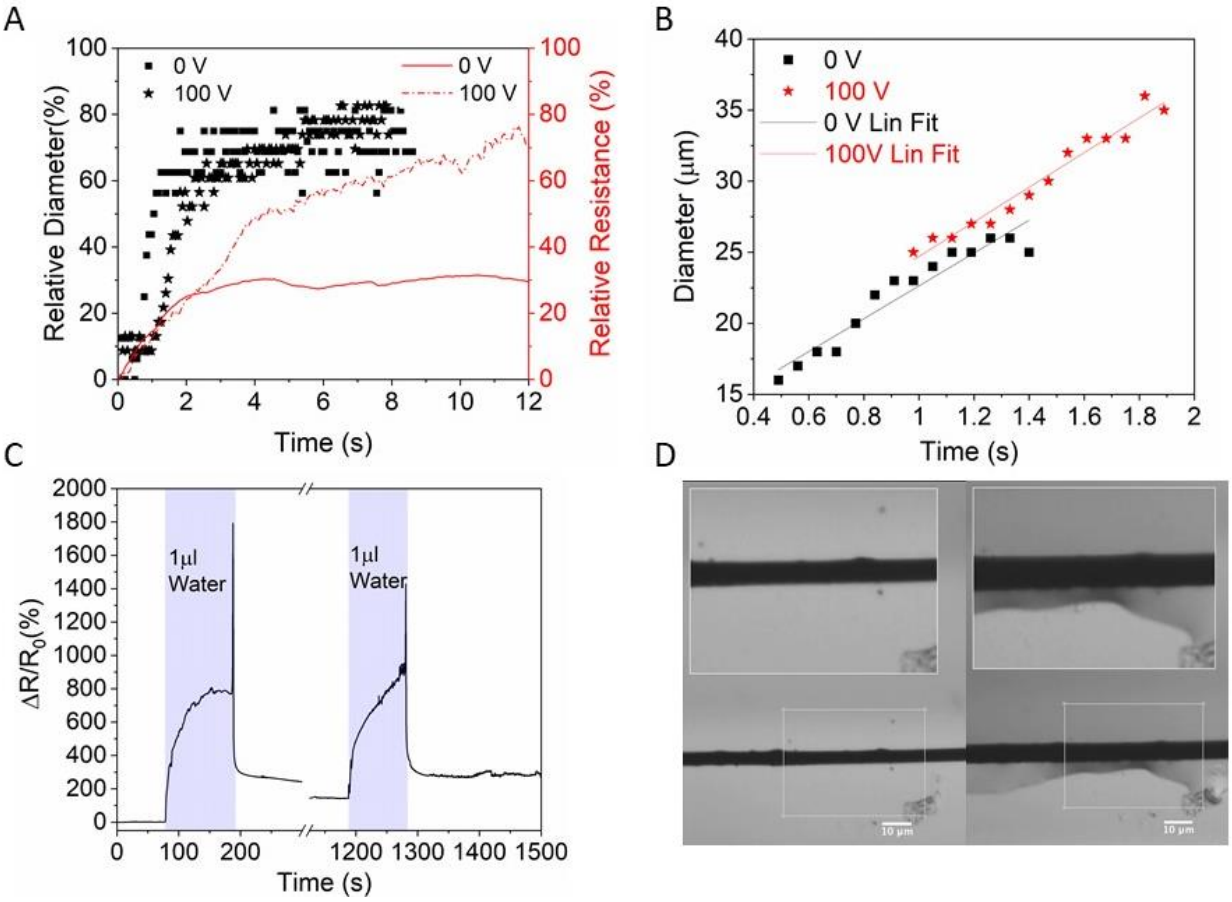

Figure 32. ***(A)*** *Relative swelling diameter and resistance changes after a 1μl drop of water is placed on 50 wt % filament produced with and without an applied electric field.* ***(B)*** *Swelling rate of aligned and unaligned 50 wt % filament with respect to time.* ***(C)*** *Cyclic water sensing of 1μl of water on a 50 wt % filament created with an applied electric field.* ***(D)*** *Microscope images 50 wt % aligned dry filament (left) and swelled filament from water exposure (right).*

3.8 Conclusion

CNF is an ideal sustainable polymeric matrix for creating conductive composites to fill a variety of complex needs involving sensing, biomedical applications, and small electronics. This

material has the added benefit of functioning as a natural dispersant for SWNTs, a necessary component due to the semiconducting nature of CNF, through mechanical wrapping and counterion interactions producing a compound dispersion with a high SWNT loading. Transforming these dispersions into filaments using a novel electric field flow focusing channel establishes anisotropy in SWNTs and improves mechanical performance of the 50 wt % SWNT filaments beyond the possibilities of pure CNF filaments and other reported CNF and nanotube composite filaments. This alignment not only directly benefits the mechanical performance, but the conductivity is also significantly increased through intentional junctions created from the SWNT alignment. This increased conductivity from alignment also translates to a higher sensitivity and a better performance overall creating sustainable multifunctional composite filament.

IV. Conclusion and Future Work

Nanocellulose is a promising alternative material to petroleum-based products offering a sustainable alternative source, but its success is dependent on its ability to fill a multitude of functionalities. This nanocellulose is a unique alternative its traits can be tailored through manipulation of its structure and thus properties.

Using a chemi-mechanical synthesis, TEMPO oxidation, we have demonstrated independent control over two critical characteristics, surface charge and fiber aspect ratio. These two traits determine the dispersion quality and dictate the future product formation as well as the successful transfer of desirable properties from the nano to the micro and macro scale. Surface charge can be controlled from approximately 0.35-1.2 mmol COOH/g CNF by tailoring the oxidation time or sodium hypochlorite concentration. Controlling the oxidation step can dictate the starting macro fiber size, but mechanical defibrillation is the primary step used to control the nano fiber aspect ratio. Nanofiber length can be decreased by increasing time and severity of mechanical defibrillation. Controlling these properties individually allows a wide variety of fiber size and surface charge combinations allowing the nanostructure to specifically be tailored to the pre-alignment process or other diverse applications.

The key to capturing the unique nano properties of CNF at the macro scale is mimicking the fiber alignment found in nature. Pre-alignment methods involving alignment before fiber fixation, offer more potential to produce a highly aligned, strong, and continuous materials as opposed to post-alignment methods. Using the knowledge gained from previous work tailored polar moieties were established on the CNF surface via controlled oxidation enabling strong polarization and spontaneous alignment of dipoles under an applied external electric field, which significantly improved the downstream nematic ordering of CNFs despite diffusion caused by Brownian motion. Fiber lengths were tailored to the appropriate length to maintain alignment from electric

field and mechanical properties of individual CNF fibers. While the upstream field-assisted alignment enhanced the CNF ordering both on the filament surface and in the bulk, its effect became dominant once a threshold voltage was applied. Filaments produced at 600 V_{pp} had greater optical anisotropy and exhibited a 16 % augmentation in orientation index compared to filaments prepared without an AC external field. The high orientation degree of CNFs observed using 2D-XRD combined with their dense packing yielded impressive improvements in the mechanical properties of the resulting filaments, with up to 120 % increase in toughness without compromising the material's stiffness. These results demonstrate for the first time that an external electric field can be applied in a continuous flow process taking advantage of individual nano fiber ordering from the electric field and quick fiber fixation offered from the flow focusing to create anisotropic continuous filaments. These strong filaments can be applied as pure cellulose textile or as a base alternative to plastic fibers. This filament was further adapted to demonstrate its ability to fill more complex functionalities such as small electronics or sensors.

CNF lacks the natural conductivity necessary to perform complex functionalities commonly associated with sensors or small electronics, but through incorporation of a secondary conductive filler, SWNTs, we created a conductive CNF/SWNT composite filament. Typically, a surfactant is required to successfully disperse SWNTs, but by tailoring CNF surface charge it acts as a natural dispersant for SWNTs. Understanding the dispersion mechanism to be mechanical wrapping and counterion interactions allowed us to produce a compound dispersion with a high SWNT loading and an aligned uniform filament. Transforming these dispersions into filaments using the novel electric field flow focusing channel established anisotropy in SWNTs and improved mechanical performance of the 50 wt % SWNT filaments beyond the possibilities of pure CNF filaments and other reported CNF and nanotube composite filaments. This alignment

also significantly increased filament conductivity by creating intentional junctions between SWNTs demonstrating potential to function in small electronics and sensors. Taking advantage of the hygroscopic nature of cellulose and the filament geometry, we displayed the filament performance as a humidity sensor and aligned filaments showed a higher sensitivity to liquid water. This conductive filament and its demonstration as a water sensor demonstrates the potential for CNF to function to fill multiple applications.

The impact of this work goes beyond the direct applications displayed here and can extend to all applications involving polymer-based networks or other petroleum products, most notably biomedical fields. The aligned CNF filament's biocompatibility could have major implications in tissue engineering.[46] Scaffolds for cellular regrowth in tissues engineering face many challenges including size control, porosity, and biocompatibility among other traits, but the tailorable nature of CNF displayed in this work allows us to achieve all the desired traits in one material. The hydrogel nature, micron size, and natural biocompatibility of the created CNF filament when it exited the channel is ideal for cellular growth and the tunability of factors give the potential scaffold an adaptability to grow many different cellular types.[136] Our novel alignment method is also unique and could be used to grow more complex tissues that require aligned scaffolds to encourage anisotropic striated muscle tissue growth. This continuous aligned filament can have major implications in aligned organoid growth and 3D cellular printing.

In addition to the innate properties of CNF obvious to applications in the biomedical field, the filament itself can be improved upon with the addition of crosslinkers to improve strength properties extending the range of applications. There is also great potential in adding other secondary compounds to change the material properties such as magnetic nanoparticles. Overall,

this work has implications that provide insight into multiple adaptations that could be used to improve and expand the filament and its functionality.

V. References

(1) Hess, J.; Bednarz, D.; Bae, J.; Pierce, J. Petroleum and Health Care: Evaluating and Managing Health Care's Vulnerability to Petroleum Supply Shifts. *Am J Public Health* **2011**, *101* (9), 1568–1579. https://doi.org/10.2105/AJPH.2011.300233.

(2) Hartline, N. L.; Bruce, N. J.; Karba, S. N.; Ruff, E. O.; Sonar, S. U.; Holden, P. A. Microfiber Masses Recovered from Conventional Machine Washing of New or Aged Garments. *Environ. Sci. Technol.* **2016**, *50* (21), 11532–11538. https://doi.org/10.1021/acs.est.6b03045.

(3) Dris, R.; Gasperi, J.; Saad, M.; Mirande, C.; Tassin, B. Synthetic Fibers in Atmospheric Fallout: A Source of Microplastics in the Environment? *Marine Pollution Bulletin* **2016**, *104* (1), 290–293. https://doi.org/10.1016/j.marpolbul.2016.01.006.

(4) Moore, C. J.; Moore, S. L.; Leecaster, M. K.; Weisberg, S. B. A Comparison of Plastic and Plankton in the North Pacific Central Gyre. *Marine Pollution Bulletin* **2001**, *42* (12), 1297–1300. https://doi.org/10.1016/S0025-326X(01)00114-X.

(5) Woods, M. N.; Hong, T. J.; Baughman, D.; Andrews, G.; Fields, D. M.; Matrai, P. A. Accumulation and Effects of Microplastic Fibers in American Lobster Larvae (Homarus Americanus). *Marine Pollution Bulletin* **2020**, *157*, 111280. https://doi.org/10.1016/j.marpolbul.2020.111280.

(6) Hansmann, R.; Mieg, H. A.; Frischknecht, P. Principal Sustainability Components: Empirical Analysis of Synergies between the Three Pillars of Sustainability. *International Journal of Sustainable Development & World Ecology* **2012**, *19* (5), 451–459. https://doi.org/10.1080/13504509.2012.696220.

(7) Puspasari, T.; Pradeep, N.; Peinemann, K.-V. Crosslinked Cellulose Thin Film Composite Nanofiltration Membranes with Zero Salt Rejection. *Journal of Membrane Science* **2015**, *491*, 132–137. https://doi.org/10.1016/j.memsci.2015.05.002.

(8) Tayeb, A. H.; Amini, E.; Ghasemi, S.; Tajvidi, M. Cellulose Nanomaterials—Binding Properties and Applications: A Review. *Molecules* **2018**, *23* (10). https://doi.org/10.3390/molecules23102684.

(9) Miyashiro, D.; Hamano, R.; Umemura, K. A Review of Applications Using Mixed Materials of Cellulose, Nanocellulose and Carbon Nanotubes. *Nanomaterials* **2020**, *10* (2), 186. https://doi.org/10.3390/nano10020186.

(10) Jozala, A. F.; de Lencastre-Novaes, L. C.; Lopes, A. M.; de Carvalho Santos-Ebinuma, V.; Mazzola, P. G.; Pessoa-Jr, A.; Grotto, D.; Gerenutti, M.; Chaud, M. V. Bacterial Nanocellulose Production and Application: A 10-Year Overview. *Appl Microbiol Biotechnol* **2016**, *100* (5), 2063–2072. https://doi.org/10.1007/s00253-015-7243-4.

(11) Kang, Y. J.; Chun, S.-J.; Lee, S.-S.; Kim, B.-Y.; Kim, J. H.; Chung, H.; Lee, S.-Y.; Kim, W. All-Solid-State Flexible Supercapacitors Fabricated with Bacterial Nanocellulose Papers, Carbon Nanotubes, and Triblock-Copolymer Ion Gels. *ACS Nano* **2012**, *6* (7), 6400–6406. https://doi.org/10.1021/nn301971r.

(12) Lee, W. J.; Clancy, A. J.; Kontturi, E.; Bismarck, A.; Shaffer, M. S. P. Strong and Stiff: High-Performance Cellulose Nanocrystal/Poly(Vinyl Alcohol) Composite Fibers. *ACS Appl. Mater. Interfaces* **2016**, *8* (46), 31500–31504. https://doi.org/10.1021/acsami.6b11578.

(13) Isogai, A.; Saito, T.; Fukuzumi, H. TEMPO-Oxidized Cellulose Nanofibers. *Nanoscale* **2011**, *3* (1), 71–85. https://doi.org/10.1039/C0NR00583E.

(14) Thomas, B.; Raj, M. C.; B, A. K.; H, R. M.; Joy, J.; Moores, A.; Drisko, G. L.; Sanchez, C. Nanocellulose, a Versatile Green Platform: From Biosources to Materials and Their Applications. *Chem. Rev.* **2018**, *118* (24), 11575–11625. https://doi.org/10.1021/acs.chemrev.7b00627.
(15) Zhu, Q.; Yao, Q.; Sun, J.; Chen, H.; Xu, W.; Liu, J.; Wang, Q. Stimuli Induced Cellulose Nanomaterials Alignment and Its Emerging Applications: A Review. *Carbohydrate Polymers* **2020**, *230*, 115609. https://doi.org/10.1016/j.carbpol.2019.115609.
(16) Plomion, C.; Leprovost, G.; Stokes, A. Wood Formation in Trees. *Plant Physiology* **2001**, *127* (4), 1513–1523.
(17) Chen, C.; Hu, L. Nanocellulose toward Advanced Energy Storage Devices: Structure and Electrochemistry. *Acc. Chem. Res.* **2018**, *51* (12), 3154–3165. https://doi.org/10.1021/acs.accounts.8b00391.
(18) Fall, A. B.; Lindström, S. B.; Sprakel, J.; Wågberg, L. A Physical Cross-Linking Process of Cellulose Nanofibril Gels with Shear-Controlled Fibril Orientation. *Soft Matter* **2013**, *9* (6), 1852–1863. https://doi.org/10.1039/C2SM27223G.
(19) Sehaqui, H.; Ezekiel Mushi, N.; Morimune, S.; Salajkova, M.; Nishino, T.; Berglund, L. A. Cellulose Nanofiber Orientation in Nanopaper and Nanocomposites by Cold Drawing. *ACS Appl Mater Interfaces* **2012**, *4* (2), 1043–1049. https://doi.org/10.1021/am2016766.
(20) Tang, H.; Butchosa, N.; Zhou, Q. A Transparent, Hazy, and Strong Macroscopic Ribbon of Oriented Cellulose Nanofibrils Bearing Poly(Ethylene Glycol). *Adv. Mater. Weinheim* **2015**, *27* (12), 2070–2076. https://doi.org/10.1002/adma.201404565.
(21) Kadimi, A.; Benhamou, K.; Habibi, Y.; Ounaies, Z.; Kaddami, H. Chapter 11 - Nanocellulose Alignment and Electrical Properties Improvement. In *Multifunctional Polymeric Nanocomposites Based on Cellulosic Reinforcements*; Puglia, D., Fortunati, E., Kenny, J. M., Eds.; William Andrew Publishing, 2016; pp 343–376. https://doi.org/10.1016/B978-0-323-44248-0.00011-0.
(22) Bordel, D.; Putaux, J.-L.; Heux, L. Orientation of Native Cellulose in an Electric Field. *Langmuir* **2006**, *22* (11), 4899–4901. https://doi.org/10.1021/la0600402.
(23) Choi, K.; Gao, C. Y.; Nam, J. D.; Choi, H. J. Cellulose-Based Smart Fluids under Applied Electric Fields. *Materials (Basel)* **2017**, *10* (9). https://doi.org/10.3390/ma10091060.
(24) Xu, S.; Liu, D.; Zhang, Q.; Fu, Q. Electric Field-Induced Alignment of Nanofibrillated Cellulose in Thermoplastic Polyurethane Matrix. *Composites Science and Technology* **2018**, *156*, 117–126. https://doi.org/10.1016/j.compscitech.2017.12.017.
(25) Kim, H. C.; Kang, J.; Park, J. H.; Akther, A.; Kim, J. Feasibility Study of Cellulose Nanofiber Alignment by High DC Magnetic Field. In *Nanosensors, Biosensors, Info-Tech Sensors and 3D Systems 2017*; International Society for Optics and Photonics, 2017; Vol. 10167, p 101670H. https://doi.org/10.1117/12.2259830.
(26) Sugiyama, J.; Chanzy, H.; Maret, G. Orientation of Cellulose Microcrystals by Strong Magnetic Fields. *Macromolecules* **1992**, *25* (16), 4232–4234. https://doi.org/10.1021/ma00042a032.
(27) Kimura, F.; Kimura, T.; Tamura, M.; Hirai, A.; Ikuno, M.; Horii, F. Magnetic Alignment of the Chiral Nematic Phase of a Cellulose Microfibril Suspension. *Langmuir* **2005**, *21* (5), 2034–2037. https://doi.org/10.1021/la0475728.

(28) Kim, J.; Chen, Y.; Kang, K.-S.; Park, Y.-B.; Schwartz, M. Magnetic Field Effect for Cellulose Nanofiber Alignment. *Journal of Applied Physics* **2008**, *104* (9), 096104. https://doi.org/10.1063/1.3006140.
(29) Mittal, N.; Ansari, F.; Gowda.V, K.; Brouzet, C.; Chen, P.; Larsson, P. T.; Roth, S. V.; Lundell, F.; Wågberg, L.; Kotov, N. A.; Söderberg, L. D. Multiscale Control of Nanocellulose Assembly: Transferring Remarkable Nanoscale Fibril Mechanics to Macroscale Fibers. *ACS Nano* **2018**, *12* (7), 6378–6388. https://doi.org/10.1021/acsnano.8b01084.
(30) Smith, D. E.; Babcock, H. P.; Chu, S. Single-Polymer Dynamics in Steady Shear Flow. *Science* **1999**, *283* (5408), 1724–1727. https://doi.org/10.1126/science.283.5408.1724.
(31) Håkansson, K. M. O.; Fall, A. B.; Lundell, F.; Yu, S.; Krywka, C.; Roth, S. V.; Santoro, G.; Kvick, M.; Prahl Wittberg, L.; Wågberg, L.; Söderberg, L. D. Hydrodynamic Alignment and Assembly of Nanofibrils Resulting in Strong Cellulose Filaments. *Nature Communications* **2014**, *5*, 4018. https://doi.org/10.1038/ncomms5018.
(32) Mittal, N.; Benselfelt, T.; Ansari, F.; Gordeyeva, K.; Roth, S. V.; Wågberg, L.; Söderberg, L. D. Ion-Specific Assembly of Strong, Tough, and Stiff Biofibers. *Angewandte Chemie International Edition* **2019**, *58* (51), 18562–18569. https://doi.org/10.1002/anie.201910603.
(33) Rosén, T.; Mittal, N.; Roth, S. V.; Zhang, P.; Lundell, F.; Söderberg, L. D. Flow Fields Control Nanostructural Organization in Semiflexible Networks. *Soft Matter* **2020**, *16* (23), 5439–5449. https://doi.org/10.1039/C9SM01975H.
(34) Hamedi, M. M.; Hajian, A.; Fall, A. B.; Håkansson, K.; Salajkova, M.; Lundell, F.; Wågberg, L.; Berglund, L. A. Highly Conducting, Strong Nanocomposites Based on Nanocellulose-Assisted Aqueous Dispersions of Single-Wall Carbon Nanotubes. *ACS Nano* **2014**, *8* (3), 2467–2476. https://doi.org/10.1021/nn4060368.
(35) Fake Silk | Yale University Press https://yalebooks.yale.edu/book/9780300204667/fake-silk (accessed May 8, 2021).
(36) S; Evans, ra. 3 Fatalities Haunt Rayon Mill Workers. *Washington Post*. December 23, 1986.
(37) Guo, W.; Liu, C.; Sun, X.; Yang, Z.; Kia, H. G.; Peng, H. Aligned Carbon Nanotube/Polymer Composite Fibers with Improved Mechanical Strength and Electrical Conductivity. *J. Mater. Chem.* **2011**, *22* (3), 903–908. https://doi.org/10.1039/C1JM13769G.
(38) Klemm, D.; Kramer, F.; Moritz, S.; Lindström, T.; Ankerfors, M.; Gray, D.; Dorris, A. Nanocelluloses: A New Family of Nature-Based Materials. *Angewandte Chemie International Edition* **2011**, *50* (24), 5438–5466. https://doi.org/10.1002/anie.201001273.
(39) Portela da Gama, F. M.; Dourado, F. Bacterial NanoCellulose: What Future? *Bioimpacts* **2018**, *8* (1), 1–3. https://doi.org/10.15171/bi.2018.01.
(40) Phanthong, P.; Reubroycharoen, P.; Hao, X.; Xu, G.; Abudula, A.; Guan, G. Nanocellulose: Extraction and Application. *Carbon Resources Conversion* **2018**, *1* (1), 32–43. https://doi.org/10.1016/j.crcon.2018.05.004.
(41) Bin, L.; Xu, C.; Kronlund, D.; Eriksson, J.-E.; Määttänen, A.; Willför, S.; Xu, W. Comparable characterization of nanocellulose extracted from bleached softwood and hardwood pulps. *Paper and Biomaterials* **2018**, *3* (4).
(42) Abdul Khalil, H. P. S.; Davoudpour, Y.; Islam, M. N.; Mustapha, A.; Sudesh, K.; Dungani, R.; Jawaid, M. Production and Modification of Nanofibrillated Cellulose Using

Various Mechanical Processes: A Review. *Carbohydr Polym* **2014**, *99*, 649–665. https://doi.org/10.1016/j.carbpol.2013.08.069.
(43) Bondeson, D.; Mathew, A.; Oksman, K. Optimization of the Isolation of Nanocrystals from Microcrystalline Celluloseby Acid Hydrolysis. *Cellulose* **2006**, *13* (2), 171. https://doi.org/10.1007/s10570-006-9061-4.
(44) Johar, N.; Ahmad, I.; Dufresne, A. Extraction, Preparation and Characterization of Cellulose Fibres and Nanocrystals from Rice Husk. *Industrial Crops and Products* **2012**, *37* (1), 93–99. https://doi.org/10.1016/j.indcrop.2011.12.016.
(45) Siró, I.; Plackett, D. Microfibrillated Cellulose and New Nanocomposite Materials: A Review. *Cellulose* **2010**, *17* (3), 459–494. https://doi.org/10.1007/s10570-010-9405-y.
(46) Khakalo, A.; Mäkelä, T.; Johansson, L.-S.; Orelma, H.; Tammelin, T. High-Throughput Tailoring of Nanocellulose Films: From Complex Bio-Based Materials to Defined Multifunctional Architectures. *ACS Appl. Bio Mater.* **2020**, *3* (11), 7428–7438. https://doi.org/10.1021/acsabm.0c00576.
(47) Chin, K.-M.; Ting, S. S.; Ong, H. L.; Omar, M. Surface Functionalized Nanocellulose as a Veritable Inclusionary Material in Contemporary Bioinspired Applications: A Review. *Journal of Applied Polymer Science* **2018**, *135* (13), 46065. https://doi.org/10.1002/app.46065.
(48) Saito, T.; Nishiyama, Y.; Putaux, J.-L.; Vignon, M.; Isogai, A. Homogeneous Suspensions of Individualized Microfibrils from TEMPO-Catalyzed Oxidation of Native Cellulose. *Biomacromolecules* **2006**, *7* (6), 1687–1691. https://doi.org/10.1021/bm060154s.
(49) Sun, B.; Gu, C.; Ma, J.; Liang, B. Kinetic Study on TEMPO-Mediated Selective Oxidation of Regenerated Cellulose. *Cellulose* **2005**, *12* (1), 59–66. https://doi.org/10.1023/B:CELL.0000049409.56806.da.
(50) Tahiri, C.; Vignon, M. R. TEMPO-Oxidation of Cellulose: Synthesis and Characterisation of Polyglucuronans. *Cellulose* **2000**, *7* (2), 177–188. https://doi.org/10.1023/A:1009276009711.
(51) Isogai, A.; Kato, Y. Preparation of Polyuronic Acid from Cellulose by TEMPO-Mediated Oxidation. *Cellulose* **1998**, *5* (3), 153–164. https://doi.org/10.1023/A:1009208603673.
(52) Hastuti, N.; Kanomata, K.; Kitaoka, T. Characteristics of TEMPO-Oxidized Cellulose Nanofibers from Oil Palm Empty Fruit Bunches Produced by Different Amounts of Oxidant. *IOP Conf. Ser.: Earth Environ. Sci.* **2019**, *359*, 012008. https://doi.org/10.1088/1755-1315/359/1/012008.
(53) Rattaz, A.; Mishra, S. P.; Chabot, B.; Daneault, C. Cellulose Nanofibres by Sonocatalysed-TEMPO-Oxidation. *Cellulose* **2011**, *18* (3), 585. https://doi.org/10.1007/s10570-011-9529-8.
(54) Ibert, M.; Marsais, F.; Merbouh, N.; Brückner, C. Determination of the Side-Products Formed during the Nitroxide-Mediated Bleach Oxidation of Glucose to Glucaric Acid. *Carbohydr. Res.* **2002**, *337* (11), 1059–1063. https://doi.org/10.1016/s0008-6215(02)00072-1.
(55) Park, K.-M.; Kim, Y. N.; Choi, S. J.; Park, J.-H.; Chang, P.-S. Chemoselective Oxidation of C6 Primary Hydroxyl Groups of Polysaccharides in Rice Bran for the Application as a Novel Water-Soluble Dietary Fiber. *International Journal of Food Properties* **2015**, *18* (8), 1664–1676. https://doi.org/10.1080/10942912.2014.926370.

(56) Levanič, J.; Šenk, V. P.; Nadrah, P.; Poljanšek, I.; Oven, P.; Haapala, A. Analyzing TEMPO-Oxidized Cellulose Fiber Morphology: New Insights into Optimization of the Oxidation Process and Nanocellulose Dispersion Quality. *ACS Sustainable Chem. Eng.* **2020**, *8* (48), 17752–17762. https://doi.org/10.1021/acssuschemeng.0c05989.

(57) Mohammadi, P.; Toivonen, M. S.; Ikkala, O.; Wagermaier, W.; Linder, M. B. Aligning Cellulose Nanofibril Dispersions for Tougher Fibers. *Scientific Reports* **2017**, *7* (1), 1–10. https://doi.org/10.1038/s41598-017-12107-x.

(58) Reising, A. B.; Moon, R. J.; Youngblood, J. P. Effect of Particle Alignment on Mechanical Properties of Neat Cellulose Nanocrystal Films. *Journal of Science & Technology for Forest Products and Processes: Volume 2, Number 6, 2012; pp. 32-41.* **2012**, *2* (6), 32–41.

(59) Wang, S.; Jiang, F.; Xu, X.; Kuang, Y.; Fu, K.; Hitz, E.; Hu, L. Super-Strong, Super-Stiff Macrofibers with Aligned, Long Bacterial Cellulose Nanofibers. *Advanced Materials* **2017**, *29* (35), 1702498. https://doi.org/10.1002/adma.201702498.

(60) Kafy, A.; Kim, H. C.; Zhai, L.; Kim, J. W.; Hai, L. V.; Kang, T. J.; kim, J. Cellulose Long Fibers Fabricated from Cellulose Nanofibers and Its Strong and Tough Characteristics. *Sci Rep* **2017**, *7*. https://doi.org/10.1038/s41598-017-17713-3.

(61) Pullawan, T.; Wilkinson, A. N.; Eichhorn, S. J. Influence of Magnetic Field Alignment of Cellulose Whiskers on the Mechanics of All-Cellulose Nanocomposites. *Biomacromolecules* **2012**, *13* (8), 2528–2536. https://doi.org/10.1021/bm300746r.

(62) Takana, H.; Guo, M. Numerical Simulation on Electrostatic Alignment Control of Cellulose Nano-Fibrils in Flow. *Nanotechnology* **2020**. https://doi.org/10.1088/1361-6528/ab703d.

(63) Mittal, N.; Ansari, F.; Gowda.V, K.; Brouzet, C.; Chen, P.; Larsson, P. T.; Roth, S. V.; Lundell, F.; Wågberg, L.; Kotov, N. A.; Söderberg, L. D. Multiscale Control of Nanocellulose Assembly: Transferring Remarkable Nanoscale Fibril Mechanics to Macroscale Fibers. *ACS Nano* **2018**, *12* (7), 6378–6388. https://doi.org/10.1021/acsnano.8b01084.

(64) Håkansson, K. M. O.; Lundell, F.; Prahl-Wittberg, L.; Söderberg, L. D. Nanofibril Alignment in Flow Focusing: Measurements and Calculations. *J. Phys. Chem. B* **2016**, *120* (27), 6674–6686. https://doi.org/10.1021/acs.jpcb.6b02972.

(65) Nechyporchuk, O.; Håkansson, K. M. O.; Gowda.V, K.; Lundell, F.; Hagström, B.; Köhnke, T. Continuous Assembly of Cellulose Nanofibrils and Nanocrystals into Strong Macrofibers through Microfluidic Spinning. *Advanced Materials Technologies* **2019**, *4* (2), 1800557. https://doi.org/10.1002/admt.201800557.

(66) Mredha, M. T. I.; Le, H. H.; Tran, V. T.; Trtik, P.; Cui, J.; Jeon, I. Anisotropic Tough Multilayer Hydrogels with Programmable Orientation. *Mater. Horiz.* **2019**, *6* (7), 1504–1511. https://doi.org/10.1039/C9MH00320G.

(67) Gupta, P.; Rajput, M.; Singla, N.; Kumar, V.; Lahiri, D. Electric Field and Current Assisted Alignment of CNT inside Polymer Matrix and Its Effects on Electrical and Mechanical Properties. *Polymer* **2016**, *89*, 119–127. https://doi.org/10.1016/j.polymer.2016.02.025.

(68) Oliva-Avilés, A. I.; Avilés, F.; Sosa, V.; Oliva, A. I.; Gamboa, F. Dynamics of Carbon Nanotube Alignment by Electric Fields. *Nanotechnology* **2012**, *23* (46), 465710. https://doi.org/10.1088/0957-4484/23/46/465710.

(69) Chen, X. Q.; Saito, T.; Yamada, H.; Matsushige, K. Aligning Single-Wall Carbon Nanotubes with an Alternating-Current Electric Field. *Appl. Phys. Lett.* **2001**, *78* (23), 3714–3716. https://doi.org/10.1063/1.1377627.
(70) Habibi, Y.; Heim, T.; Douillard, R. AC Electric Field-Assisted Assembly and Alignment of Cellulose Nanocrystals Part B Polymer Physics. **2008**.
(71) Kalidindi, S.; Ounaies, Z.; Kaddami, H. Toward the Preparation of Nanocomposites with Oriented Fillers: Electric Field-Manipulation of Cellulose Whiskers in Silicone Oil. *Smart Mater. Struct.* **2010**, *19* (9), 094002. https://doi.org/10.1088/0964-1726/19/9/094002.
(72) Aguié-Béghin, V.; Molinari, M.; Hambardzumyan, A.; Foulon, L.; Habibi, Y.; Heim, T.; Blossey, R.; Douillard, R. Preparation of Ordered Films of Cellulose Nanocrystals. In *Model Cellulosic Surfaces*; ACS Symposium Series; American Chemical Society, 2009; Vol. 1019, pp 115–136. https://doi.org/10.1021/bk-2009-1019.ch005.
(73) Kadimi, A.; Benhamou, K.; Ounaies, Z.; Magnin, A.; Dufresne, A.; Kaddami, H.; Raihane, M. Electric Field Alignment of Nanofibrillated Cellulose (NFC) in Silicone Oil: Impact on Electrical Properties. *ACS Appl. Mater. Interfaces* **2014**, *6* (12), 9418–9425. https://doi.org/10.1021/am501808h.
(74) Xu, S.; Liu, D.; Zhang, Q.; Fu, Q. Electric Field-Induced Alignment of Nanofibrillated Cellulose in Thermoplastic Polyurethane Matrix. *Composites Science and Technology* **2018**, *156*, 117–126. https://doi.org/10.1016/j.compscitech.2017.12.017.
(75) Tatsumi, M.; Kimura, F.; Kimura, T.; Teramoto, Y.; Nishio, Y. Anisotropic Polymer Composites Synthesized by Immobilizing Cellulose Nanocrystal Suspensions Specifically Oriented under Magnetic Fields. *Biomacromolecules* **2014**, *15* (12), 4579–4589. https://doi.org/10.1021/bm501629g.
(76) Ten, E.; Jiang, L.; Wolcott, M. P. Preparation and Properties of Aligned Poly(3-Hydroxybutyrate-Co-3-Hydroxyvalerate)/Cellulose Nanowhiskers Composites. *Carbohydrate Polymers* **2013**, *92* (1), 206–213. https://doi.org/10.1016/j.carbpol.2012.09.033.
(77) Csoka, L.; Hoeger, I. C.; Peralta, P.; Peszlen, I.; Rojas, O. J. Dielectrophoresis of Cellulose Nanocrystals and Alignment in Ultrathin Films by Electric Field-Assisted Shear Assembly. *J Colloid Interface Sci* **2011**, *363* (1), 206–212. https://doi.org/10.1016/j.jcis.2011.07.045.
(78) Lebreton, L. C. M.; van der Zwet, J.; Damsteeg, J.-W.; Slat, B.; Andrady, A.; Reisser, J. River Plastic Emissions to the World's Oceans. *Nature Communications* **2017**, *8* (1), 1–10. https://doi.org/10.1038/ncomms15611.
(79) Goodman, S. M.; Ferguson, N.; Dichiara, A. B. Lignin-Assisted Double Acoustic Irradiation for Concentrated Aqueous Dispersions of Carbon Nanotubes. *RSC Adv.* **2017**, *7* (9), 5488–5496. https://doi.org/10.1039/C6RA25986C.
(80) Isogai, A.; Saito, T.; Fukuzumi, H. TEMPO-Oxidized Cellulose Nanofibers. *Nanoscale* **2011**, *3* (1), 71–85. https://doi.org/10.1039/C0NR00583E.
(81) Gu, J.; Hu, C.; Zhang, W.; Dichiara, A. B. Reagentless Preparation of Shape Memory Cellulose Nanofibril Aerogels Decorated with Pd Nanoparticles and Their Application in Dye Discoloration. *Applied Catalysis B: Environmental* **2018**, *237*, 482–490. https://doi.org/10.1016/j.apcatb.2018.06.002.
(82) Segal, L.; Creely, J. J.; Martin, A. E.; Conrad, C. M. An Empirical Method for Estimating the Degree of Crystallinity of Native Cellulose Using the X-Ray

Diffractometer. *Textile Research Journal* **1959**, *29* (10), 786–794. https://doi.org/10.1177/004051755902901003.
(83) Fall, A. B.; Lindström, S. B.; Sundman, O.; Ödberg, L.; Wågberg, L. Colloidal Stability of Aqueous Nanofibrillated Cellulose Dispersions. *Langmuir* **2011**, *27* (18), 11332–11338. https://doi.org/10.1021/la201947x.
(84) Gu, J.; Dichiara, A. Hybridization between Cellulose Nanofibrils and Faceted Silver Nanoparticles Used with Surface Enhanced Raman Scattering for Trace Dye Detection. *International Journal of Biological Macromolecules* **2020**, *143*, 85–92. https://doi.org/10.1016/j.ijbiomac.2019.12.018.
(85) Nishiyama, Y. Molecular Interactions in Nanocellulose Assembly. *Philos Trans A Math Phys Eng Sci* **2018**, *376* (2112). https://doi.org/10.1098/rsta.2017.0047.
(86) Nascimento, D. M.; Nunes, Y. L.; Figueirêdo, M. C. B.; Azeredo, H. M. C. de; Aouada, F. A.; Feitosa, J. P. A.; Rosa, M. F.; Dufresne, A. Nanocellulose Nanocomposite Hydrogels: Technological and Environmental Issues. *Green Chem.* **2018**, *20* (11), 2428–2448. https://doi.org/10.1039/C8GC00205C.
(87) Sydney Gladman, A.; Matsumoto, E. A.; Nuzzo, R. G.; Mahadevan, L.; Lewis, J. A. Biomimetic 4D Printing. *Nature Materials* **2016**, *15* (4), 413–418. https://doi.org/10.1038/nmat4544.
(88) Xu, Y.; Atrens, A. D.; Stokes, J. R. Liquid Crystal Hydroglass Formed via Phase Separation of Nanocellulose Colloidal Rods. *Soft Matter* **2019**, *15* (8), 1716–1720. https://doi.org/10.1039/C8SM02288G.
(89) Alizadehgiashi, M.; Khabibullin, A.; Li, Y.; Prince, E.; Abolhasani, M.; Kumacheva, E. Shear-Induced Alignment of Anisotropic Nanoparticles in a Single-Droplet Oscillatory Microfluidic Platform. *Langmuir* **2018**, *34* (1), 322–330. https://doi.org/10.1021/acs.langmuir.7b03648.
(90) Gierlinger, N.; Schwanninger, M.; Reinecke, A.; Burgert, I. Molecular Changes during Tensile Deformation of Single Wood Fibers Followed by Raman Microscopy. *Biomacromolecules* **2006**, *7* (7), 2077–2081. https://doi.org/10.1021/bm060236g.
(91) Wiley, J. H.; Atalla, R. H. Band Assignments in the Raman Spectra of Celluloses. *Carbohydrate Research* **1987**, *160*, 113–129. https://doi.org/10.1016/0008-6215(87)80306-3.
(92) Hsieh, Y.-C.; Yano, H.; Nogi, M.; Eichhorn, S. J. An Estimation of the Young's Modulus of Bacterial Cellulose Filaments. *Cellulose* **2008**, *15* (4), 507–513. https://doi.org/10.1007/s10570-008-9206-8.
(93) Agarwal, U. P. Analysis of Cellulose and Lignocellulose Materials by Raman Spectroscopy: A Review of the Current Status. *Molecules* **2019**, *24* (9). https://doi.org/10.3390/molecules24091659.
(94) Munier, P.; Gordeyeva, K.; Bergström, L.; Fall, A. B. Directional Freezing of Nanocellulose Dispersions Aligns the Rod-Like Particles and Produces Low-Density and Robust Particle Networks. *Biomacromolecules* **2016**, *17* (5), 1875–1881. https://doi.org/10.1021/acs.biomac.6b00304.
(95) Ureña-Benavides, E. E.; Kitchens, C. L. Wide-Angle X-Ray Diffraction of Cellulose Nanocrystal−Alginate Nanocomposite Fibers. *Macromolecules* **2011**, *44* (9), 3478–3484. https://doi.org/10.1021/ma102731m.
(96) Hooshmand, S.; Aitomäki, Y.; Norberg, N.; Mathew, A. P.; Oksman, K. Dry-Spun Single-Filament Fibers Comprising Solely Cellulose Nanofibers from Bioresidue. *ACS*

Appl. Mater. Interfaces **2015**, *7* (23), 13022–13028. https://doi.org/10.1021/acsami.5b03091.
(97) Henriksson, M.; Berglund, L. A.; Isaksson, P.; Lindström, T.; Nishino, T. Cellulose Nanopaper Structures of High Toughness. *Biomacromolecules* **2008**, *9* (6), 1579–1585. https://doi.org/10.1021/bm800038n.
(98) Galland, S.; Berthold, F.; Prakobna, K.; Berglund, L. A. Holocellulose Nanofibers of High Molar Mass and Small Diameter for High-Strength Nanopaper. *Biomacromolecules* **2015**, *16* (8), 2427–2435. https://doi.org/10.1021/acs.biomac.5b00678.
(99) Zubris, K. A. V.; Richards, B. K. Synthetic Fibers as an Indicator of Land Application of Sludge. *Environmental Pollution* **2005**, *138* (2), 201–211. https://doi.org/10.1016/j.envpol.2005.04.013.
(100) Habib, D.; Locke, D. C.; Cannone, L. J. Synthetic Fibers as Indicators of Municipal Sewage Sludge, Sludge Products, and Sewage Treatment Plant Effluents. *Water, Air, & Soil Pollution* **1998**, *103* (1), 1–8. https://doi.org/10.1023/A:1004908110793.
(101) Browne, M. A.; Crump, P.; Niven, S. J.; Teuten, E.; Tonkin, A.; Galloway, T.; Thompson, R. Accumulation of Microplastic on Shorelines Woldwide: Sources and Sinks. *Environ. Sci. Technol.* **2011**, *45* (21), 9175–9179. https://doi.org/10.1021/es201811s.
(102) Products Made from Petroleum | Ranken Energy Corporation.
(103) Dufresne, A. Nanocellulose: A New Ageless Bionanomaterial. *Materials Today* **2013**, *16* (6), 220–227. https://doi.org/10.1016/j.mattod.2013.06.004.
(104) Nogi, M.; Iwamoto, S.; Nakagaito, A. N.; Yano, H. Optically Transparent Nanofiber Paper. *Advanced Materials* **2009**, *21* (16), 1595–1598. https://doi.org/10.1002/adma.200803174.
(105) Wise, H. G.; Takana, H.; Ohuchi, F.; Dichiara, A. B. Field-Assisted Alignment of Cellulose Nanofibrils in a Continuous Flow-Focusing System. *ACS Appl. Mater. Interfaces* **2020**, *12* (25), 28568–28575. https://doi.org/10.1021/acsami.0c07272.
(106) Grossiord, N.; Loos, J.; Laake, L. van; Maugey, M.; Zakri, C.; Koning, C. E.; Hart, A. J. High-Conductivity Polymer Nanocomposites Obtained by Tailoring the Characteristics of Carbon Nanotube Fillers. *Advanced Functional Materials* **2008**, *18* (20), 3226–3234. https://doi.org/10.1002/adfm.200800528.
(107) Le Bras, D.; Strømme, M.; Mihranyan, A. Characterization of Dielectric Properties of Nanocellulose from Wood and Algae for Electrical Insulator Applications. *J. Phys. Chem. B* **2015**, *119* (18), 5911–5917. https://doi.org/10.1021/acs.jpcb.5b00715.
(108) Ajayan, P. M. Nanotubes from Carbon. *Chem. Rev.* **1999**, *99* (7), 1787–1800. https://doi.org/10.1021/cr970102g.
(109) Premkumar, T.; Mezzenga, R.; Geckeler, K. E. Carbon Nanotubes in the Liquid Phase: Addressing the Issue of Dispersion. *Small* **2012**, *8* (9), 1299–1313. https://doi.org/10.1002/smll.201101786.
(110) Liu, Y.; Kumar, S. Polymer/Carbon Nanotube Nano Composite Fibers–A Review. *ACS Appl. Mater. Interfaces* **2014**, *6* (9), 6069–6087. https://doi.org/10.1021/am405136s.
(111) Lu, W.; Zu, M.; Byun, J.-H.; Kim, B.-S.; Chou, T.-W. State of the Art of Carbon Nanotube Fibers: Opportunities and Challenges. *Advanced Materials* **2012**, *24* (14), 1805–1833. https://doi.org/10.1002/adma.201104672.

(112) Vaisman, L.; Wagner, H. D.; Marom, G. The Role of Surfactants in Dispersion of Carbon Nanotubes. *Adv Colloid Interface Sci* **2006**, *128–130*, 37–46. https://doi.org/10.1016/j.cis.2006.11.007.
(113) Shin, J.-Y.; Premkumar, T.; Geckeler, K. E. Dispersion of Single-Walled Carbon Nanotubes by Using Surfactants: Are the Type and Concentration Important? *Chemistry – A European Journal* **2008**, *14* (20), 6044–6048. https://doi.org/10.1002/chem.200800357.
(114) Li, Y.; Zhu, H.; Shen, F.; Wan, J.; Lacey, S.; Fang, Z.; Dai, H.; Hu, L. Nanocellulose as Green Dispersant for Two-Dimensional Energy Materials. *Nano Energy* **2015**, *13*, 346–354. https://doi.org/10.1016/j.nanoen.2015.02.015.
(115) Song, K.; Zhang, Y.; Meng, J.; Green, E. C.; Tajaddod, N.; Li, H.; Minus, M. L. Structural Polymer-Based Carbon Nanotube Composite Fibers: Understanding the Processing–Structure–Performance Relationship. *Materials* **2013**, *6* (6), 2543–2577. https://doi.org/10.3390/ma6062543.
(116) Hajian, A.; Lindström, S. B.; Pettersson, T.; Hamedi, M. M.; Wågberg, L. Understanding the Dispersive Action of Nanocellulose for Carbon Nanomaterials. *Nano Lett.* **2017**, *17* (3), 1439–1447. https://doi.org/10.1021/acs.nanolett.6b04405.
(117) Sengezer, E. C.; Seidel, G. D.; Bodnar, R. J. Phenomenological Characterization of Fabrication of Aligned Pristine-SWNT and COOH-SWNT Nanocomposites via Dielectrophoresis under AC Electric Field. *Polymer Composites* **2015**, *36* (7), 1266–1279. https://doi.org/10.1002/pc.23031.
(118) Goodman, S. M.; Ferguson, N.; Dichiara, A. B. Lignin-Assisted Double Acoustic Irradiation for Concentrated Aqueous Dispersions of Carbon Nanotubes. *RSC Adv.* **2017**, *7* (9), 5488–5496. https://doi.org/10.1039/C6RA25986C.
(119) Stemmler, D. I.; Backes, D. C. Absorption Spectroscopy as a Powerful Technique for the Characterization of Single-Walled Carbon Nanotubes. 6.
(120) Sofla, M. R. K.; Brown, R. J.; Tsuzuki, T.; Rainey, T. J. A Comparison of Cellulose Nanocrystals and Cellulose Nanofibres Extracted from Bagasse Using Acid and Ball Milling Methods. *Adv. Nat. Sci: Nanosci. Nanotechnol.* **2016**, *7* (3), 035004. https://doi.org/10.1088/2043-6262/7/3/035004.
(121) Lasseuguette, E.; Roux, D.; Nishiyama, Y. Rheological Properties of Microfibrillar Suspension of TEMPO-Oxidized Pulp. *Cellulose* **2008**, *15* (3), 425–433. https://doi.org/10.1007/s10570-007-9184-2.
(122) Sahoo, N. G.; Rana, S.; Cho, J. W.; Li, L.; Chan, S. H. Polymer Nanocomposites Based on Functionalized Carbon Nanotubes. *Progress in Polymer Science* **2010**, *35* (7), 837–867. https://doi.org/10.1016/j.progpolymsci.2010.03.002.
(123) Yang, L.; Zhang, B.; Liang, Y.; Yang, B.; Kong, T.; Zhang, L.-M. In Situ Synthesis of Amylose/Single-Walled Carbon Nanotubes Supramolecular Assembly. *Carbohydrate Research* **2008**, *343* (14), 2463–2467. https://doi.org/10.1016/j.carres.2008.06.031.
(124) Li, Y.; Zhu, H.; Wang, Y.; Ray, U.; Zhu, S.; Dai, J.; Chen, C.; Fu, K.; Jang, S.-H.; Henderson, D.; Li, T.; Hu, L. Cellulose-Nanofiber-Enabled 3D Printing of a Carbon-Nanotube Microfiber Network. *Small Methods* **2017**, *1* (10), 1700222. https://doi.org/10.1002/smtd.201700222.
(125) Huang, F.; Ananth Tamma, V.; Mardy, Z.; Burdett, J.; Kumar Wickramasinghe, H. Imaging Nanoscale Electromagnetic Near-Field Distributions Using Optical Forces. *Scientific Reports* **2015**, *5* (1), 10610. https://doi.org/10.1038/srep10610.

(126) Fiber Polymers. *Molecular Vista*.
(127) *ISTFA 2018: Proceedings from the 44th International Symposium for Testing and Failure Analysis*; ASM International, 2018.
(128) Nowak, D.; Morrison, W.; Wickramasinghe, H. K.; Jahng, J.; Potma, E.; Wan, L.; Ruiz, R.; Albrecht, T. R.; Schmidt, K.; Frommer, J.; Sanders, D. P.; Park, S. Nanoscale Chemical Imaging by Photoinduced Force Microscopy. *Science Advances* **2016**, *2* (3), e1501571. https://doi.org/10.1126/sciadv.1501571.
(129) Tasis, D.; Tagmatarchis, N.; Bianco, A.; Prato, M. Chemistry of Carbon Nanotubes. *Chem. Rev.* **2006**, *106* (3), 1105–1136. https://doi.org/10.1021/cr050569o.
(130) Hou, Y.; Guan, Q.-F.; Xia, J.; Ling, Z.-C.; He, Z.; Han, Z.-M.; Yang, H.-B.; Gu, P.; Zhu, Y.; Yu, S.-H.; Wu, H. Strengthening and Toughening Hierarchical Nanocellulose via Humidity-Mediated Interface. *ACS Nano* **2021**, *15* (1), 1310–1320. https://doi.org/10.1021/acsnano.0c08574.
(131) Qi, H.; Schulz, B.; Vad, T.; Liu, J.; Mäder, E.; Seide, G.; Gries, T. Novel Carbon Nanotube/Cellulose Composite Fibers As Multifunctional Materials. *ACS Appl. Mater. Interfaces* **2015**, *7* (40), 22404–22412. https://doi.org/10.1021/acsami.5b06229.
(132) Wan, Z.; Chen, C.; Meng, T.; Mojtaba, M.; Teng, Y.; Feng, Q.; Li, D. Multifunctional Wet-Spun Filaments through Robust Nanocellulose Networks Wrapping to Single-Walled Carbon Nanotubes. *ACS Appl. Mater. Interfaces* **2019**, *11* (45), 42808–42817. https://doi.org/10.1021/acsami.9b15153.
(133) Steinert, B. W.; Dean, D. R. Magnetic Field Alignment and Electrical Properties of Solution Cast PET–Carbon Nanotube Composite Films. *Polymer* **2009**, *50* (3), 898–904. https://doi.org/10.1016/j.polymer.2008.11.053.
(134) Choi, E. S.; Brooks, J. S.; Eaton, D. L.; Al-Haik, M. S.; Hussaini, M. Y.; Garmestani, H.; Li, D.; Dahmen, K. Enhancement of Thermal and Electrical Properties of Carbon Nanotube Polymer Composites by Magnetic Field Processing. *Journal of Applied Physics* **2003**, *94* (9), 6034–6039. https://doi.org/10.1063/1.1616638.
(135) Guo, X.; Wu, Y.; Xie, X. Water Vapor Sorption Properties of Cellulose Nanocrystals and Nanofibers Using Dynamic Vapor Sorption Apparatus. *Scientific Reports* **2017**, *7* (1), 14207. https://doi.org/10.1038/s41598-017-14664-7.
(136) Ferreira, F. V.; Otoni, C. G.; De France, K. J.; Barud, H. S.; Lona, L. M. F.; Cranston, E. D.; Rojas, O. J. Porous Nanocellulose Gels and Foams: Breakthrough Status in the Development of Scaffolds for Tissue Engineering. *Materials Today* **2020**, *37*, 126–141. https://doi.org/10.1016/j.mattod.2020.03.003.